TARGETED THREE-WAY-JUNCTION RNA NANOPARTICLE REPROGRAMMED CYCLOOXYGENASE-2 CATALYZED DIHOMO-ϒ-LINOLENIC ACID PEROXIDATION PATTERN IN LUNG CANCER

A Dissertation
Submitted to the Graduate Faculty
of the
North Dakota State University
of Agriculture and Applied Science

By

Lizhi Pang

In Partial Fulfillment of the Requirements
for the Degree of
DOCTOR OF PHILOSOPHY

Major Department:
Pharmaceutical Sciences

August 2021

Fargo, North Dakota

North Dakota State University
Graduate School

Title

TARGETED THREE-WAY-JUNCTION RNA NANOPARTICLE REPROGRAMMED CYCLOOXYGENASE-2 CATALYZED DIHOMO-ϒ-LINOLENIC ACID PEROXIDATION PATTERN IN LUNG CANCER

By

Lizhi Pang

The Supervisory Committee certifies that this ***disquisition*** complies with North Dakota State University's regulations and meets the accepted standards for the degree of

DOCTOR OF PHILOSOPHY

SUPERVISORY COMMITTEE:

Dr. Sathish Venkatachalem
Chair

Dr. Sanku Mallik

Dr. Sijo Mathew

Dr. Danling Wang

Approved:

August 18, 2021
Date

Dr. Jagdish Singh
Department Chair

ABSTRACT

As the second most common cancer and the first leading cause of cancer deaths, lung cancer attracts much research attention. Since cyclooxygenase-2 (COX-2) is overexpressing in nearly 80% of lung cancer patients, COX-2 inhibitors may benefit cancer patients via breaking the COX-2/arachidonic acid (AA)/ prostaglandin E_2 (PGE_2) axis, which is highly relevant to cancer progression. However, the COX-2 inhibitors fail to improve survival of cancer patients in clinical studies. To effectively take advantage of COX-2 overexpression in lung cancer, in this study, we advanced a novel strategy, instead of direct COX-2 inhibition, redirecting COX-2 catalyzed dihomo-γ-linolenic acid peroxidation by knocking down delta-5-desaturase (D5D) in lung cancer cells. We found that the D5D siRNA knockdown could repress the AA and PGE_2 formation in lung cancer cells. While a distant free radical byproduct, 8-hydroxyoctanoic acid (8-HOA) was derived from DGLA by COX-2. Both exogenous 8-HOA and DGLA-derived endogenous 8-HOA resulted in inhibition of proliferation, survival, migration but activation of apoptosis in lung cancer cells. We believe that the inhibitory effect of 8-HOA lung cancer is possibly due to histone deacetylase (HDAC) and YAP1/TAZ inhibition. Additionally, we demonstrated the synergistic effect between 8-HOA and first-line chemo cisplatin on lung cancer. To improve the efficiency of D5D inhibition, we used innovative RNA nanotechnology to specifically deliver D5D siRNA to lung cancer *in vitro* and *in vivo*. The D5D siRNA was harbored by 3 way-junction (3WJ) RNA nanoparticle along with epithelial cell adhesion molecule (EpCAM) aptamer as targeting module, and Alexa 647 as imaging module. By using lung cancer and normal lung epithelial cell models, we demonstrated that 3WJ-EpCAM-D5D siRNA nanoparticles could suppress lung cancer cell growth by promoting 8-HOA formation in a COX-2 dependent manner. The EpCAM aptamer ensured the specific *in vivo* delivery of RNA nanoparticles to lung tumors, avoiding damage to

other tissues and toxic/off-target effect. 3WJ-EpCAM-D5D siRNA nanoparticle significantly inhibited xenograft tumor growth in nude mice by regulating apoptosis, metastasis, and proliferation. Overall, our strategy generated an effective and safer outcome and paved the road to COX-2-based precise medicine for lung cancer therapy.

ACKNOWLEDGMENTS

It is my great pleasure to acknowledge my deepest gratitude to Dr. Steven Qian, who was my supervisor since I joined the Department of Pharmaceutical Sciences, NDSU. His vision, enthusiasm, sincerity, dynamism, and motivation have deeply inspired me. He has taught me the methodology to carry out the cancer research and to present the research as clearly as possible in writing and seminar. His guidance helped me in my first two years at NDSU of not only research but also my personal life. Unfortunately, Dr. Qian sadly passed away in 2019. It was a tough time for me to keep my research up without support from him. Thanks to the help of Dr. Sathish Venkatachalem, my committee members, Dr. Sanku Mallik, Dr. Sijo Mathew, Dr. Danling Wang, and the Chair of the Department, Dr. Jagdish Singh, I can continuously proceed with my dissertation.

I am extremely grateful to my current supervisor Dr. Sathish Venkatachalem for allowing me to complete my dissertation in his lab. His guidance helped me in all the time of research and writing of this thesis. I could not have imagined this thesis can be done without his help. My sincere thanks also go to my labmates and collaborators who helped me with my experiment, Harshit Shah, Dr. Yi Xu, Dr. Xiaoyu Yang, Ashish Kumar, Niyati A. Borkar, Sangeeta Bhallamudi, Subashini Varadharajan, Dr. Nilesh S Ambhore, Dr. Premanand Balraj, Dr. Priyanka Banerjee, Dr. Peixuan Guo, Dr. Dan Shu, and Hongzhi Wang. I would like to thank Dr. Jagdish Singh for providing me with the opportunity to work in the department. Also, I thank my friends and colleague in Department of Pharmaceutical Sciences for support and encouragement.

Last but not the least, I wish to thank my family: my parents Yujuan Li and Donghui Pang, for giving birth to me and supporting me spiritually throughout my life.

TABLE OF CONTENTS

LIST OF TABLES

LIST OF FIGURES

LIST OF SCHEMES

LIST OF ABBREVIATIONS

15-PGDH .....15-hydroxyprostaglandin dehydrogenase

3WJ .....3 way-junction

5-FU 5-fluorouracil

5-LOX 5-lipoxygenase

8-HOA.....8-hydroxyloctanoic acid

AA.....Arachidonic acid

AA.....Arachidonic acid

AcH3 .....Acetyl-Histone H3

ALT.....Alanine aminotransferase

ASOs .....Antisense oligonucleotides

AST .....Aspartate aminotransferase

ATCC.....American Type Culture Collection

BAX .....Bcl-2-associated X protein

Bcl-2.....B-cell lymphoma 2

CId.....Combination index

COX .....Cyclooxygenase

CT .....Computed tomography

CTGF .....Connective tissue growth factor

Cyr61.....Cysteine-rich angiogenic inducer 61

D5D.....Delta-5 desaturase

D5D-*KD*.....D5D siRNA knock down

D6D.....Delta-6 desaturase

DDX58.....Retinoic acid-inducible gene I

DGLA .....Dihomo-γ-linolenic acid

DMEM .....Dulbecco's Modified Eagle Medium

DMSO .....Dimethyl sulfoxide

DNase.....Deoxyribonuclease

DNMT3B .....DNA-methyltransferase 3B

ELOVL5 .....Fatty acid elongase 5

EMT .....Epithelial-to-mesenchymal transition

EPA .....Eicosapentaenoic acid

EpCAM .....Epithelial cell adhesion molecule

ER .....Endoplasmic reticulum

ETA.....Eicosatetraenoic acid

EtBr .....Ethidium bromide

FBS .....Fetal Bovine Serum

FDA.....U.S. Food and Drug Administration

GaINAc .....N-Acetylgalactosamine

GC-MS.....Gas chromatography–mass spectrometry

GPX4.....Glutathione Peroxidase 4

GWAS.....Genome-wide association study

HAS.....Highest single agent

HAT .....Histone Acetyltransferase

HDAC .....Histone deacetylase

IC50.....Half maximal inhibitory concentration

IVIS.....In Vivo Imaging System

LC-MS .....Liquid chromatography–mass spectrometry

LDH .....Lactate dehydrogenase

LNPs .....Lipid nanoparticles

LXR.....Liver X receptor

MDSCs.....Myeloid-derived-suppressor cells

miRNA.....MicroRNA

MMP .....Matrix metallopeptidase

mPGES1.....Microsomal prostaglandin E synthase-1

mRNA.....Messenger RNA

MTT .....Thiazolyl Blue tetrazolium bromide

NBF.....Neutral buffered formalin

NC-si .....Negative control siRNA

NS .....Not significant

NSCLC.....Non-small cell lung cancer

PARP.....Poly (ADP-ribose) polymerase

PBS .....Phosphate buffer saline

PD-L1.....Programmed death-ligand 1

PDX.....Patient-derived xenograft

PFB .....Pentafluorobenzyl bromide

PGE_2.....Prostaglandin E_2

PI.....Propidium Iodide

PK .....Pharmacokinetic

POBN.....α-(4-Pyridyl N-oxide)-N-tert-butylnitrone

PPARα .....Peroxisome proliferator-activated receptor α

pSIVA .....Polarity Sensitive Indicator of Viability & Apoptosis

PTPN14.....Protein tyrosine phosphatase non-receptor type 14

PUFA .....Polyunsaturated fatty acids

RIPK3	Receptor-interacting protein kinase 3
RISC	RNA-induced silencing complex
RNAi	RNA interference
RNase	Ribonuclease
SCRIB	Scribble planar cell polarity protein
SD	Standard deviation
SDS	Sodium dodecyl sulfate
SEM	Standard error of the mean
siRNA	Small (or short) interfering RNA
SREBP	Sterol regulatory element-binding protein
TAZ	Transcriptional co-activator with a PDZ-binding motif
TCGA	The Cancer Genome Atlas Program
TLR	Toll-like receptor
TRIS	Tris(hydroxymethyl)aminomethane
VEGFs	Vascular Endothelial Growth Factors
YAP1	Yes-associated protein 1

1. INTRODUCTION

Lung cancer (small cell and non-small cell) is the second most common cancer in both men and women. Non-small cell lung cancer (NSCLC) is the major type of lung cancer. A variety of therapeutic and adjuvant approaches have so far been studied for treating lung cancer, including chemotherapy, targeted therapy, cyclooxygenase-2 (COX-2) inhibition, and polyunsaturated fatty acids (PUFAs) manipulation [1,2]. PUFAs can be classified as n-3 or n-6 fatty acids according to the position of the final double bound. Although n-6 PUFAs are inevitable and more widespread in the human daily diet than n-3s, n-6-based dietary strategies in cancer treatment have not received much research attention. In downstream of n-6 PUFAs pathway, COX-2 plays a key role in cancer progression via promoting the generation of prostaglandin E_2 (PGE_2). Thus, the classic strategy of limiting COX-2-catalyzed n-6 fatty acid peroxidation and subsequent PGE_2 formation has been tested as an adjuvant approach to improve chemotherapy outcomes for many types of cancers, including lung cancer [3,4]. However, many COX-2 inhibitors suffer from safety issues, and clinical responses remain limited [5,6]. To improve the clinical management of lung cancer, there is a critical need to develop better strategies addressing both the overexpression of COX-2 in cancer cells and the inevitable COX-2-catalyzed peroxidation of n-6 PUFAs, which are the primary fatty acids in our diet.

Delta-5 desaturase (D5D) is a rate-limiting enzyme in the downstream of PUFAs synthesis pathway that introduces double-bonds to the delta-5 position in the fatty acid chain [7]. Given the key role of the PUFAs synthesis pathway in energy homeostasis, the act of D5D has been commonly studied in metabolic diseases, such as hepatic steatosis and type 2 diabetes [8,9]. The main function of D5D is to catalyze eicosatetraenoic acid (ETA) to eicosapentaenoic acid (EPA) in the n-3 PUFAs pathway and dihomo-γ-linolenic acid (DGLA) to AA in the n-6 PUFAs pathway

[7]. However, the function of D5D on cancer has remained poorly understood. Our lab recently provided evidence that DGLA derived free radical byproduct, 8-hydroxyloctanoic acid (8-HOA), appears to work in an autocrine manner to not only suppress pancreatic and colon cancer growth but also inhibit cancer metastasis [10,11]. We also demonstrated that the genetic knockdown of D5D via siRNA or shRNA could elicit anticancer effects from DGLA by promoting the formation of 8-HOA [11–17]. Despite the effective knocking-down of D5D by siRNA *in vitro*, the RNA interference (RNAi) system has been hindered by several roadblocks for *in vivo* study and clinical applications, such as low stability and off-target effect [18,19]. Therefore, the active and target delivery system is required to improve the efficiency of D5D siRNA in the *in vivo* and *in vitro* system.

To improve the efficiency of D5D siRNA and investigate the effect of this new strategy on lung cancer, we applied the innovative RNA nano-technology to deliver D5D siRNA to lung tumors. The feasibility of RNA nanotechnology in cancer therapy is exemplified by the bacteriophage phi29 pRNA system, which naturally forms dimers and hexamers via hand-in-hand interactions between right- and left-interlocking loops [20]. The crystal structure of the pRNA-3-Way Junction (3WJ) motif held at the center of the pRNA monomer was recently reported, allowing the construction of ultra-stable and self-assembling nanoparticles with very high affinity. Various targeting modules have been tested successfully with the pRNA-3WJ nanoparticle to specifically target cancers. In the current thesis plan, we combined our novel COX-2 cancer biology concept with innovative RNA nanotechnology to deliver the therapeutic D5D siRNA specifically to tumor tissues. We demonstrated that 3WJ RNA nanoparticles could selectively deliver D5D siRNA to lung cancer cells with high epithelial cell adhesion molecule (EpCAM) expression, whereas it avoids damage to normal cells. EpCAM targeted 3WJ D5D siRNA

nanoparticle successfully redirected the DGLA peroxidation pattern in lung cancer, resulting in the generation of 8-HOA. Both, our *in vitro* and *in vivo* results suggested that DGLA-derived 8-HOA could serve as an HDAC inhibitor that suppresses cancer progression through inhibiting cancer cell proliferation, metastasis, and promoting apoptosis. Our study not only challenged the classic cancer treatment strategies on how to manipulate *in situ* high COX-2 levels and D5D catalyzed n-6 fatty acid metabolism in the diet for cancer treatment, but also provide new insights in overcoming significant barriers that restrict therapeutic delivery to tumors by using unique RNA-nanotechnology.

1.1. The Structure and Distribution of D5D

D5D and delta-6 desaturase (D6D) are respectively coded by *FADS1* and *FADS2* genes, which are located on chromosome 11q12-13.1 [21]. These two genes are oriented as a cluster with <11 kb region in a head-to-head pattern, whereas *FADS3* is in the same cluster (6.0 kb away from *FADS2*) in a tail-to-tail manner with *FADS2*. *FADS1*, *FADS2*, and *FADS3* genes consist of 11 introns and 12 exons and occupy 100 kb regions in total. The closely associated *FADS* genes on chromosome 11 may explain the phenomenon that *FADS1* could replace the function of *FADS2* in *FADS2* deficient breast cancer cells [22]. The variants of the *FADS* gene cluster have been reported that are closely associated with fatty acid consumption, pregnancy, auto-immune diseases, and cancers. The minor allele carriers of the single-nucleotide polymorphism (SNP) rs136261927, rs174537, rs174541, rs174545, rs174546, rs174547, rs174548, rs174549, rs174550, rs174553, rs174555, rs174556, rs174561, and rs42187261 in *FADS1* have been found correlated to change of D5D activity in certain populations and dietary oils, such as EPA, eicosadienoic acid (EDA), and AA [23].

FADS1 and *FADS2* genes contain 1335 bp for encoding 444 amino acids. D5D is a typical front-end fatty acyl-CoA desaturase, which binds to the endoplasmic reticulum (ER) membrane and catalyzes the synthesis of downstream PUFAs. The D5D enzyme belongs to the superfamily of iron-dependent enzymes that consists of two domains, cytochrome b5 domain at N-terminal with heme-binding motifs and desaturase domain at the C-terminal with histidine boxes where one of the histidine residue is replaced by glutamine, which is responsible for the activity of desaturase. The replacement of the glutamine back to histidine (or isoleucine) could result in abrogating the desaturase's activity [7,22]. However, the precise crystal structure of D5D is still unclear as to the difficulties in stabilizing the membrane-bound enzyme with full activities [24]. Since the D5D and D6D shared many similarities in gene SNP, protein structure, and function, it could be a challenge to isolate enzymes that exclusively exhibit D5D activity on their substrates (DGLA and ETA) rather than catalyzing on broad PUFAs' precursors. Fatty acid desaturases are widely distributed in most tissues in animals as the essential function to synthesize PUFAs for energy supply and signaling transduction (serve as first/second messengers). The D5D enzyme is highly expressed in the brain, lung, pancreas, liver (highest), and variety of cancer cells [7]. The low D5D activity in serum lipids has been identified as a potential biomarker in the prediction of disease status, such as metabolic risk in children, hepatic steatosis, type 2 diabetes, and cancers [9,25–27]. A recent The Cancer Genome Atlas (TCGA) database analysis indicated that the mRNA expression levels of *FADS1* are increased in head-neck squamous cell carcinoma tissues in comparison with noncancerous tissues [28].

1.2. The Physiological Function of D5D

D5D and D6D in the n-3/-6 PUFAs pathway are responsible to convert dietary essential fatty acids (α-linolenic acid and linolenic acid) to a series of downstream PUFAs by introducing

double-bonds to the fatty acid chain from the carboxylic end, increasing unsaturation (Scheme 1). Another type of desaturase catalyzing PUFAs synthesis from methyl-end to pre-existing double bonds, such as D12D and D15D, are not present in humans/mammals. Therefore, mammals have to uptake α-linolenic acid and linoleic acid from their daily diet to maintain the balance of fatty acid compositions. Saturated fatty acids have a higher transition temperature compared to unsaturated fatty acids. Therefore, the ratio of saturated to unsaturated fatty acid has been identified as the primary determinant of the melting temperature of triglycerides for regulating cellular membrane fluidity [7,24,29]. In our daily diet, α-linolenic acid and linoleic acid are the major resource of n-3 and omega-6 fatty acids, respectively [30]. Both n-6/-3 fatty acid synthesis pathways shared the same set of enzymes, including D6D, elongase, and D5D, of which D5D is in response to catalyze the formation of EPA in the n-3 pathway and AA in the n-6 pathway [21]. Interestingly, EPA and AA are the precursors of a variety of inflammatory mediators, such as prostaglandins (PGs) and leukotrienes (LTs), for regulating physiological and pathological functions [31]. Selective knocking down *FADS1* by *in vivo* antisense oligonucleotide has been found to induce hepatic inflammation and atherosclerosis in mice [32,33]. *In vitro* study further confirmed the knockdown of *FADS1* activates classic M1 macrophages and inhibits M2 activation, and cause alterations of liver X receptor (LXR) associated gene expression, implicating the key role of D5D in liver lipid metabolism [34]. Additionally, a population-based Kuopio Ischaemic Heart Disease Risk Factor Study has suggested that higher D5D activity is favorably associated with stroke and metabolic risk factors, including low systolic/diastolic blood pressure, insulin level, C-reactive protein concentrations, BMI, and better homeostatic model assessment indices [35]. A high DGLA concentration and low D5D activity in blood is a valuable predictor of hepatic steatosis as the significant correlation between the ratio of abdominal computed tomography (CT)

attenuation for the liver to the spleen and DGLA/D5D level in the patient's serum [8]. The activity of D5D also has been identified as a risk factor of type 2 diabetes where plasma apoB is negatively correlated with D5D activity [9]. Moreover, the D5D activity is also negatively associated with serum triiodothyronine in adolescents with eating disorders, indicating that D5D may participate in thyroid hormone regulation [36].

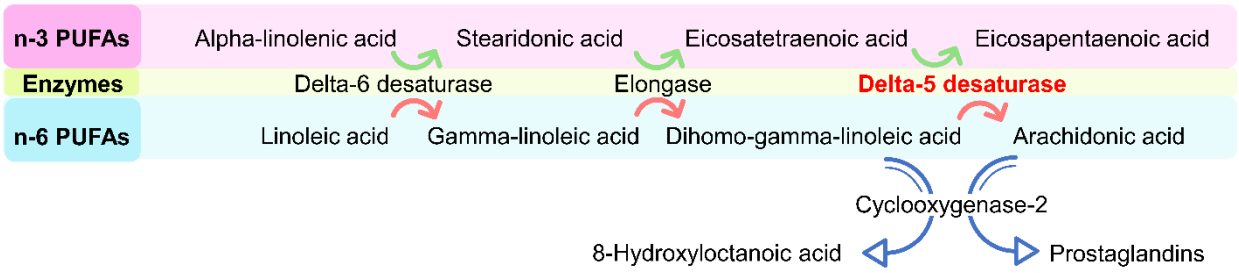

Scheme 1. Pathway of n-3 and n-6 polyunsaturated fatty acids (PUFAs) synthesis. (Reprint from L. Pang, H. Shah, Y. Xu, S. Qian, Delta-5-desaturase: A novel therapeutic target for cancer management, Translational Oncology 14:11 (2021) 101207, under the terms of the Creative Commons CC BY license).

Several rodent studies report that the expression and activity of D5D could be influenced by diet. Indeed, the PUFAs synthesis is regulated under a strong feedback pathway [7]. The D5D is inhibited by dietary PUFA, especially the high-fat diet [37]. Different transcription factors, including peroxisome proliferator-activated receptor α (PPARα), retinoid X receptor (RXR), sterol regulatory element-binding protein 1c (SREBP-1c), have been reported with a strong regulatory effect on D5D expression [7]. All three desaturases, D5D, D6D, and D9D, can be activated by SREBP-1c via regulating mRNA expression. Mouse with overexpression of SREBP-1a, -1c, and -2 appears a higher expression of hepatic D5D than the wild-type mouse. After a fast/refed cycle, supplementation of carbohydrate diet with linoleate or EPA significantly inhibited D5D expression, indicating PUFA induced feedback suppression on D5D [38]. PPARα is another transcription factor that controls β-oxidation in the liver [7]. Activation of PPARα also has been found could induce D5D in the liver, especially in fast conditions. The cross-talk between SREBP-

1c and PPARα may build the basic mechanism of how D5D be regulated under different nutritional statuses and energy states [32,38]. A recent study based on UK Biobank reveals the positive association between FADS1 with rs174561 variant in the frontal cortex and daytime napping. Two-sample Mendelian randomization analyses further confirmed that more frequent daytime napping is correlating to independent risk factors (waist circumference and blood pressure) of cardiometabolic diseases [39]. Given the fact that many downstream inflammatory mediators are generated by the D5D-catalyzed n-6 PUFAs pathway, the correlation between daytime napping and cardiometabolic risks may be explained by activation of AA/PGs-mediated inflammatory response.

1.3. Correlation between D5D and Cancer

The function of D5D is to produce AA and downstream eicosanoids, which are contributing to the progression of inflammation. The relationship between D5D and inflammatory diseases, such as cardiovascular diseases, metabolic syndrome, and diabetes has been well established [21,31]. Additionally, more newer studies recently revealed the potential correlation between D5D expression and cancer [27,40,41]. Since inflammation plays a key role in cancer development, the D5D may be involved in carcinogenesis via mediating PUFAs metabolism in the tumor microenvironment. Interestingly, the divergence of how D5D correlated to cancer development has been seen in different studies. The positive correlation between *FADS1* expression and cancer progression has been observed in non-small cell lung cancer and esophageal squamous cell carcinoma where the patients with low *FADS1* expression corresponding with poor overall survival and disease-free survival, indicating *FADS1* as a predictor of worse prognosis in cancer [41]. Conversely, a recent study based on TCGA suggests high *FADS1* expression in bladder cancer patients with poor prognosis, indicating a negative correlation [40]. The *in vitro*

study further shows that overexpression of *FADS1* could lead to bladder cancer proliferation, whereas the *FADS1* knockdown could arrest the cell cycle [27]. Moreover, *FADS1* is upregulated by a long non-coding RNA linc00460 in osteosarcoma, resulting in distant metastasis and reduced overall survival [42]. A genome-wide association study (GWAS) of colorectal cancer in East Asians suggests that higher *FADS1* expression in colon tumor tissues than normal tissues [43]. Additionally, *FADS1* is also upregulated in patients with hepatocellular carcinoma [44]. Why these opposite correlations have been observed in the above studies? One possible explanation is that the function of D5D may vary in different organs and cancers. D5D is one of the enzymes that participated in PUFAs synthesis. Other enzymes, such as D6D, cyclooxygenase (COX), 5-lipoxygenase (5-LOX), need to be coupled with D5D to generate corresponding eicosanoids [31]. Since both n-3 and n-6 PUFAs pathways compete for the same set of enzymes, the function of different eicosanoids could be contrary. The classical concept considers that n-6 PUFAs are pro-inflammatory, whereas n-3 PUFAs are anti-inflammatory [45]. Worth noting, the positive correlations of *FADS1* with lung cancer and esophageal squamous cell carcinoma are established by analyzing tumor samples from patients in the same region [41,46]. Given the fact that the diet structure varies according to the region, more studies may need to be conducted to further validating the function of D5D in cancer in larger populations across different regions with a variety of dietary habits. Not only *FADS1* expression, but also certain SNPs of *FADS1*, such as rs174549, rs174548, and rs174550 have been identified as independent and favorable factors in predicting oral, lung cancer, colorectal cancer, and laryngeal squamous cell carcinoma progression [47–50].

1.4. D5D Regulates Cancer Progression via Mediating Prostaglandin E_2 (PGE_2) Production

The role of fatty acid metabolism in cancer has been extensively studied as fatty acids could serve as an alternative fuel for providing energy to support cancer cell growth and proliferation [51]. However, fatty acids also contribute to tumorigenesis by mediating various signaling pathways. D5D is a rate-limiting enzyme that catalyzes the formation of AA/EPA from DGLA/ETA [21]. The newly formed AA could be continuously transformed to PGE_2 by COX and PGE synthase in cancer cells [31]. As the most abundant prostaglandin, PGE_2 has been identified that is involved in many aspects of tumorigenesis [52]. COX-2/PGE_2 axis contributes to the formation of the inflammatory microenvironment in the tumor, resulting in proliferation, invasion, epithelial-mesenchymal transition (EMT), cancer cell stemness, and inhibition of apoptosis via autocrine and paracrine regulation (Scheme 2) [52,53]. Therefore, to explore the mechanism of PGE_2 on cancer progression, it is necessary to consider the tumor microenvironment and the function of non-cancer cells. For example, in macrophages, PGE_2 activates the EP4 receptor, leading to M2 polarization. M2 macrophage further promotes the secretion of vascular epithelial growth factors (VEGFs) and accelerates tumor growth [54]. Moreover, PGE_2 promotes migration and stromal formation by regulating EP2/4 signaling in cancer-associated fibroblasts [55]. Tumor growth and migration are also depending on angiogenesis for transporting energy and chemical signals. The activation of PGE_2-EP2/4 could promote angiogenesis through CXCR4 and upregulation of Src [56,57]. Additionally, Orai1 has recently been identified as one of the downstream molecules of the EP4/PI3K pathway, which is responding to PGE_2-induced cancer cell migration [58]. Taken together, PGE_2 may serve as a hub of communication in D5D-mediated cancer progression.

In breast cancer cells, DNA methyltransferase 3B (DNMT3B) can be induced by PGE_2. However, the addition of the PGE_2 receptor antagonist (AH-6809) reverses the change of DNMT3B. This DNMT3B enzyme plays a key role in DNA methylation, which is a significant epigenetic change in tumors and metastatic sites [59]. Moreover, reducing PGE_2 could further activate the $CD8^+$ T cells, preventing breast tumor growth. Therefore, inhibition of PGE_2 by COX-2 inhibitors (etodolac and meloxicam) and natural compound sulforaphane appears to be a promising supplementary therapy to combine with doxorubicin on breast cancer development [60].

Given the vital role of inflammation in cancer, the over-activation of the COX-2/PGE_2 pathway has been reported that could upregulate the protein expression of phospho- NF-κB p65. However, AH6809 and BAY11-7082 (κB kinase inhibitor) suppress the NF-κB pathway, resulting in less invasion and proliferation in ovarian cancer cells [61]. Additionally, another study indicated that myeloid-derived suppressor cells (MDSCs) are also involved in PGE_2-mediated ovarian cancer progression by promoting programmed death-ligand 1 (PD-L1) expression and cancer stemness [62]. More studies investigated the relationship of MDSCs and the NF-κB/COX-2/PGE_2 axis in colorectal carcinogenesis. Yan et al. found that PGE_2 promotes tumor growth through deteriorating the immunosuppressive activity of MDSCs. In the colorectal tumor microenvironment, MDSCs act as the bridge that connecting tumor cells and other immune cells via receptor-interacting protein kinase 3 (RIPK3)-PGE_2 circuit, resulting in immunosuppression and tumor cell proliferation [63]. Not only inhibition of the immune system, but a recent study also revealed that PGE_2 could promote colorectal cancer progression by upregulation of miRNA 675-5p (miR675-5p) [64]. By using RNA-ChIP assays, Cen et al. identified that p53 is the downstream target of miR675-5p. PGE_2 activates Akt/NF-κB/β-catenin pathway, upregulating the expression of Myc, resulting in the expression of miR675-5p in LS174T colorectal cancer cells.

miR675-5p further binds to *TP53* mRNA, decreasing p53 expression [64]. To verify this mechanism *in vivo*, researchers injected p53 depleted cells into the colorectal cancer orthotopic model in NSG mice. It has been shown that PGE_2 treatment results in tumor metastasis almost at the same level as the effect of p53 depletion, implicating the role of miR675-5p in PGE_2-mediated colorectal cancer development [64]. Besides miR675-5p, other miRNAs and molecules, such as miR-370-3p, miR-206, miR-146a, syntenin-1 also could regulate PGE_2 production and inactivation in colorectal cancer [65–67]. The increased PGE_2 in cancer cells could further trigger a positive activation loop of YAP1/COX-2/EP4, resulting in colorectal cancer cell proliferation and polyp formation [68]. Another miRNA miR-194-5p has been found that could improve pancreatic tumor repopulation. After radiotherapy, the dying tumor cells are a major source of PGE_2, which promotes the proliferation of tumor repopulating cells. Aspirin could block the generation of exosomal miR-194-5p via inhibiting the production of PGE_2 in dying pancreatic tumor cells [69]. Additionally, MDSCs infiltration is one of the pathological features of bladder cancer. Prima et al. demonstrated that the COX-2/microsomal prostaglandin E synthase1 (mPGES1)/PGE_2 pathway could promote the expression of programmed death-ligand 1 (PD-L1) in MDSCs. This mechanism helps the bladder cancer cells being attacked by the immune system. However, the treatment of celecoxib and CAY10526 (mPGES1 inhibitor) suppresses PD-L1 expression in myeloid cells. Interestingly, overexpression of 15-hydroxyprostaglandin dehydrogenase (15-PGDH) also inhibits PD-L1 expression through converting PGE_2 to inactive form 15-keto PGE_2 [70].

Despite the importance of PGE_2 synthesis in cancer, the interrelationships and relevance of D5D expression and activity in PGE_2-mediated cancer progression have remained poorly understood. One reason is that compared to D5D, COX-2 is a more conspicuous and accessible

target for regulating PGE_2 production, because the structure and function of COX-2 have been widely studied. Many studies have demonstrated the effect and mechanism of COX-2 inhibitors on various types of cancers *in vitro* and *in vivo*. However, clinical studies indicated that long-term and high-dose treatment of COX-2 inhibitor is required for the PGE_2 inhibition in clinical practices [71,72]. Worth noting, not only in cancer cells but also COX-2 is the key molecule regulating inflammation and other physiological function throughout the body. Thus, the usage of COX-2 inhibitors in cancer treatment may raise safety concerns. Indeed, a significant increase in cardiovascular side effects has been observed in the clinical study when cancer patients received the addition of COX-2 inhibitors in the standard treatment [6]. Moreover, another study suggested that COX-2 inhibitors failed to improve the overall and progression-free survival in cancer patients irrespective of COX-2 expression in tumors [73]. Therefore, continued research into upstream molecules of COX-2/PGE_2 pathways, such as D5D could help us to better understand the role of fatty acid metabolism in cancer progression and to overcome the limitation of COX-2 inhibitors.

1.5. D5D Regulates Cancer Progression through Activating Ferroptosis

Ferroptosis is the iron-dependent manner of cell death and regulated by lipid peroxidation in many types of cells, including cancer cells. Studies suggested that induction of ferroptosis could inhibit cancer development and enhance the efficacy of chemotherapy, targeted therapy, and radiotherapy [74]. The contribution of D5D and lipid peroxidation to ferroptosis has been recently explored in cancer cells. The differential expression of D5D has been observed between intestinal-type and mesenchymal-type gastric cancer cells. By knocking out the D5D gene or using small molecule D5D inhibitor CP-24879, researchers have demonstrated that the expression and activity of D5D are positively correlated with the ferroptosis sensitivity of gastric cancer cells. Indeed, inhibition of D5D diminishes the glutathione peroxidase 4 (GPX4) inhibitor RSL3-induced

ferroptosis in YCC-16 gastric cancer cells. However, the addition of AA to D5D depleted gastric cancer cells could reverse the effect of D5D inhibition, restoring the ferroptosis sensitivity of cancer cells. Not only D5D but also fatty acid elongase 5 (ELOVL5) is essential for ferroptosis. During n-6 PUFA synthesis, ELOVL5 catalyzes gamma-linolenic acid to DGLA, which is the substrate of D5D. Inhibition of ELOVL5 decreases the sensitivity of cancer cells to ferroptosis. However, the addition of exogenous D5D substrate (DGLA) triggers cell death via activating the ferroptosis pathway in fibrosarcoma cells. Worth noting, this phenomenon has been observed in cells treated with a high dose of DGLA (500 μM), whereas low dose (less than 250 μM) appears no anti-cancer effect *in vitro*. Therefore, D5D may serve as a central checkpoint in ferroptosis via manipulating PUFA synthesis [75].

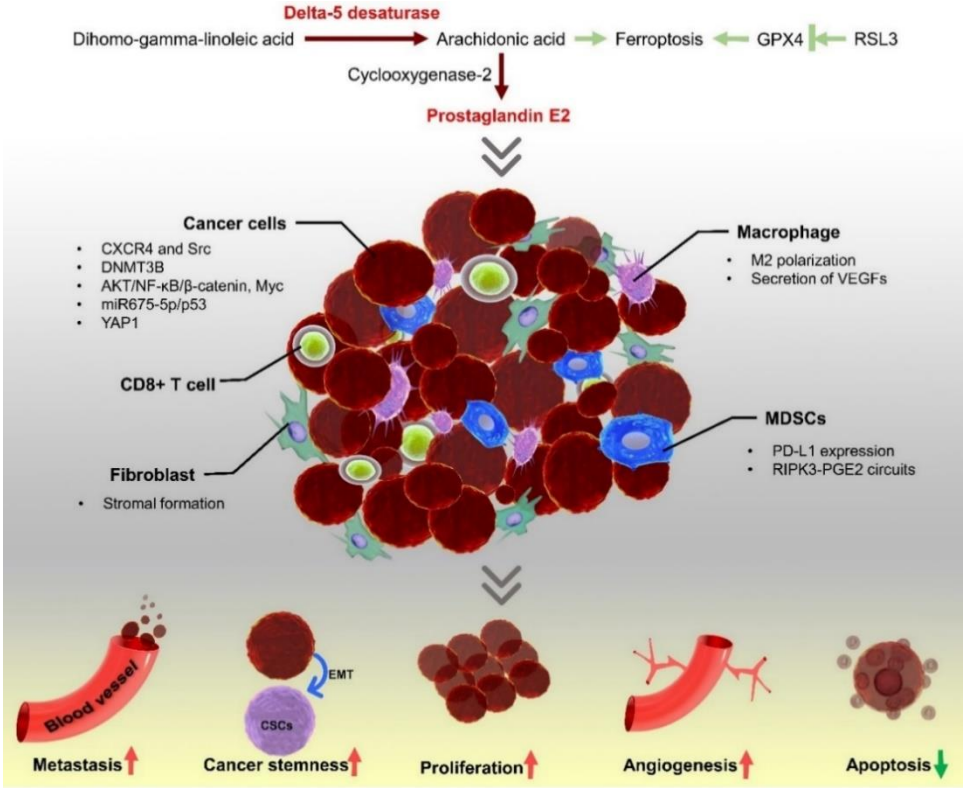

Scheme 2. Delta-5 desaturase (D5D) regulates cancer progression via mediating arachidonic acid (AA) and prostaglandin E_2 (PGE_2) production. (Reprint from L. Pang, H. Shah, Y. Xu, S. Qian, Delta-5-desaturase: A novel therapeutic target for cancer management, Translational Oncology 14:11 (2021) 101207, under the terms of the Creative Commons CC BY license).

1.6. Inhibition of D5D as a New Strategy for Cancer Treatment

Since D5D is an independent prognostic biomarker in many types of cancers, targeting D5D seems like a promising alternative strategy for cancer therapy. By transfecting laryngeal cancer cells with lentivirus vector with *FADS1* shRNA, Zhao et al. found that D5D knockdown inhibited cancer cell proliferation and migration. Additionally, D5D knocking down cells also exhibit the prolonged G1 phase and more apoptosis, indicating that inhibition of D5D expression could suppress laryngeal cancer cell growth. The microarray assay and protein-protein interaction network indicate that the effect of D5D knocking down may be associated with the AKT/mTOR pathway. The activation of AKT, mTOR, and S6K1 are decreased in D5D knocking down laryngeal cancer cells and xenograft tumor tissues in nude mice. It is plausible that *FADS1* silencing reduces the production and activation of AA/PGE_2/EPs, leading to inactivation of the AKT/mTOR pathway and cancer cell death [28].

Not only inhibition of PGE_2 generation, but suppression of D5D may also trigger free radical reactions by reprogramming COX-2-catalyzed DGLA peroxidation (Scheme 3). Xiao et al. identified a series of free radicals from DGLA peroxidation by LC/ESR/MS with α-(4-Pyridyl 1-oxide)-N-tert-butylnitrone (POBN), which is a spin trap for stabilizing free radicals. Two unique free radicals (POBN adducts) have been identified from DGLA/COX-2 C-8 oxygenation, POBN/ $^{\bullet}C_7H_{13}O_2$ (m/z 324) and POBN/ $^{\bullet}C_8H_{15}O_3$ (m/z 354). These two free radicals appear exclusively in DGLA peroxidation, but not AA peroxidation, indicating that alternative downstream pathways of DGLA are existing rather than the AA/PGE_2 pathway [76]. Gu et al. further improved the spin trapping/solid-phase extraction approach and investigated the association between these two free radicals and colon cancer cell growth. In a cellular environment, $^{\bullet}C_7H_{13}O_2$ and $^{\bullet}C_8H_{15}O_3$ could immediately capture hydrogen to form corresponding derivates, heptanoic acid, and 8-HOA. MTS

assay and cell cycle analysis suggest that 8-HOA could decrease the cell viability and delay the G_1 phase of HCA-7 colon cancer cells. However, heptanoic acid did not affect the cancer cell cycle and proliferation [77]. To better understand the role of DGLA-derived free radicals in cancer, Xu et al. assessed the apoptosis of HCA-7 colon cancer cells treated with 8-HOA or hexanol. 8-HOA (1 μM) significantly induced apoptosis in colon cancer cells by regulating the protein expression of p53 and procaspase-9. However, the effect of other DGLA's free radical derivatives (hexanol and heptanoic acid) on apoptosis is modest. Moreover, 8-HOA also drops the IC50 of fluorouracil (5-FU) on HCA-7 cells from 1 mM to 0.5 mM, indicating that 8-HOA may serve as the supplementary treatment for chemotherapy [13]. Moreover, Yang et al. found that 8-HOA also could suppress the BxPC-3 pancreatic cancer cell proliferation and promote apoptosis. Additionally, the wound healing assay suggested that 8-HOA could inhibit the migration of HCA-7 and BxPC-3 cancer cells. The addition of 8-HOA significantly improved the efficacy of gemcitabine (first-line chemo) on inhibiting pancreatic cancer cell growth. Interestingly, the increased protein expression of acetyl-histone H3 has been observed in both colon and pancreatic cancer cells treated with 8-HOA, indicating that histone deacetylase (HDAC) may act as the downstream effector of 8-HOA [11]. Additionally, the HDAC activity response curve to 8-HOA has been established on A549 lung cancer cells [78]. A similar effect of 8-HOA also has been observed on breast cancer cells (MDA-MB 231 and 4T1) [79]. Therefore, it is reasonable to believe that 8-HOA is a broad-spectrum antitumor agent that regulating many aspects of cancer progression.

However, it has been observed in the above-mentioned studies that the treatment of 8-HOA alone without combination with other chemotherapies only can result in less than 30% of inhibition of cancer cell growth. One possible reason is that the effect of exogenous 8-HOA cannot fully

represent the effect of endogenous 8-HOA, which is derived from $^{\bullet}C_8H_{15}O_3$ [76]. Although the free radical form of 8-HOA ($^{\bullet}C_8H_{15}O_3$) is transient in the cellular environment, it may still provide additional cytotoxicity rather than the derivate form of 8-HOA ($C_8H_{16}O_3$). However, in normal cellular conditions, the free radical form of 8-HOA ($^{\bullet}C_8H_{15}O_3$) is not the main product of DGLA, which is more likely to be converted to AA by D5D. To enforce the generation of 8-HOA, Xu et al. knocked down D5D in HCA-7 cells by siRNA transfection. The DGLA consumption is significantly slower in D5D knockdown cells compared to cells with full D5D expression. After 48 h of the transfection, the 8-HOA level increased from ~0.3 μM to more than 0.8 μM, indicating the activation of the DGLA/8-HOA pathway. It has been observed that supplementation of DGLA (100 μM) to D5D knockdown cells could activate p53-dependent apoptosis and enhance the effect of 5-FU, irinotecan, and regorafenib [80]. A similar effect of siRNA-based D5D knockdown has also been found in pancreatic and breast cancer cells [15,81]. By cross-comparison of all these studies, among three cancer types, breast cancer cells (4T1 and MDA-MB 231) generated more 8-HOA (~1.2 μM) after 48 h of transfection than 8-HOA in colon and pancreatic cancer cells (~0.8 μM). However, the difference between the effect of D5D siRNA on breast, colon, and pancreatic cancer cells is minimal. Interestingly, an *in vitro* threshold of endogenous 8-HOA level (0.5 μM) has been identified in these studies. No matter colon, pancreatic, or breast cancer cells, the effect of D5D knockdown only can be elicited if the threshold (0.5 μM 8-HOA) is achieved [15,80,81]. Therefore, it is plausible that the long-term exposure of 8-HOA may provide a bonus benefit than a high concentration but in a short exposure time. This phenomenon may also explain why a high concentration of exogenous 8-HOA appears a lower efficacy than DGLA-derived 8-HOA.

Despite siRNA transfection has high efficiency on D5D knocking down, the off-target effect and stability are still the major concerns of siRNA-based drugs, especially in animal models

and patients [18]. To ensure the continuous generation of 8-HOA, Yang et al. established the stable D5D knockdown cancer cells using shRNA transfection. Supplementation of DGLA to D5D shRNA transfected BxPC-3 and HCA-7 cancer cells inhibit the protein expression of matrix metallopeptidase 2 and 9 (MMP2/9), which are key enzymes for degradation of type IV collagen, extracellular matrix, and basement membrane, resulting in suppression of cancer cell invasion [11]. Additionally, knocking down D5D triggered the expression of cell adhesion protein E-cadherin but decreased the expression of structural protein vimentin and snail, which are critical proteins for EMT during cancer metastasis [79]. Not only exogenous 8-HOA, but DGLA-derived 8-HOA also enhanced the inhibitory effect of gemcitabine and 5-FU on pancreatic and colon cancer cells possibly through co-regulating transcriptional activation of genes in cancer metastasis pathways [11]. Furthermore, the *in vivo* study has demonstrated that shRNA transfected tumor tissues only have about a half expression of D5D compared to mice bearing wild-type tumors. Lacking D5D expression limited the AA generation but significantly improved the 8-HOA production from ~0.1 to ~0.5 μg/g in tumor tissues. Consequently, about 26% tumor size reduction has been observed in nude mice with D5D knocking down tumors [10].

Not only genetically knocking down, but small molecule D5D inhibitor may also hold promise for cancer treatment. However, classical D5D inhibitors, such as sesame, curcumin, and CP-24879 are lacking specificity [82–84]. Thus, even though these inhibitors showed an ideal inhibitory effect on cancer, it is unconvincing this is exclusively resulting from D5D inhibition. Furthermore, few selective D5D inhibitors have been identified by Takeda Pharmaceutical Company, such as D5D-IN-326, T-3364366, and 3,5-diphenyl-4-methyl-1,3-oxazolidin-2-ones; however, these molecules have only been evaluated in other diseases models (such as insulin resistance, obesity, and atherosclerosis) rather than cancer [85–88]. Additionally, another molecule

iminodibenzyl has been found as a promising D5D inhibitor that redirects COX-2 catalyzed DGLA peroxidation to generate 8-HOA in cancer cells [89]. The slow advance of the development of D5D inhibitors may be reasoned by 1) the missing identification of the fine crystal structure of the D5D enzyme and 2) the difficulty to obtain D5D with high stability and activity [24]. Another obstacle is the current methods to quantify PUFAs metabolites of D5D are laborious and time-consuming. Thus, a faster and reliable method needs to be established for accelerating the development of D5D inhibitors for cancer treatment. For instance, a recent study has demonstrated a 2D nanomaterial Ti3C2 MXene-based sensor that simplified the procedures for assessing PGE_2 and 8-HOA concentration in cell lysis, tumor tissues, and blood [90].

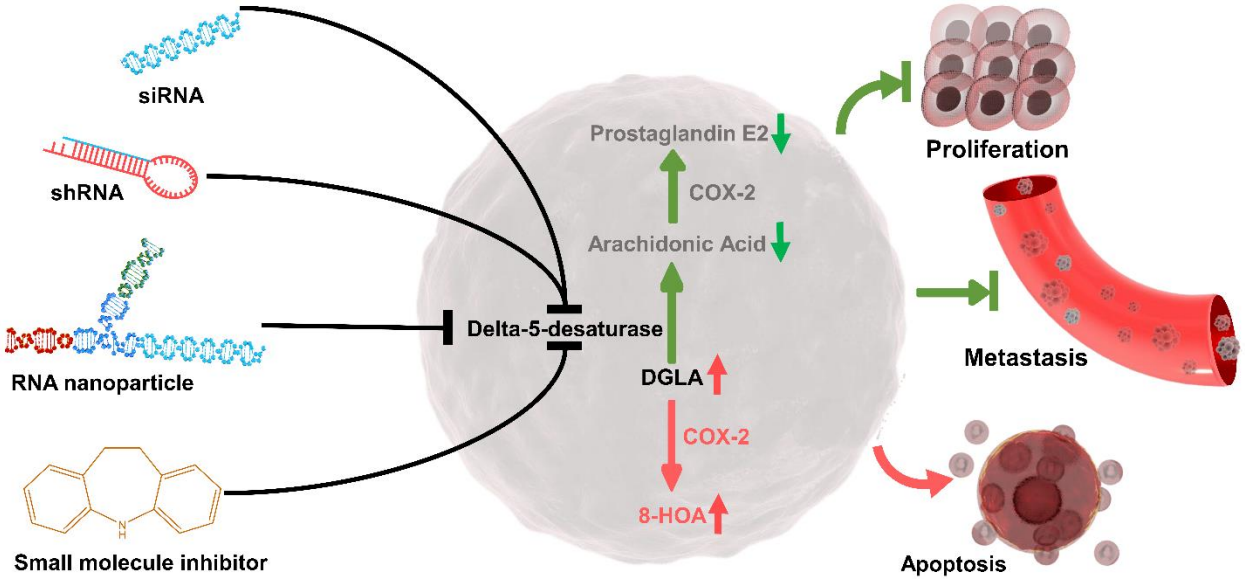

Scheme 3. Inhibition of D5D as a new strategy for cancer treatment. (Reprint from L. Pang, H. Shah, Y. Xu, S. Qian, Delta-5-desaturase: A novel therapeutic target for cancer management, Translational Oncology 14:11 (2021) 101207, under the terms of the Creative Commons CC BY license).

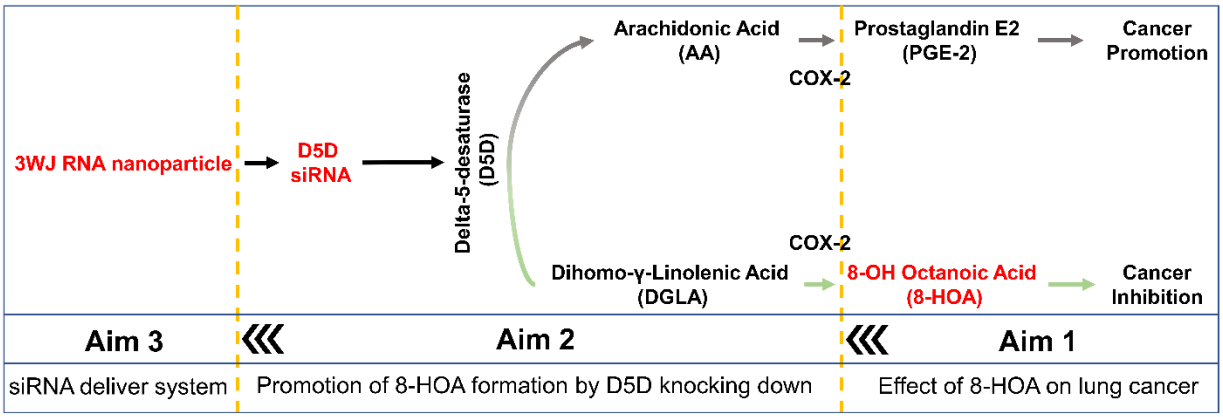

Scheme 4. Conceptual framework. The experiments designed in the following aims we will assess the effect of 8-hydroxyloctanoic acid (8-HOA) on A549 lung cancer *in vitro* (Aim 1). We will stimulate the formation of 8-HOA from COX-2 catalyzed dihomo-γ-linolenic acid (DGLA) peroxidation *via* knocking down D5D (Aim 2). Finally, we will employ 3 way-junction (3WJ) RNA nanoparticle to specifically deliver D5D siRNA to lung tumors *in vivo* (Aim 3).

1.7. Summary of Research Aims in Present Study

D5D is the key enzyme for regulating PUFAs synthesis. The D5D and certain SNPs expression has been found that associated with cancer progression. In the n-6 PUFA synthesis pathway, DGLA is catalyzed by D5D to form arachidonic acid, which is a precursor of PGE_2 and an inflammation mediator. The COX-2 catalyzed PGE_2 could activate EP receptors and promote cancer cell growth and metastasis via regulating tumor microenvironment and immunosuppression. Additionally, COX-2 could directly catalyze DGLA peroxidation, resulting in the generation of a distinct anti-cancer free radical byproduct, 8-HOA. It has been demonstrated that inhibition of D5D could activate the apoptosis pathway, but suppress cancer cell survival, proliferation, migration, and invasion. All these reports suggested that D5D may serve as the central hub and ideal target for the regulation of different aspects of cancer progression. Therefore, continued research into targeted nanoparticle delivery systems for D5D siRNA may help elucidate the controversial mechanisms underlying PUFAs metabolism in cancer and may aid the development of D5D siRNA-based therapeutical strategies.

To further improve the efficiency of the D5D knocking down approach, in this study, we hypothesized that targeted 3WJ RNA nanoparticles could specifically deliver the D5D siRNA to the lung tumor region. Unlike other nanoparticles, RNA nanoparticle does not encapsulate the drug/siRNA in the center; however, all the therapeutical siRNA/miRNA are directly conjugated on the branches of the RNA nanoparticle core. We believe that 3WJ RNA nanoparticles could significantly increase the 8-HOA production, resulting in lung tumor reduction. Moreover, we will explore the targeting efficiency and safety of 3WJ RNA nanoparticles in lung cancer by comparing the internalization and effect of this nanoparticle in cancer cells versus in normal cells. To test these hypotheses, we aimed to 1) determine the role of DGLA-derived free radical byproduct (8-HOA) in lung cancer, 2) promote the formation of 8-HOA from COX-2-catalyzed DGLA peroxidation via knockdown of D5D in NSCLC cells to suppress cancer cell growth, 3) evaluate *in vivo* therapeutic outcomes of DGLA supplementation and siRNA molecules delivered via 3WJ-RNA nanoparticles in mouse models (Scheme 4). We expect that this novel RNA nanoparticle-based therapy will not only suppress tumor growth and cancer development effectively but also avoid the side effects. Our strategy should also generate a much more effective and safer outcome in lung cancer treatment versus the classic COX-2 inhibition strategy, as cancer cells and tumors not only express much higher COX-2 levels but also have a greater need for and much higher uptake rate of fatty acids during their growth.

2. METHODS AND MATERIALS

2.1. Cell Lines and Culture Information

All cell lines were acquired from American Type Culture Collection (ATCC). A549 (CRM-CCL-185™) and H1299 (CRL-5803™) are human lung carcinoma cells. BEAS-2B (CRL-9609™) is a human normal lung epithelial cell. In a biosafety level-2 (BSL-2) lab, cells were individually cultured in HyClone™ Classical Liquid Media, Dulbecco's Modified Eagles Medium (DMEM) with 10% HyClone™ Defined Fetal Bovine Serum (FBS) in cell culture flasks with vent cap from Corning with 5% CO_2 at 37°C in a suitable incubator. For subculture, cells were washed with Dulbecco's phosphate-buffered saline (DPBS). Trypsin was incubated with cells in the incubator till releasing adherent cells from the tissue culture flask. Trypsinization was stopped by adding DMEM 10% FBS media to the flask. Cells and media were collected and transferred into a 15 mL tube for centrifuge at 1000 rpm for 10 min. The cell pellet was resuspended in fresh cell culture media and transferred into a new flask or plates for further experiments.

2.2. Chemical and Reagents

2.2.1. Chemical and Materials

Analytical standard grades of AA-d_8, AA, DGLA, and DGLA-d_6 were purchased from Cayman Chemical (MI, USA). The Costar transwell chamber with the non-coated membrane (6.5 mm insert and 24 well plate 8.0 μm polycarbonate membrane) was purchased from Corning Life Sciences. SampliQ Silica C18 ODS reverse phase SPE cartridge was bought from Agilent Technology (CA, USA). For in vivo treatment, DGLA ethyl ester (0531920-3) was purchased from Cayman Chemical (MI, USA). Cell culture multiwell microplates (6, 12, 24, and 96 wells, sterile with clear flat bottoms) were collected from Santa Cruz Biotechnology. Pipette tips in sterile racks (20, 200, and 1000 μL) and serological pipettes (individually wrapped and bulk) were purchased

from Santa Cruz Biotechnology. Automated cell counters, Countess™ cell counting chamber slides, and trypan blue stain (0.4%) were bought from Thermo Fisher Scientific (MA, USA). Sodium phosphate, sodium phosphate dibasic, ethyl acetate, and sodium phosphate tribasic were purchased from Mallinckrodt Pharmaceuticals. Cis-diamineplatinum dichloride (cisplatin), 2-mercaptoethanol, potassium phosphate dibasic, potassium phosphate monobasic, triton-100X, and 8-hydroxyoctanoic acid, were purchased from Sigma-Aldrich. Acetonitrile, water, methanol, dichloromethane, and acetone were purchased from EMD Millipore. Acetic acid, calcium chloride, potassium chloride, and calcium phosphate were obtained from Fisher Scientific. Chloroform was purchased from J.T.Baker. Crystal violet and dimethyl sulfoxide (DMSO) were acquired from Alfa Aesar. Dry milk (powder) was purchased from Santa Cruz Biotechnology. Sodium dodecyl sulfate (SDS) was purchased from Bio-Rad Laboratories. Sodium chloride, tween-20, and tris(hydroxymethyl)aminomethane (TRIS, Trometamol) were purchased from VWR International. X-ray-film was acquired from Phoenix Research Product. Chemicals not noted were purchased from Sigma-Aldrich.

2.2.2. Biological Reagents

D5D-targeted siRNA, Lipofectamine™ RNAiMAX transfection reagent, MEM reduced serum medium, and Negative Control siRNA was purchased from Thermo Fisher Scientific Inc (MA, USA). RIPA lysis buffer was purchased from Thermo Fisher Scientific (MA, USA). Fetal bovine serum (FBS) and Dulbecco's Modified Eagle's Medium (DMEM) were obtained from Hyclone Laboratories (GE Healthcare, IL, USA). Trypsin EDTA 1X 0,05% Trypsin/0,53 mM EDTA in HBSS with sodium bicarbonate (without calcium and magnesium) were purchased from Corning. PVDF transfer membrane (0.2 μm), extra thick western blotting filter paper, Novex 10% zymogram plus gelatin gel, and Pierce BCA protein assay kit were acquired from Thermo Fisher

Scientific (MA, USA). Spin-X UF 6 10K MWCO PES concentrator was purchased from Corning. Coomassie brilliant blue R-250 staining solution, 10X zymogram renaturation buffer, 10X Zymogram development buffer, mini-PROTEAN TGX stain-free gels (4-20%, 10-well comb), 30% acrylamide/bis solution (29:1), transfer-blot turbo 5X transfer buffer, and 4X laemmli sample buffer was bought from Bio-Rad. Quick-RNA MinPrep was purchased from ZYMO Research. Safe-Green 2X PCR Bestaq MasterMix and OneScript cDNA synthesis kit were purchased from Applied Biological Materials Inc. For immunofluorescence staining, primary antibodies (YAP1, TAZ, D5D, COX-2, MMP-2, E-cadherin, cleaved-PARP, and Ki-67), Alexa fluor-conjugated secondary antibodies (Alexa 647 and Alexa 488), and Phalloidin-iFluor 488 Reagent were acquired from Abcam (MA, USA). Fluoro-Gel II with DAPI was obtained from Electron Microscopy Sciences (PA, USA). For Western analysis, primary antibodies for Bax, p53, Bcl-2, cleaved PARP, procaspase-9, procaspase-3, Acetyl-Histone H3 (Lys9) (C5B11), and β-actin were bought from Cell Signaling (MA, USA). CTGF (E-5), Cyr61 (A-10), Histone H3 (1G1) antibodies were purchased from Santa Cruz Biotechnology (TX, USA). IRDye 800 CW Goat anti-Rabbit or anti-Mouse IgG Secondary Antibodies were purchased from LI-COR Biosciences (NE, USA). Thiazolyl Blue tetrazolium bromide (MTT) was obtained from Alfa Aesar (MA, USA). The 3WJ-EpCAM-Alexa 647 nanoparticle was acquired from ExonanoRNA (Columbus, OH, USA). Phosphoramidites and synthesizer reagents for the synthesis of 3WJ-EpCAM-D5D siRNA nanoparticles were obtained from Glen Research (USA). Histone deacetylase (HDAC), histone acetyltransferase (HAT), lactate dehydrogenase (LDH), and sirtuins activity colorimetric assay kits were purchased from BioVision. Annexin V detection kit was purchased from BD Pharmingen. Human *FADS1* primers (FWD: 5'-GTC CTA AGG CAT GTT GGG ATA G-3'; REV: 5'-GGA CTT GGT CTT GGC TCA ATA G-3') and human S16 primers (FWD: 5'-CAA

TGG TCT CAT CAA GGT GAA CGG-3'; REV: 5'-CTG GAT AGC ATA AAT CTG GGC-3') were purchased from Integrated DNA Technologies. Kinetic Apoptosis Kit (Microscopy) was purchased from Abcam.

2.3. Synthesis of 3WJ RNA Nanoparticles

The 3WJ-EpCAM-Alexa 647 nanoparticle (with targeting and imaging module) was acquired from ExonanoRNA to evaluate cellular binding, internalization, and *in vivo* biodistribution of RNA nanoparticles. 3WJ-EpCAM nanoparticle (only with targeting module, as the vehicle) and 3WJ-EpCAM-D5D siRNA nanoparticle (with D5D siRNA) were synthesized as described in the previous study [91]. The 3WJa D5D siRNA sense strand (5′-uuG ccA uGu GuA uGu GGG uuA cAu cAu ccA cuc Acu AAA tt −3′) and antisense strand (5′-UUU AGU GAG UGG AUG AUG UCG-3′) was purchased from TriLink BioTechnologies (San Diego, CA, USA). Note, the lowercase letters in sequences represent 2'-F modified nucleotides. Assembly of 3WJs was performed by mixing corresponding strands at the equimolar molar concentration in TES buffer (10 mM TRIS pH=7.5, 50 mM NaCl, 1 mM EDTA) and annealing at 85 °C for 5 min followed by slow cooling to 4 °C over about 50 min. 3WJ nanoparticle formation was confirmed on a 12% native PAGE in TBE running buffer (89 mM Tris, 200 mM boric acid, and 5 mM MgCl2). Gels were stained with ethidium bromide (EtBr) followed by imaging by Typhoon FLA 7000 (GE Healthcare).

2.4. siRNA Transfection

D5D siRNA (Silencer Select validated siRNA) transfection was conducted on A549 cells as described in our previous study [12]. Briefly, 3×10^5 A549 cells were seeded into each well of a 6-well plate for overnight incubation. The DMEM cell culture medium was removed, and cells were washed with phosphate buffer saline (PBS) solution. Transfection mixture containing D5D

siRNA (150 nM) and Lipofectamine™ RNAiMAX transfection reagent (6 μL) were treated to A549 cells for 6 h with 500 μL of GlutaMAX Opt-MEM reduced serum media. After incubation, the reduced serum media was replaced by DMEM with 10% (v/v) FBS. At 12 h, 24 h, and 48 h, the transfected A549 cells were collected to verify the knockdown efficiency of D5D siRNA by using Western and immunofluorescence analysis. The appropriate post-transfection time was determined by comparing the D5D expression at different time points. D5D siRNA transfected A549 cells were ready for further treatments and experiments. A549 cells transfected with negative control siRNA were used as the vehicle group.

2.5. Xenograft Lung Tumor Model

Six-week-old nude mice (nu/nu) purchased from The Jackson Laboratory were used to investigate the *in vivo* effect of 3WJ-EpCAM-D5D siRNA nanoparticle on lung tumors. All the animal experiments in this study were approved by the Institutional Animal Care and Use Committees at North Dakota State University (#A19047). Nude mice were acclimated to the animal house for a week upon arriving. Before the *in vivo* study, A549 cells were shipped to IDEXX BioResearch for IMPACT rodent pathogen testing as required of the Institutional Animal Care and Use Committees (IACUC) at North Dakota State University. 2×10^6 A549 cells in 50 μL DMEM media (no FBS) were injected into the hind flank (subcutaneous) of each nude mouse. The nude mice were randomly assigned into different treatment groups (n=6), including the Vehicle group (treated with the same volume of the 3WJ-EpCAM RNA nanoparticles), DGLA group (5 mg/mouse, oral gavage, 20ga polypropylene feeding tubes, every day), 3WJ-EpCAM-D5D siRNA nanoparticle group (intravenous injection, twice a week, 20 μM in 50 μL PBS), and DGLA+ 3WJ-EpCAM-D5D siRNA nanoparticle group [10]. All the treatments were last for 4

weeks. Organs, tumors, and blood were collected after euthanasia. All the samples were immediately used for testing or storing in -80 ℃ freezer.

2.6. MTT Cell Viability Assay

The cell viability was determined by MTT assay. The cells were seeded at 8000 cells per well (in 100 uL medium) into 96-well plates and overnight incubation was done. To evaluate the effect of 8-HOA *in vitro*, we treated cells with 0.01, 0.1, 1, 10, 100 μM 8-HOA for 6, 12, 24, or 48 h. To investigate synergy effect between 8-HOA and cisplatin, cells were treated with 0.35, 0.5, 1, 15, 50, 100 μM 8-HOA and/or 0.35, 0.75, 1.5, 15, 50, 100 μM cisplatin for 48 h. To evaluate the *in vitro* effect of RNA nanoparticles, The 3WJ-EpCAM-D5D siRNA nanoparticle (1, 10, 100, or 1000 nM) and/or DGLA (100 μM) were treated to each well for 48 h. The vehicle group was treated with the same volume of the 3WJ-EpCAM nanoparticle. After treatment, each sample was received 10 μL 0.5% (w/v) MTT and incubated for 4 h in a cell culture incubator. The supernatant of each well was replaced with 100 μL DMSO to dissolve the crystal and determining absorbance at 570/650 nm. The cell viability of the treatment group was normalized by the absorbance in the vehicle group.

2.7. Colony Formation Assay

To evaluate the effect of 8-HOA on cell survival, we seeded 1000 cells to each well of a 6-wells plate. Cells were treated with 8-HOA (0.5 or 1 μM) and/or cisplatin (0.75 or 1.5 μM) for 48 h. After 48 h of 8-HOA and cisplatin treatment, cells were washed with PBS and incubated with fresh DMEM containing 10% (v/v) FBS for 10 days to allow for the formation of colonies. The plate was washed with 3 times PBS. The plate was fixed with 10% Neutral buffered formalin (NBF) for 15 min. After crystal violet staining (0.25% crystal violet in PBS for 30 min), the colonies of cells in each well of 6-well plates were counted by ImageJ (NIH, Bethesda, MD, USA).

The survival fraction was calculated by the equation: the number of colonies in the treatment group divided by the number of colonies in the vehicle group. To evaluate the effect of D5D siRNA transfection on cell survival, the negative control siRNA (*NC-si*) and D5D siRNA (D5D-*KD*) transfected A549 cells were trypsinized and seeded into the new 6-wells plates at the density of 1,000 cells per well. Cells were randomly assigned into 4 different groups, including the *NC-si* group (transfected with negative control siRNA), *NC-si*+ DGLA group (transfected with negative control siRNA and treated with 100 μM DGLA), D5D-*KD* group (transfected with D5D siRNA), and D5D-*KD*+ DGLA group (transfected with D5D siRNA and treated with 100 μM DGLA). After 48 h of DGLA treatment, cells were washed with PBS and fresh DMEM with 10% (v/v) FBS was added for 10 days to allow the formation of colonies. After crystal violet staining, the colonies of cells in each well of 6-wells plates were counted by ImageJ (NIH, Bethesda, MD, USA). The survival fraction was calculated by the equation: the number of colonies in the treatment group divided by the number of colonies in the *NC-si* group [15]. To evaluate the effect of RNA nanoparticles on cell survival, we seeded 1000 cells to each well of a 6-wells plate. Cells were treated with 3WJ-EpCAM RNA nanoparticle (100 nM, as the vehicle), 3WJ-EpCAM-D5D siRNA nanoparticle (100 nM), and/or DGLA (100 μM) for 48 h. After 48 h, cells were washed with PBS. The fresh DMEM with 10% (v/v) FBS was added to each well for 10 days to allow the formation of colonies. After crystal violet staining, the colonies of cells in each well of 6-wells plates were counted by ImageJ (NIH, Bethesda, MD, USA). The survival fraction was calculated by the equation: the number of colonies in the treatment group divided by the number of colonies in the vehicle group.

2.8. Transwell Migration Assay

The Costar transwell chamber with the non-coated membrane (6.5 mm insert and 24 well plate 8.0 μm polycarbonate membrane) was purchased from Corning Life Sciences. To evaluate the effect of 8-HOA on cell migration, cells were treated with 8-HOA (1 μM) and/or cisplatin (1.5 μM) for 48 h. To evaluate the effect of D5D siRNA transfection, cells were incubated with negative control siRNA or D5D siRNA for 6 h as mentioned in the method of siRNA transfection. We replaced media with fresh DMEM with or without DGLA (100 μM) for 48 h. After treatment, each group of cells was trypsinized and collected into a separate vial. About 5 x 10^4 A549 cells from each group were seeded into the insert with DMEM and 10% (v/v) FBS overnight. The medium was replaced by the fresh DMEM (FBS-free) in the insert, DMEM with 10% (v/v) FBS in the lower chamber. After 48 h of incubation, the A549 cells were fixed with neutral buffered formalin solution and stained with crystal violet solution as described in the previous study [92]. The migrated cells on the lower surface of the insert were observed and counted in the inverted microscopy (Lecia Microsystems Model DMi8). The percentage of relative migration rate was calculated by the equation: the number of migrated cells in the treatment group divided by the number of migrated cells in the *NC-si* group [15].

2.9. Wound Healing Assay

About 3 x 10^5 cells were seeded into 6 wells plates overnight. The wound was made by scratching with a sterile pipette. Each well was washed with PBS to clear dislodged cells and replaced by the fresh DMED with 1% (v/v) FBS as described in the previous study [92]. To evaluate the effect of 8-HOA on cell migration, cells were treated with 8-HOA (1 μM) and/or cisplatin (1.5 μM) for 48 h. To evaluate the effect of D5D inhibition on cell migration, cells were transfected with *NC-si* or D5D siRNA with/without DGLA. The wound area of each well was

measured by using ImageJ at 0, 24, and 48 h of post-treatment, respectively. The migrated size of each well was calculated by the equation: the wound area at 24, or 48 h minus the wound area at 0 h. The relative migration rate was normalized by the wound area at 0 h. The smaller wound is representing a higher migration ability of cells in this treatment group.

2.10. Annexin V Detection Kit

The cell apoptosis was evaluated by flow cytometry using FITC Annexin V Apoptosis Detection Kit (556547, BD Pharmingen). Briefly, 3 x 10^5 cells were seeded into each well of 6 well plates overnight. To evaluate the effect of 8-HOA on cell apoptosis, cells were treated with 8-HOA (1 μM) and/or cisplatin (1.5 μM) for 48 h. To evaluate the effect of D5D inhibition on cell apoptosis, cells were transfected with *NC-si* or D5D siRNA with/without DGLA. Cells were harvested by trypsinization and washed with PBS. After centrifugation, 1 x 10^6 cells of each sample were resuspended in 100 μL binding buffer and incubated with 5 μL FITC Annexin V and 5 μL propidium iodide (PI) solution for 15 min in the dark. The samples were analyzed in Accuri C6 flow cytometry as previously described [12].

2.11. Flow Cytometry for Nanoparticle Binding

About 3 x 10^5 cells were trypsinized and washed with PBS. After centrifugation, A549 cells were resuspended in the PBS solution or 100 nM 3WJ-EpCAM-Alexa 647 nanoparticle (in 100 μL PBS) solution. A549 cells were incubated at 37℃ for 2 h. After incubation, cells were washed and resuspended in PBS, followed by flow cytometry analysis (BD Accuri C6 Flow Cytometer) of Alexa 647 intensity [91]. The population of control cells was represented as a blue peak. The red peak represented the cell population with the treatment of the 3WJ-EpCAM-Alexa 647 nanoparticle.

2.12. Live Imaging Kinetic Apoptosis Assay

About 1 x 10^4 cells were seeded into 12 wells plate. Cells were treated with 8-HOA (1 μM) and/or cisplatin (1.5 μM) with fresh DMEM cell culture media (10% FBS). Simultaneously, we added 10 μL/mL Polarity Sensitive Indicator of Viability & Apoptosis (pSIVA-IANBD) and 10 μL/mL PI to each well in a dark cell culture cabinet. The plate was incubated in the Lionheart FX Automated Microscope for observation during 48 h with 5% CO_2 at 37 ℃. The number of total cells and the number of pSIVA positive cells (in green) were recorded at each time point. The apoptosis-positive rate was determined by the number of pSIVA positive cells versus the number of total cells.

2.13. Western Analysis

Protein from cells was collected by scratching off the cells from plates with RIPA Buffer (mixed with protease and phosphatase inhibitor cocktail) on the ice. The protein concentration of each sample solution was determined by using Pierce™ BCA Protein Assay Kit (Thermo Fisher Scientific) as the instruction. Briefly, 5 μL protein samples and 20 μL RIPA buffer were added to each well of the 96-wells plate. The standard curve was made with diluted albumin (BSA) as the instruction in the manual of the BCA Protein Assay Kit. The working solution was prepared by mixing solution A with solution B (50:1). We added 200 μL working solution to each well of the 96-wells plate and mixed it thoroughly on a plate shaker for 30 s. We covered the plate and incubated it for 30 min at 37 ℃. The plate was cooled down in a shaker. The absorbance was measured at 562 nm on a plate reader. The protein concentration was calculated by plotting sample readings into a standard curve. Each sample (containing 80 μg protein) was loaded onto a well of 4-15% Mini-PROTEAN TGX Stain-Free Gels (Bio-Rad Laboratories) for electrophoresis at a constant voltage of 80 V. The proteins were transferred to the 0.2 μm PVDF Transfer Membrane

(Thermo Fisher Scientific) in the Trans-Blot Turbo Transfer System (Bio-Rad Laboratories) in a 30 min standard program as the instruction manual. After blocking by 5% non-fat dry milk, the PVDF membrane was incubated with primary antibodies overnight at 4℃ and followed with secondary antibodies for 1 h. Protein signals were captured in a Li-Cor Odyssey XL System, and densitometry analysis was performed by using ImageJ or Image Studio v.5.2 software. For *in vivo* study, the collected tumor tissues (100 mg) were frozen in liquid nitrogen and crushed to fine powders by mortar. The protein expression was determined as same as *in vitro* samples.

2.14. Histone Deacetylase (HDAC) Activity Colorimetric Assay

2.14.1. HDAC Activity *in vivo*

After 4 weeks of treatment with 3WJ-EpCAM-D5D siRNA nanoparticle (20 μM in 50 μL PBS) and DGLA (5 mg/mouse), tumor tissues were harvested from the nude mice and tissue homogenate was prepared for assessing the HDAC activity. The HDAC activity in tumor tissues was determined by the HDAC Activity Colorimetric Assay Kit (catalog #K331-100, BioVision) as the given protocol. About 100 μg of tissue lysate to 85 μL of water was added to each well of the 96-wells plate. We added 10 μL 10X HDAC assay buffer and 5 μL HDAC colorimetric substrate to each well. The plate was incubated at 37 ℃ for 1 h. The reaction was stopped by adding 10 μL of lysine developer for 30 min incubation at 37 ℃. The absorbances were read at 405 nm on a plate reader.

2.14.2. HDAC Activity *in vitro*

The dose-response curve of HDAC activity to 8-HOA was determined *in vitro*. About 3.0 $x10^5$ A549 cells were seeded into 6 wells plates, followed the treatment of 8-HOA in different concentration (0.0001, 0.001, 0.01,0.05, 0.1, 0.2, 0.5, 1, 50, 315, 1000 μM) for 48 h. To evaluate the effect of RNA nanoparticles on HDAC activity, we treated cells with 3WJ-EpCAM-D5D

siRNA nanoparticles (100 nM) and/or DGLA (100 μM) for 48 h. The cell lysate was prepared in RIPA lysis buffer. The HDAC activity in each well was determined followed by the same protocol as the quantification of HDAC activity *in vivo*.

2.15. Histone Acetyltransferase (HAT) Activity Colorimetric Assay

2.15.1. HAT Activity *in vivo*

After 4 weeks of treatment with 3WJ-EpCAM-D5D siRNA nanoparticle (20 μM in 50 μL PBS) and DGLA (5 mg/mouse), tumor tissues were harvested from the nude mice and tissue homogenate was prepared for assessing the HAT activity. The HAT activity in tumor tissues was determined by the HAT Activity Colorimetric Assay Kit (catalog #K332-100, BioVision) as the given protocol. About 50 μg of tissue lysate to 40 μL of water was added to each well of the 96-wells plate. The cocktail containing: 50 μL 2X HAT assay buffer, 5 μL HAT substrate I, 5 μL HAT substrate II, and 8 μL NADH generating enzyme were added to each well. The plate was incubated at 37 ℃ for 2 h. The absorbances were read at 440 nm on a plate reader.

2.15.2. HAT Activity *in vitro*

About 3.0 $x10^5$ A549 cells were seeded into 6 wells plates, followed by the treatment of 3WJ-EpCAM-D5D siRNA nanoparticle (100 nM) and/or DGLA (100 μM) for 48 h. The cell lysate was prepared in RIPA lysis buffer. The HAT activity in each well was determined followed by the same protocol as the quantification of HAT activity *in vivo*.

2.16. Sirtuins Activity Fluorescence Assay

2.16.1. Sirtuins Activity *in vivo*

After 4 weeks of treatment with 3WJ-EpCAM-D5D siRNA nanoparticle (20 μM in 50 μL PBS) and DGLA (5 mg/mouse), tumor tissues were harvested from the nude mice and tissue homogenate was prepared for assessing the activity of the sirtuin. The sirtuins activity in tumor

tissues was determined by the Sirtuins Activity Fluorometric Assay Kit (catalog #K324 -100, BioVision) as the given protocol. The DTT was added to the homogenization buffer to the final concentration of 2 mM. 200 µL of cold homogenization buffer containing protease inhibitor cocktail to 3 $x10^6$ cells and homogenize tissues on ice. The tissue lysate was agitated on a rotary shaker at 4 ℃ for 15 min. The supernatant was collected after centrifugation at 16,000 g for 20 min at 4 ℃. We added 25 µL of tissue extract into the 96-wells plate. The volume of the sample was made up to 50 µL/well with sirtuins assay buffer. The reaction mix was made with 36 µL of sirtuins assay buffer, 2 µL of the substrate, and 2 µL NAD. We added a 40 µL reaction mix to each sample for 60 min at 37 ℃. The fluorescence was measured under Ex/Em: 400/505. The HDAC activity can be calculated by plotting absorbance into the standard curve.

2.16.2. Sirtuins Activity *in vitro*

About 3.0 $x10^5$ A549 cells were seeded into 6 wells plates, followed by the treatment of 3WJ-EpCAM-D5D siRNA nanoparticle (100 nM) and/or DGLA (100 µM) for 48 h. The cell lysate was prepared in RIPA lysis buffer. The sirtuins activity in each well was determined followed by the same protocol as the quantification of sirtuins activity *in vivo*.

2.17. Lactate Dehydrogenase (LDH) Activity Colorimetric Assay

The LDH-cytotoxicity was determined by the LDH-Cytotoxicity colorimetric assay kit (K311-400) from BioVision. About 1.5 $x10^4$ cells were seeded into 96 wells plates in the 200 µL assay medium (DMEM with 1% BSA). The background control was prepared by adding the 200 µL assay medium into triplicate wells. The background value was subtracted from other groups. The vehicle group was prepared by adding the 200 µL assay medium into triplicate wells. The positive control group was prepared by adding the 200 µL assay medium containing 1% Triton X-100 into triplicate wells. The plate was incubated for 48 h and centrifuged at 250 g for 10 min. The

supernatant of each well was transferred into a new 96 wells plate. The reaction mixture was added to each well for 30 min incubation at room temperature. The absorbance was determined at 495 nm in a plate reader, 600 nm as reference. The cytotoxicity was calculated by comparing the ratio between test sample- vehicle and positive control- vehicle.

2.18. Liquid Chromatography-Mass Spectrometry (LC-MS) for Fatty Acids Quantification

The concentration of DGLA, AA, and PGE_2 in cells or tumor tissues was determined by LC/MS as described in the previous studies [12,91–93]. For the *in vitro* test, 3.0 x 10^5 cells were seeded into each well of 6 wells plates, followed by D5D siRNA transfection or treatment of 100 nM 3WJ RNA nanoparticles. At different treatment duration (12, 24, 48 h for D5D siRNA; 48 h for nanoparticle), cells were scratched off from the plate and collected with 1 mL of cell culture medium. The medium was blended with 0.45 mL LC-MS grade methanol and 1.55 mL water. After mixing with the internal standards (5.0 µL of DGLA-d_6, AA-d_8, and PGE_2-d_9 for each sample), the sample was centrifuged for separating supernatant and purified by using the solid phase extraction (SampliQ Silica C18 ODS). The analysis system consisting of the HPLC system (Agilent 1200 series) and LC/MSD SL ion trap mass (Agilent 6300) was used to determine DGLA, AA, and PGE_2 concentration in the collected samples. The concentration of DGLA, AA, and PGE_2 in cell samples was determined by comparing the peak areas with their internal standards. For *in vivo* study, the tumor tissues were crushed in mortar after being frozen in the liquid nitrogen. 1 mL tissue lysis was prepared for LC/MS as the same procedures as the quantification *in vitro*.

2.19. Gas Chromatography-Mass Spectrometry (GC-MS) for 8-HOA Quantification

For *in vitro* study, 3.0 x10^5 cells were seeded into 6 well plates, followed by siRNA transfection or 100 nM 3WJ-EpCAM-D5D siRNA nanoparticle with 100 µM DGLA. After the extraction and evaporation, the dry samples were reconstituted in 1.0% diisopropylethylamine in

LC-MS grade acetonitrile and reacted with 1.0% PFB-bromide in acetonitrile for 30 min. The acetonitrile was removed using the vacuum evaporator, residues were reconstituted by dichloromethane for GC/MS analysis as described in the previous study [12,91–93]. Briefly, 2.0 µL of the reconstituted sample was injected into an Agilent 7890A gas chromatograph. At 25˚C/min, the temperature of the GC oven is programmed from 60 to 300˚C, gradually. The injector and transfer line were kept at 280˚C. Quantitative analysis was conducted by using a Mass selective detector with a source temperature of 230˚C. An extracted ion with m/z 181 (base peak for both 8-HOA-PFB and hexanoic acid-PFB derivatives) was used to monitor the peak area of 8-HOA and hexanoic acid derivatives. The contents of 8-HOA were determined by using the internal standard curve of hexanoic acid (comparing the peak area to the internal standard). For *in vivo* study, the collected tumor tissues were crushed in a mortar after freezing in the liquid nitrogen. The procedures of 8-HOA quantification are the same as *in vitro*.

2.20. Nanoparticle Internalization Assay

A549 cells were trypsinized and seeded into each well (300 µL per well) of µ-Slide 8 Well (ibidi) with complete DMEM (10% (v/v) FBS) overnight. 200 nM of 3WJ-EpCAM-Alexa 647 nanoparticles (in 100 µL PBS) was treated to cells for 4 h. The cells were washed with a warm PBS-Calcium solution and fixed with the neutral buffered formalin solution. Phalloidin-iFluor 488 Reagent was treated to each well for 30 min to stain the actin filaments of cells. The reagent was removed and washed with a PBS-Calcium solution 3 times. Fluoro-Gel II with DAPI was applied to each well for the staining of the nucleus. The µ-Slide 8 Well was observed under confocal microscopy (LSM900 with Airyscan 2, Carl Zeiss Microscopy) [91].

2.21. Immunofluorescence Analysis

About 5.0 x10^4 cells were trypsinized and seeded into each well (300 µL per well) of µ-Slide 8 Well (ibidi) with the complete DMEM (10% (v/v) FBS) overnight. After treatment of 3WJ RNA nanoparticle or D5D siRNA transfection, cells were fixed by using 4% paraformaldehyde in PBS pH 7.4 for 20 min. The permeabilization was conducted on µ-Slide by incubating samples for 20 min with PBS containing 0.15% Triton X-100. Cells were incubated with 5% BSA for 1 h to block the unspecific binding of antibodies. Followed by blocking, cells were incubated overnight with primary antibodies at 4℃, followed by secondary antibodies for 1 h. Phalloidin-iFluor 488 Reagent was used to stain actin filaments. Cell nuclear was stained by DAPI. The fluorescence images of cells were captured by LSM900 confocal microscopy with Airyscan 2 (Carl Zeiss Microscopy). For *in vivo* samples, collected tumor tissues were sent to Advanced Imaging & Microscopy Laboratory in NDSU to cut into slices for fluorescence analysis as described in the previous study [93]. The tumor tissue images were captured with a Zeiss Axio Imager M2 microscope (20x/0.75). The relative intensity of D5D, MMP-2, and E-cadherin in tumors was determined by using Image-Pro software (Media Cybernetics). The positive rate of Ki-67 and cleaved PARP were illustrated as the K-i67 (or cleaved PARP-positive cells) percentages versus the total number of counted cells [91].

2.22. qPCR Analysis

2.22.1. mRNA Extraction

About 3.0 x10^5 cells were seeded into 6 well plates overnight, followed by administration of 100 nM 3WJ-EpCAM-D5D siRNA nanoparticle with 100 µM DGLA for 48 h. Cells were washed in ice-cold PBS two times. Cells were scraped off from the plate with 1 mL PBS. The mixture was centrifuged at 12,000 rpm for 10 min at 4 ℃. The RNA was extracted by Quick-RNA

MiniPrep (R1054&r1055) from ZOMO Research. Briefly, the pellet was resuspended in 300 μL RNA lysis buffer and gently mixed buffer with the sample. The mixture was loaded into the spin-away filter and centrifuged at 12,000g for 30 s. 300 μL ethanol was added into the flow-through and mix well. The mixture was added into the Zymo-Spin IIICG column and centrifuged at 12,000g for 30 s. 400 μL RNA wash buffer was added into the Zymo-Spin IIICG column and centrifuge at 12,000g for 30 s. DNase buffer was prepared by mixing 5 μL with 75 μL DNA digestion buffer. DNase buffer was added to the Zymo-Spin IIICG column for 15 min incubation at room temperature. We discarded the waste medium in flow-through. 400 μL RNA prep buffer was added to each Zymo-Spin IIICG column and centrifuged at 12,000g for 30 s. We discarded the waste medium in flow-through once again. 700 μL RNA wash buffer was added to each Zymo-Spin IIICG column and centrifuged at 12,000g for 30 s. We discarded the waste medium in flow-through once again. 400 μL RNA wash buffer was added to each Zymo-Spin IIICG column and centrifuged at 12,000g for 2 min. The Zymo-Spin IIICG column was moved to the top of a new tube. 100 μL DNase/RNase free water was added to each Zymo-Spin IIICG column and centrifuged at 12,000g for 30 s. The prepared sample tubes were kept on ice. The RNA concentration and 260/280 were determined by SYNERGY HTX multi-mode reader from BioTek under the mode of nucleic acid quantification.

2.22.2. cDNA Preparation

The cDNA was prepared in an RNase-free PCR tube by mixing 200 ng sample RNA, 2.5 μL 10 mM Oligo (dT), 2.5 μL 10 mM dNTP, and nuclease-free water to the total volume of 50 μL. The PCR tubes were incubated in the MULTIGENE OPTIMAX Thermal Cycler with 96 Well Block from Labnet International for 5 min at 65 ℃. We added 5x RT buffer (10 μL), 1.25 μL RNaseOFF ribonuclease inhibitor (40 U/ μL), and 2.5 μL OneScriptRTase (200 U/ μL) to each

sample. The PCR tube was incubated in the Thermal Cycler as the standard program (15 min at 42 ℃ and 5 min at 85 ℃).

2.22.3. RT-PCR Analysis

The PCR mix was prepared by mixing 2 μL cDNA, 5 μL LightCycler® 480 SYBR Green I Master, 1 μL human *FADS1* primers (FWD: 5'-GTC CTA AGG CAT GTT GGG ATA G-3'), 1 μL human *FADS1* primers (REV: 5'-GGA CTT GGT CTT GGC TCA ATA G-3'), and 1 μL DNase/RNase free water. The house-keeping gene mix was prepared as 2 μL cDNA, 5 μL LightCycler® 480 SYBR Green I Master, 1 μL human *S16* primers (FWD: 5'-CAA TGG TCT CAT CAA GGT GAA CGG-3'), 1 μL human *S16* primers (REV: 5'-CTG GAT AGC ATA AAT CTG GGC-3'), and 1 μL DNase/RNase free water. After adding the PCR mixture to the PCR plate, we covered the plate with the film and centrifuged the plate at 4 ℃ and 2,500 rpm for 30 s. The plate was loaded into QuantStudio 3 Real-Time PCR Systems from Thermo Fisher Scientific. The program was set as 3.3 ℃/s to 95 ℃ for 10 min, 45 cycles of 95 ℃ for 15 s, 2.2 ℃/s to 55.5 ℃ for 20 s, 3.3 ℃/s to 60 ℃ for 1 min, heat plate to 95 ℃ by 3.3 ℃/s for 5 s, 2.2 ℃/s to 65 ℃ for 1 min, 0.15 ℃/s to 97 ℃ for 4 s, 1.6 ℃/s to 40 ℃ for 10 min. The amplification plot and cycle threshold (Ct) value were determined in QuantStudio Design & Analysis software (v1.5.1). ΔCt was calculated by Ct of *FADS1* substrated Ct of *S16*. ΔΔCt was normalized with ΔCt of the vehicle group. Fold change was calculated as 2^- ΔΔCt.

2.23. Biodistribution Imaging System Spectrum Analysis

Six-week-old homozygous nude mice (NU/J, Stock No:002019) were bought from The Jackson Laboratory (Sacramento, USA). Mice were raised in a pathogen-free Innovive IVC system a week before the study. Before the *in vivo* study, cells were shipped to IDEXX BioResearch for IMPACT rodent pathogen testing as required of the Institutional Animal Care and Use Committees

at North Dakota State University. Briefly, 2×10^6 pathogen-free A549 cells were injected into the mouse hind flank subcutaneously. The mice were fed a standard diet for 2 weeks to allow the xenograft tumor formation on the hind flank. 20 μM 3WJ-EpCAM-Alexa 647 nanoparticle (in the 50 μL PBS) or 3WJ-EpCAM nanoparticle (in the same volume, served as a vehicle) was administrated to the nude mice by *i.v.* injection. After 8 h of the injection, the mice were euthanized, and the major organs (heart, liver, lung, spleen, and kidney) and tumors were harvested. All the organs and tumor tissues were stored in a styrofoam box with dry ice. Samples were sent to Dorothy M. Davis Heart and Lung Research Institute and James Comprehensive Cancer Center, The Ohio State University (Columbus, OH, USA) for analysis. The *in vivo* biodistribution of the 3WJ-EpCAM-Alexa 647 nanoparticle was determined by the In Vivo Imaging System (IVIS) Spectrum station [91,94].

2.24. Whole-body Distribution Analysis

Six-week-old homozygous nude mice (NU/J, Stock No:002019) were bought from The Jackson Laboratory (Sacramento, USA). Mice were raised in a pathogen-free Innovive IVC system a week before the study. Before the *in vivo* study, A549 cells were shipped to IDEXX BioResearch for IMPACT rodent pathogen testing as required of the Institutional Animal Care and Use Committees at North Dakota State University. Briefly, 2×10^6 pathogen-free A549 cells were injected into the mouse hind flank subcutaneously. The mice were fed a standard diet for 2 weeks to allow the xenograft tumor formation. 20 μM 3WJ-EpCAM-Alexa 647 nanoparticle (in the 50 μL PBS) or 3WJ-EpCAM nanoparticle (in the same volume, served as a vehicle) was administrated to the nude mice by *i.v.* injection. At 1, 4, and 8 h of post-injection, the mice were anesthetized with 3% isoflurane. The relative fluorescence intensity of nanoparticles in the nude mouse was measured by the Near-Infrared (NIR) imaging system as described in the previous study [95].

2.25. Ultrasound Imaging

To set up an ultrasound imaging system, we weighed the two charcoal canisters using the scale and recorded the weight and date on the side of the canisters. The directional knob on the platform tubing line was in the closed position and the knob on the dropbox tubing line was in the open position. The mouse was placed in the dropbox and securely closed. We turned on the oxygen tank and adjusted the setting to 1.0 mL/min by using the meters of isoflurane canister. We turned the top dial to 3%. Once the mouse falls to one side and does not move around the dropbox, we took it out. We turned on the heated platform and set it to 39°C. The mouse was placed on the platform. We closed the tubing and turned the top dial on the canister down to 2%. We applied Systane eye ointment to both eyes of the mouse for protection. AquaGel lubricating gel was gently inserted into the mouse to monitor temperature during ultrasounding. Aquasonic Clear gel was warmed up by a gel warmer. The gel was applied to the top of the tumor by avoiding introduces bubbles. Vevo 3100 VisualSonics Imaging System (FUJIFILM VisualSonics, Toronto, Canada) was used to scan the tumor area weekly.

2.26. Zymogram for MMPs' Activities

Zymogram gels containing gelatin were purchased from Thermo Fisher Scientific (MA, USA). Cells were collected from a 6-wells plate with the treatment of DGLA and/or 3WJ-EpCAM-D5D siRNA nanoparticles with serum-free DMEM cell culture media. Protein from cells was collected by scratching off the cells from plates. Cell lysis was concentrated by centrifuge in the concentrator. 40 μL concentrated sample was mixed with 10 μL zymogram sample buffer. Samples were not heated before addition to gel. Samples were loaded to the gel and ran slowly at 80 V with fresh running buffer. The gel was removed from the apparatus and placed in a 1X renaturation buffer for 1 h on a slow rocker at room temperature. The gel was washed with double distilled

water (dd water) for 5 mins. The 1x developing buffer was made in dd water. The gel was covered completely by 1x developing buffer and placed in the 37 ℃ water bath for 48 hours. The gel was rinsed in double-distilled water and added Coomassie brilliant blue R-250 staining solution for 1 h incubation. The dye was washed with double distilled water and destaining solution (10% acetic acid, 40% methanol, and 50% water) 2 times for 15 mins. The gel was washed again with double distilled water and developed in Li-Cor Odyssey XL System.

2.27. Hematoxylin and Eosin Staining

The tissues were made into the paraffin section by Advanced Imaging & Microscopy Laboratory at NDSU as described in the previous study [93]. The slides were incubated for 2 h at 55-65 ℃. In a fume hood, we deparaffinized slides in xylene 3 times for 5 min. Slides were washed in 100% ethanol 2 times for 5 min, 95% ethanol for 5 min, 75% ethanol for 5 min, tap water for 5 min, double distilled water for 5 min. Slides were stained in hematoxylin (Gill's III, Sigma GHD332-1L) for 2 min. Slides were washed with double distilled water for 5 min and 1% acid alcohol (1mL HCL/100 mL 70% ethanol) for 10 s. Slides were washed with double distilled water for 5 min. Slides were incubated in 0.3% ammonia water for 1 min and washed again with double distilled water. Slides were washed in 70% ethanol for 60 s, 95% ethanol for 60 s, eosin Y (Polysciences) for 60 s. The slides were dehydrated with 95% ethanol 2 times for 60 s, 100% ethanol 2 times for 60 s, xylene 2 times for 5 min. Slides were covered manually with the mounting solution. The images of tissues were captured by using a Zeiss Axio Imager M2 microscope (20x/0.75).

2.28. ALT and AST Activity Assay

ALT and AST activity in mouse serum were measured by AST or ALT activity colorimetric assay kit (Cat#K752/753, BioVision). The serum was acquired by centrifuging blood

at 2500 rpm for 10 min. The production of pyruvate (catalyzed by ALT) or glutamate (catalyzed by AST) was detected in a reaction that concomitantly converts a nearly colorless probe to color (λ = 570 nm). According to the pyruvate standard curve or glutamate standard curve, the activity of ALT and AST were calculated by using the following formula:

$$\text{Activity} = \frac{B}{(T2 - T1) * V}$$

In this formula, B is the pyruvate (from ALT) or glutamate (from AST) amount from the standard curve; T1 is the first reading OD value at 15 min after the beginning of the reaction; T2 is the OD value read at 60 min after incubation in the 37℃ incubator; V is the sample volume added into reaction (20 μL). The ALT and AST activity was measured in units/liter (U/L) as the instruction manual.

2.29. Statistics

Statistical analysis was conducted using Prism 5 (GraphPad Software, U.S.A). *In vitro* and *in vivo* measurement data were presented as the means ± standard error of the mean (SEM). For MTT assay, colony formation assay, transwell assay, wound healing assay, Annexing V apoptosis assay, live-cell apoptosis analysis, Western analysis, HDAC activity, HAT activity, Sirtuins activity, LDH release, mRNA expression, tumor weight analysis, fatty acids and byproducts profiles, immunofluorescence analysis, and ALT and AST activity tests, multiple comparisons among groups were evaluated using a one-way ANOVA test in Tukey's method. Differences with the minimum of $P < 0.05$ were indicated statistically significant. For Combenefit analysis, the one-sample t-test was conducted for each group in comparison with the single treatment group.

3. THE ROLE OF DGLA-DERIVED FREE RADICAL BYPRODUCT (8-HOA) IN LUNG CANCER

In the n-6 PUFAs synthesis pathway, DGLA could be catalyzed by D5D to generate AA [21]. COX-2 could further take over the reaction, resulting in PGE_2 production [31]. By activating downstream PGE_2 receptors (EPs), PGE_2 suppresses apoptosis of cancer cells by inhibiting the phosphorylation of AKT [96]. Additionally, PGE_2 also increases the adhesion, migration, and angiogenesis of cancer cells by activating Rac and MMP pathways [97,98]. The AA/PGE_2 axis creates an inflammatory microenvironment, leading to immune suppression and cancer progression [52].

However, AA is not the only fatty acid product of DGLA. Our previous studies have demonstrated that DGLA also can be directly catalyzed by COX-2 to form free radical byproducts, such as heptanoic acid and 8-HOA [76,77]. We have demonstrated that 8-HOA could inhibit colon and pancreatic cancer cell survival and proliferation [11,13]. Therefore, the role of DGLA in cancer may correlate with the accessibility (expression and activity) of D5D and COX-2 in cancer cells. In normal cellular conditions where D5D is overexpressed, DGLA is primarily catalyzed by D5D, resulting in PGE_2 production and cancer development [28]. However, in the scenario of D5D inhibition, DGLA may take advantage of high COX-2 expression in cancer cells to produce 8-HOA [11,81]. We have demonstrated that 8-HOA is a potential DNA-damaging reagent affecting cancer cell growth, apoptosis, and migration. Moreover, 8-HOA doses not only promote cancer cell death *via* p53-dependent pro-apoptotic pathways but also activate p53-independent apoptotic pathways in many cancers (*e.g.*, colon, pancreatic, and breast) [10,13,15]. Additionally, we have observed significantly inhibited migration of pancreatic and colon cancer cells upon direct treatment with 8-HOA [80,93]. Furthermore, 8-HOA enhances the efficacies of other chemos- and

target-drugs, *e.g.*, 5-FU, regorafenib, *etc* [12,15,16]. However, the effect and mechanism of 8-HOA on lung cancer are still underexplored. Since the effectiveness of the D5D inhibition-based therapeutical strategy is relying on 8-HOA generation, it is critical to first confirm the sensitivity of lung cancer cells to the 8-HOA. We evaluated the effect and possible mechanism of 8-HOA on A549 and H1299 non-small cell lung cancer cells by assessing many aspects, including survival, proliferation, migration, and apoptosis.

3.1. 8-HOA Inhibited the Survival and Proliferation of Lung Cancer Cells

To evaluate the effect of 8-HOA on lung cancer, we assessed the cell viability of A549 cells treated with 8-HOA by MTT assay. A549 cells were treated with 1 μM 8-HOA for different periods (8, 12, 24, and 48 h) or different concentration (0.01, 0.1, 1, 10, 100 μM) 8-HOA for 48 h. Based on the reading of absorbance from the MTT assay, we observed that 1, 10, and 100 μM 8-HOA for 48 h could lead to a significant decrease of viability in A549 cells ($p<0.05$, Fig. 1A and B). However, the cell viability of A549 cells treated with 10 and 100 μM 8-HOA was not significantly different than A549 cells treated with 1 μM 8-HOA ($p>0.05$, Fig. 1B), indicating that 1 μM 8-HOA is the optimum dose for lung cancer treatment *in vitro*. To further evaluate the effect of 8-HOA on lung cancer cell survival, we performed colony formation assay on A549 cells treated with 8-HOA (1 μM) or the combination of 8-HOA (1 μM) and cisplatin (1.5 μM) for 48 h. Cisplatin is the first-line chemo drug for lung cancer, especially NSCLC [99]. We observed that 8-HOA (1 μM) significantly reduced the number of colonies and survival fraction of A549 cells to less than 70% versus the Vehicle group ($p<0.05$, Fig. 1C). Moreover, the effect of the combination of 8-HOA (1 μM) and cisplatin (1.5 μM) is significantly superior to the effect of 8-HOA ($p<0.01$, Fig. 1C) or cisplatin ($p<0.05$, Fig. 1C) alone on inhibiting cell viability of A549 cells, suggesting that 8-HOA may enhance the effect of cisplatin on lung cancer. Indeed, although

low dose 8-HOA (0.5 μM) and cisplatin (0.75 μM) alone has limited effect on the survival fraction of A549 lung cancer cells, the combination of 8-HOA (0.5 μM) and cisplatin (0.75 μM) could significantly drop the survival fraction to about 40% after 48 h treatment (p<0.01, Fig. 1D). Taken together, cisplatin and 8-HOA may affect lung cancer cell proliferation and survival in a synergistic pattern.

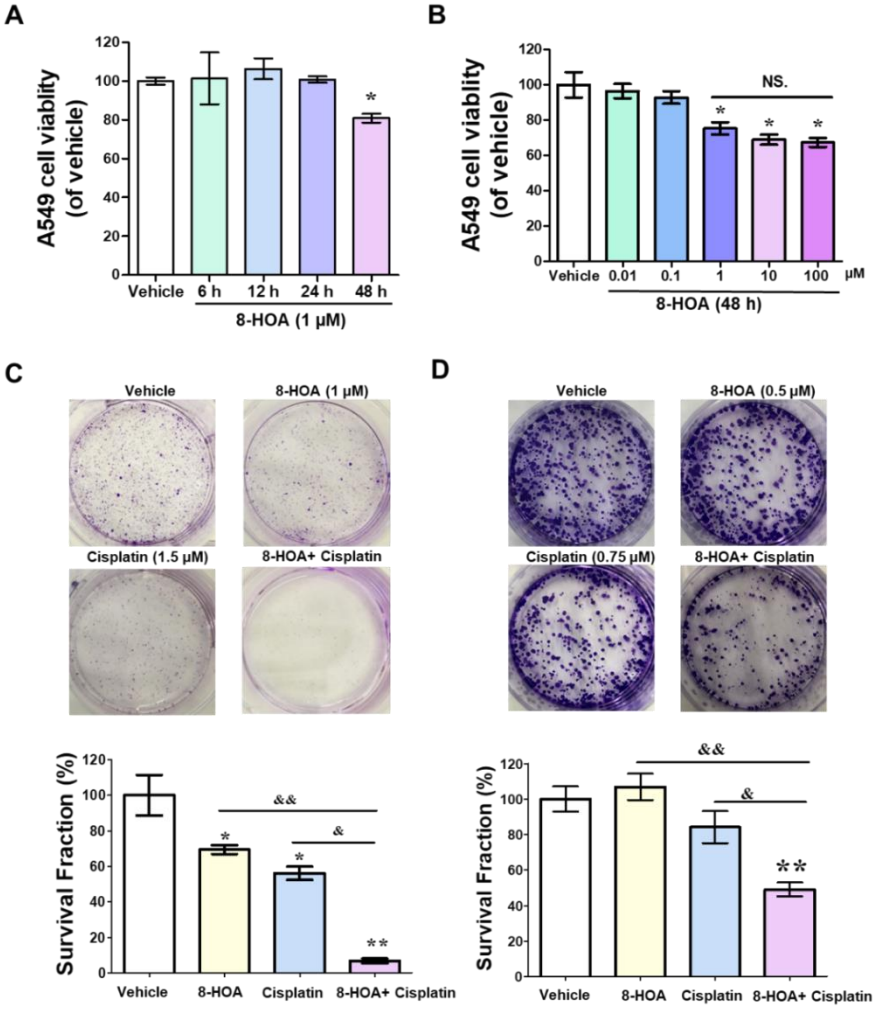

Figure 1. 8-hydroxyoctanoic acid (8-HOA) inhibited the proliferation of A549 lung cancer cells and enhanced the effectiveness of cisplatin. (A) The cell viability of A549 cells treated with 1 μM 8-HOA for 6, 12, 24, and 48 h. (B) The cell viability of A549 cells treated with 0.01, 0.1, 1, 10, and 100 μM 8-HOA for 48 h. Colony formation of A549 lung cancer cells treated with (C) 1 μM 8-HOA and 1.5 μM cisplatin or (D) 0.5 μM 8-HOA and 0.75 μM cisplatin. The survival fraction (%) of A549 cells was normalized by vehicle group. Data represent mean ± SEM for n=6. $^{**}P$<0.01, $^{*}P$<0.05 *vs* Vehicle group; $^{\&\&}P$<0.01, $^{\&}P$<0.05 *vs* 8-HOA+ Cisplatin group; NS.= not significant.

To assess the synergistic pattern and possible interrelationship between 8-HOA and cisplatin, based on the result of colony formation assay, we calculated the combination index (CId) for 8-HOA and cisplatin in different dose combinations, respectively (Table 1). The dose-response equations were established by plotting the survival fraction to each dose of 8-HOA or cisplatin. According to the previously established method [100], the equivalent doses of 8-HOA to cisplatin or cisplatin to 8-HOA were calculated based on the dose-response equations. The CId of 0.5 μM 8-HOA is 1.29; CId of 0.75 μM cisplatin is 1.44; The CId of 1 μM 8-HOA is 1.02; CId of 1.5 μM cisplatin is 1.07. Based on the calculation, the both CId of 8-HOA and cisplatin are higher than 1, indicating the synergistic effect of 8-HOA and cisplatin on regulating lung cancer cell survival.

To further confirm the synergy effect between 8-HOA and cisplatin in a larger dose range, we created the synergy matrix for these two drugs on the Combenefit platform based on the result of the MTT assay. The Combenefit platform allows us to distinguish whether the effect between 8-HOA and cisplatin is synergy, antagonism, or additive in different dose combinations. The synergy score of each dose combination was calculated by using HAS synergy model. The significantly high synergistic effect effects have been found in cells treated with the combination of 0.5 μM 8-HOA and 0.75 μM cisplatin ($p<0.05$), 1 μM 8-HOA and 0.35 μM cisplatin ($p<0.05$), 1 μM 8-HOA and 0.75 μM cisplatin ($p<0.05$), and 1 μM 8-HOA and 1.5 μM cisplatin ($p<0.001$, Fig. 2). Since 1 μM 8-HOA + 1.5 μM cisplatin has the most significant synergistic effect and desirable effectiveness on A549 cells, the dose of 1 μM 8-HOA and 1.5 μM cisplatin was used for treating lung cancer cells in the following studies.

To validate our conclusion, we also assessed the effect of 8-HOA on H1299 lung cancer cells. The cell viability of H1299 cells was determined by MTT assay. The survival fraction was measured by colony formation assay. We observed that 1 μM 8-HOA for 48 h significantly

suppressed the H1299 cell viability (p<0.01, Fig. 3A). The survival fraction of H1299 cells was suppressed by 1 μM 8-HOA (p<0.01, Fig. 3A). Furthermore, the combination of 8-HOA and cisplatin displayed a significantly stronger inhibitory effect on the cell viability and survival fraction of H1299 cells than the single dose of 8-HOA or cisplatin (p<0.001, Fig. 3A and B).

Table 1. Combination index for 8-HOA and cisplatin

Combination dose		**Equivalent dose**		**Expected additive effect**		**Actual observed effect**		**CI_{d1}**	**CI_{d2}**	**Judgement**
8-HOA (Am)	Cisplatin (Bn)	8-HOA (An)	Cisplatin (Bm)	f(Am +An)	g(Bm +Bn)	Y_{obs}				
0.5	0.75	0.68	0.52	39.37	35.19	50.93	50.93	1.29	1.44	Synergistic
1	1.5	1.28	1.14	91.00	86.82	93.22	93.22	1.02	1.07	Synergistic

Notes: Calculation of the combination index for 8-HOA and cisplatin after sequential equivalent doses exchange. Calculation based on formula: Y=f(x); Y=g(x). Y: inhibition rate of survival fraction. f(x): dose-effect relationship of 8-HOA to inhibition rate of survival fraction; g(x): dose-effect relationship of cisplatin to inhibition rate of survival fraction. Am and Bm are equivalent doses, An and Bn are equivalent doses. An=arcf[g(Bn)]; Bm=arcg[f(Am)]. CId: combination index based on dose.

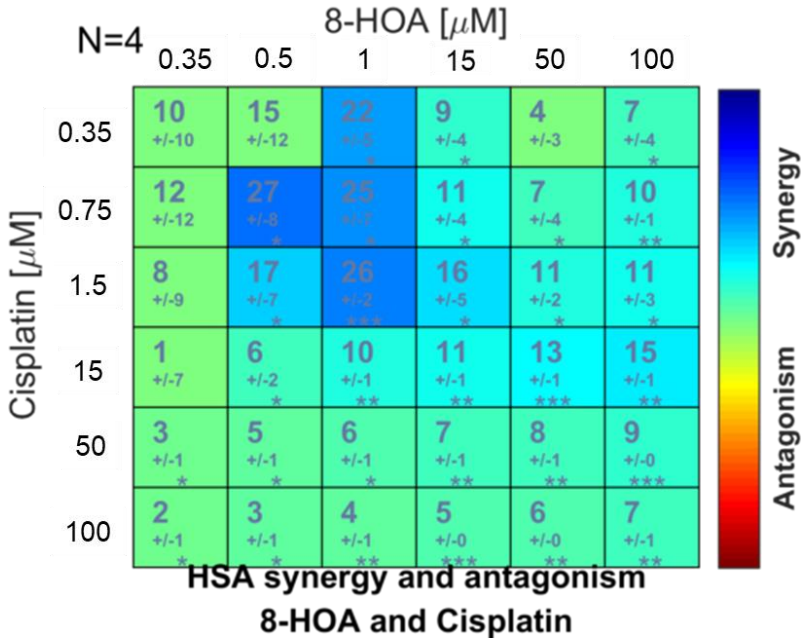

Figure 2. A synergetic effect between 8-HOA and cisplatin was assayed using the Highest Single Agent (HSA) synergy model. The synergy score of each dose combination was shown in the matrix synergy plot. The score represents mean ± SD for n=4. $^{***}P$<0.001, $^{**}P$<0.01, $^{*}P$<0.05 was determined following a one-sample t-test for each group.

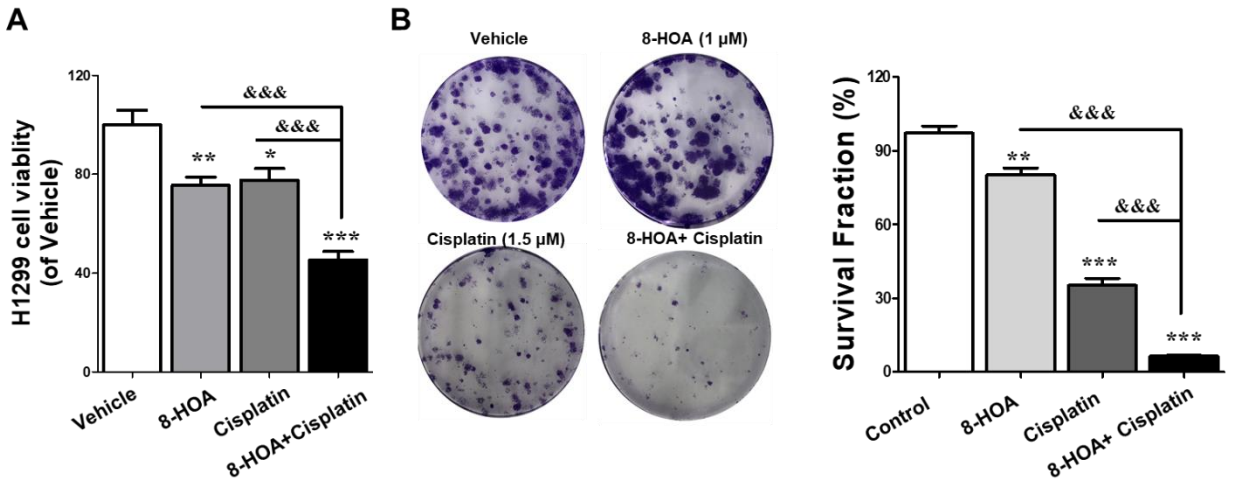

Figure 3. 8-HOA inhibited the proliferation of H1299 lung cancer cells and enhanced the effectiveness of cisplatin. (A) The cell viability of H1299 cells was normalized by vehicle group. H1299 cells were treated with 1 μM 8-HOA for 48 h. (B) Colony formation of H1299 lung cancer cells treated with 1 μM 8-HOA and 1.5 μM cisplatin. The survival fraction (%) of H1299 cells was normalized by vehicle group. Data represent mean ± SEM for n=6. $^{***}P<0.001$, $^{**}P<0.01$, $^{*}P<0.05$ *vs* Vehicle group; $^{\&\&\&}P<0.001$ *vs* 8-HOA+ Cisplatin group.

3.2. 8-HOA Inhibited the Migration of A549 Lung Cancer Cells

The poor survival of lung cancer patients is primarily due to the high occurrence of metastasis [101]. In the late stages of lung cancer, cancer cells would migrate to other organs, including the kidney, brain, liver, and bone, resulting in difficulty in cancer management and a less than 20% of 5-year survival rate of lung cancer patients [1]. To evaluate the effect of 8-HOA on lung cancer cell migration, we performed the transwell migration assay on A549 cells treated with 8-HOA and/or cisplatin (Fig. 4A). We observed that 8-HOA could significantly inhibit the migration rate of A549 lung cancer cells ($p<0.01$, Fig. 4A), indicating the suppression of cancer cell migration. Additionally, the combination of 8-HOA and cisplatin resulted a significantly lower migration rate in A549 cells compared with 8-HOA or cisplatin alone ($p<0.01$, Fig. 4A). Moreover, in wound healing assay, the relative migration rate was decreased by the 8-HOA or the combination of 8-HOA and cisplatin at 24 h ($p<0.05$) and 48 h ($p<0.01$, Fig. 4B) of post-treatment. We observed that cells treated with 8-HOA+ cisplatin have significantly larger wound areas

compared with cells treated with 8-HOA or cisplatin (p<0.05, Fig. 4B), suggesting that 8-HOA could enhance the effect of cisplatin on lung cancer cell migration.

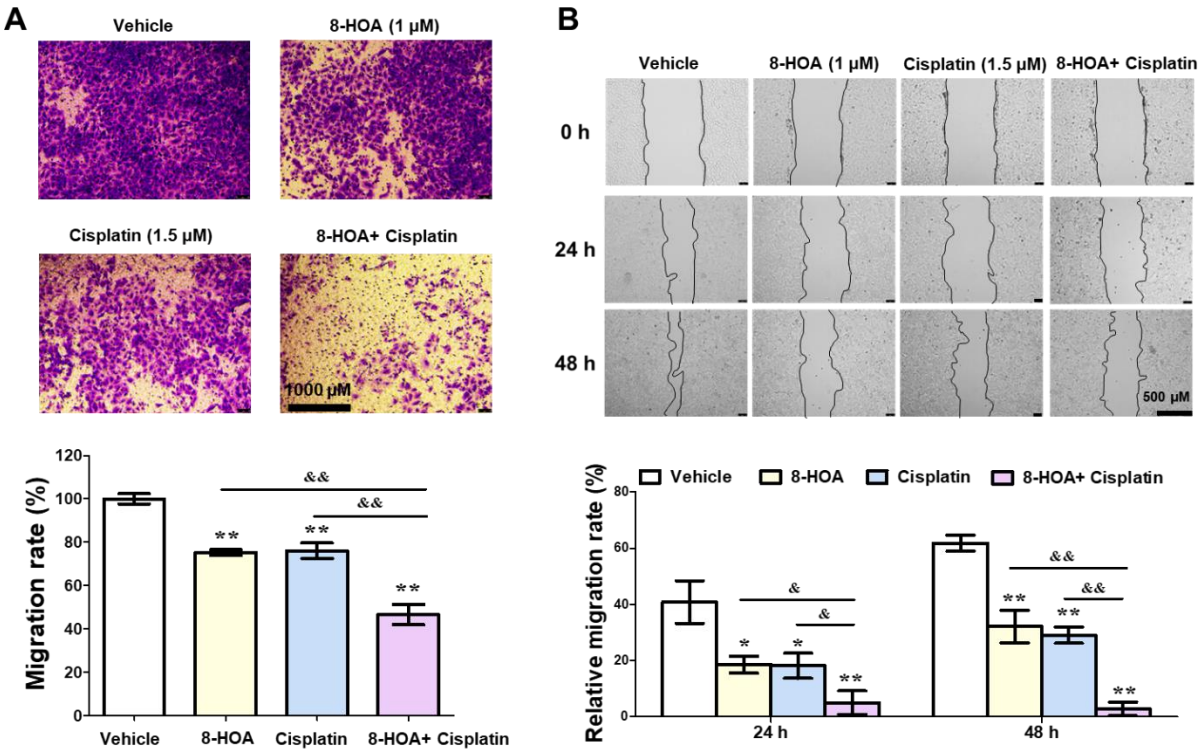

Figure 4. 8-HOA inhibited the migration of A549 lung cancer cells. (A) Transwell migration assay of A549 cells treated with 1 μM 8-HOA and/or 1.5 μM cisplatin. The migration rate (%) of A549 cells was normalized by vehicle group. (B) Wound healing assay of A549 cells treated with 8-HOA and/or cisplatin. The relative migration rate (%) of A549 cells was normalized by vehicle group. Data represent mean ± SEM for n=3. $^{**}P$<0.01, $^{*}P$<0.05 *vs* Vehicle group; $^{\&\&}P$<0.01, $^{\&}P$<0.05 *vs* 8-HOA+ Cisplatin group.

3.3. 8-HOA Induced the Apoptosis in A549 Lung Cancer Cells

We have previously demonstrated that apoptosis can be regulated by 8-HOA in colon and breast cancers [79,81]. However, it is still unknown whether 8-HOA also could trigger apoptosis in the lung cancer cell. Here, we used flow cytometry to quantify the apoptosis level of A549 cells treated with 8-HOA and/or cisplatin (Fig. 5). Annexin V-FITC/PI staining was used to determine the apoptosis and necrosis of A549 cells. We observed that 8-HOA significantly increased the early apoptosis-positive rate from of A549 cells 1.86 ± 0.78 % to 3.61± 2.52 % (p<0.05, Fig. 5).

The higher apoptosis-positive rate was observed in cells treated with the combination of 8-HOA and cisplatin, 5.19 ± 0.78 %, which is significantly higher than the Vehicle group (p<0.001, Fig. 4B). Additionally, given the fact that cisplatin is a DNA damage reagent [102], the synergy effect of 8-HOA and cisplatin may attribute to their effect on induction of apoptosis in lung cancer cells.

To illustrate the kinetic apoptotic change in lung cancer cells, we further performed a pSIVA/PI test on A549 cells for 48 h observation under time-lapse Lionheart FX Automated Microscope microscopy (Fig. 6). The number of pSIVA positive cells (in green) is significantly higher in cells treated with 8-HOA (p<0.05), cisplatin (p<0.01), and 8-HOA+ cisplatin (p<0.01) from 24 h of post-treatment (Fig. 6). However, few to no PI-positive cells (in red) have been observed during 48 h of treatment, indicating that 8-HOA activated apoptosis, not necrosis in lung cancer cells.

To explore the possible mechanism of 8-HOA on apoptosis, we assessed the protein expression of p53, Bcl-2, BAX, procaspase-3, and procaspase-9 by Western analysis (Fig. 7). The protein expression of procaspase-3 and procaspase-9 were significantly decreased in A549 cells treated with 8-HOA (p<0.05, Fig. 7A and B), implicating that 8-HOA could promote the cleavage of caspase-3/9 in lung cancer cells. The procaspases need to be cleaved to form active enzymes for intrinsic apoptosis [103]. Thus, it is reasonable to believe that 8-HOA could induce intrinsic apoptosis in lung cancer cells by activating caspases. Bcl-2 is an anti-apoptosis protein [104]. We found that A549 lung cancer cells have overexpressed Bcl-2, indicating the inhibition of apoptosis in cancer cells (Fig. 7A). However, the Bcl-2 expression was significantly suppressed by 8-HOA (p<0.05, Fig. 7A). Additionally, 8-HOA upregulated the protein expression of BAX (p<0.05, Fig. 7C), which is an apoptotic activator. The BAX/Bcl-2 ratio was significantly increased by 8-HOA in A549 cells (p<0.05, Fig. 7C). Moreover, p53 protein expression was significantly increased in

A549 cells treated with 8-HOA (p<0.01, Fig. 7B). Given that p53 is a vital inducer of apoptosis [105], 8-HOA may activate p53 dependent apoptosis pathway in lung cancer cells. Additionally, the combination of 8-HOA and cisplatin significantly induced intrinsic apoptosis in lung cancer cells in comparison with 8-HOA or cisplatin alone. Indeed, compared to 8-HOA or cisplatin, the protein expression of procaspase-3, procaspase-9, and Bcl-2 were significantly lower in A549 cells treated with the combination of 8-HOA and cisplatin (p<0.001, Fig. 4A and B); however, the protein expression of p53 and BAX were significantly higher in A549 cells treated with the combination of 8-HOA and cisplatin (p<0.001, Fig. 4B and C). These observations confirmed that 8-HOA may enhance the effect of cisplatin on lung cancer via co-regulating apoptosis.

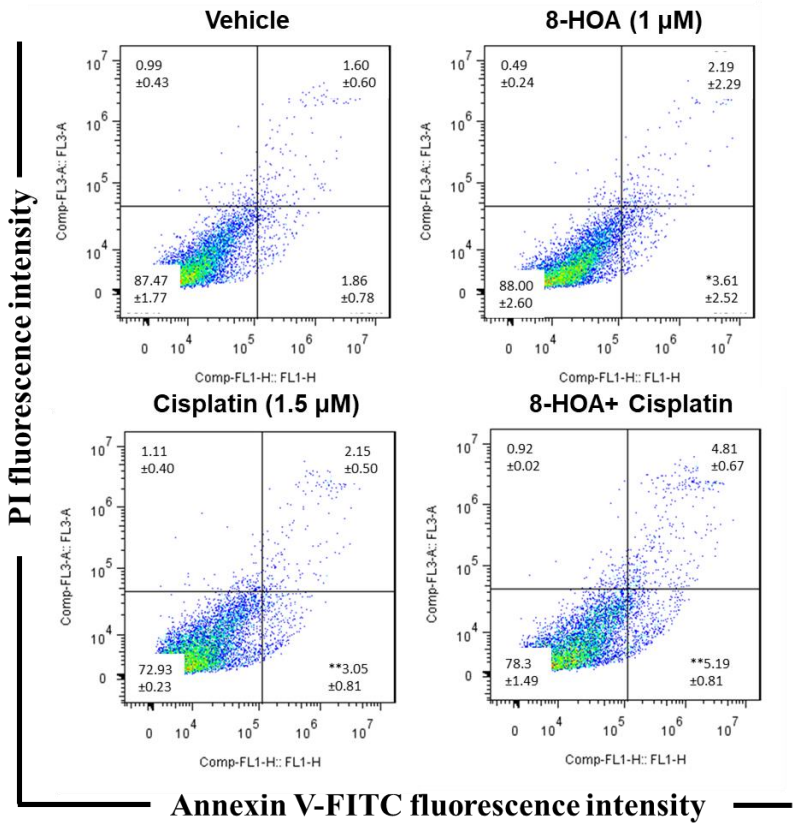

Figure 5. 8-HOA promoted apoptosis in A549 lung cancer cells. Cellular apoptosis was determined by flow cytometry on A549 cells in staining of Annexin V-FITC/PI. A549 cells were treated with 1 μM 8-HOA and 1.5 μM cisplatin for 48 h before flow cytometry analysis. Data represent mean ± SEM for n=3. $^{**}P$<0.01, $^{*}P$<0.05 *vs* Vehicle group.

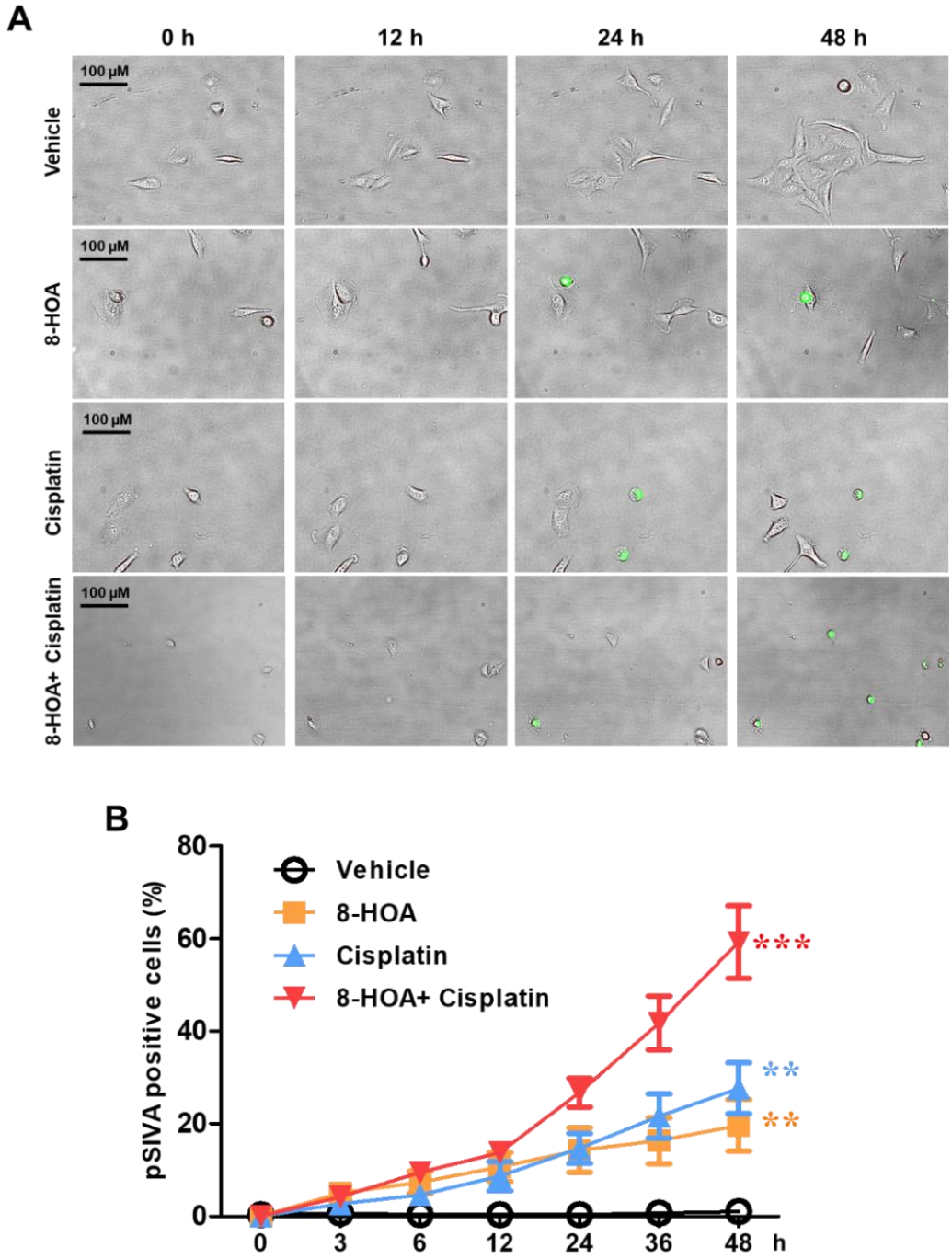

Figure 6. Real-time live A549 lung cancer cell imaging of apoptosis. (A) A549 cells treated with 8-HOA and/or cisplatin. During 48 h of treatment, cells were incubated with the DMEM culture medium (37°C, 5% CO_2) contained Polarity Sensitive Indicator of Viability & Apoptosis (pSIVA) probe and propidium iodide for imaging under time-lapse Lionheart FX Automated Microscope microscopy of the same fields over time. Green fluorescence indicated pSIVA positive cells. (B) The percentage of pSIVA positive cells was quantified at different time points. Data represent mean ± SEM for n=5. $^{***}P<0.001$, $^{**}P<0.01$ *vs* Vehicle group.

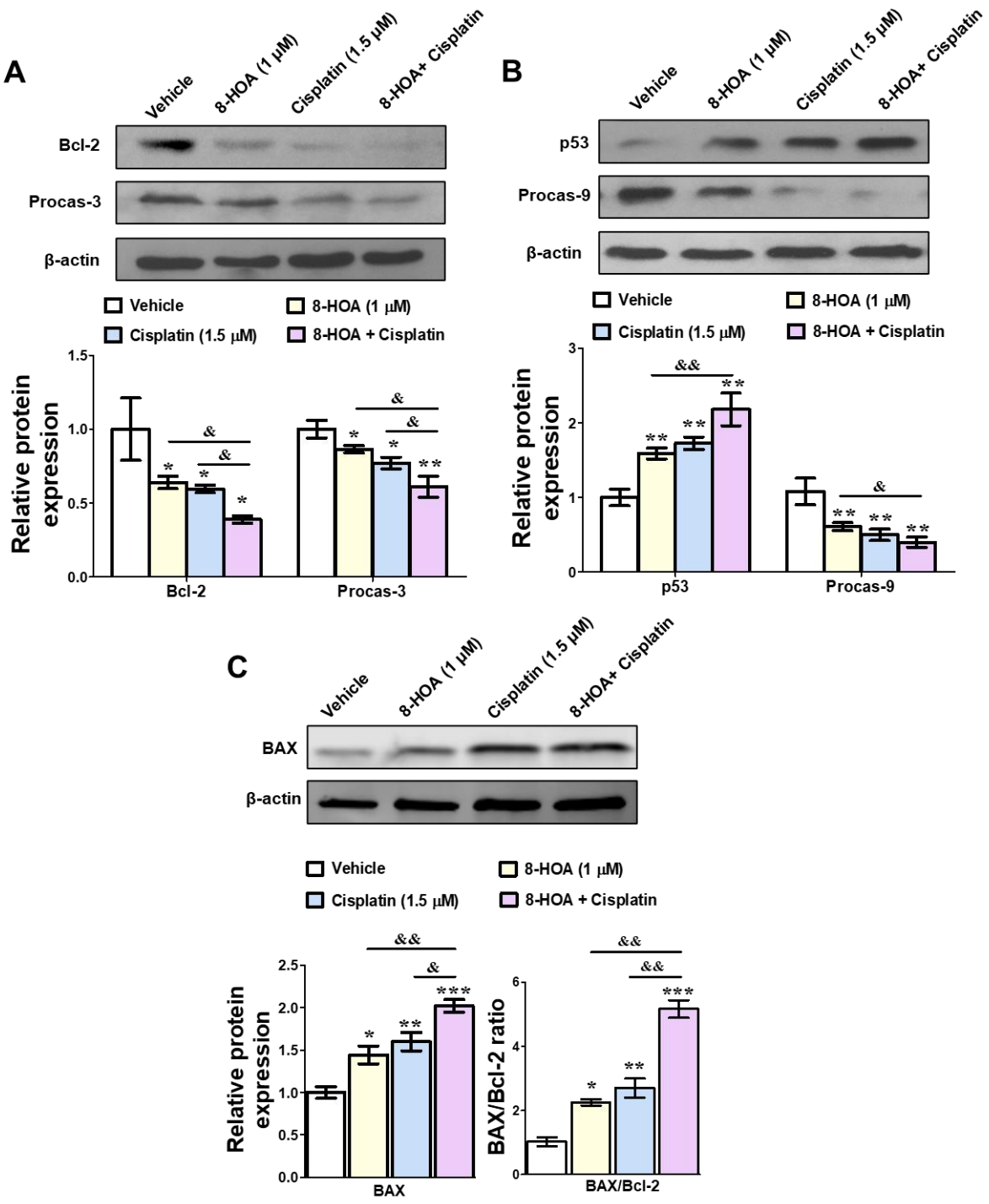

Figure 7. 8-HOA activated p53-dependent intrinsic pathway in A549 lung cancer cells. (A) Bcl-2, Procaspase-3, and (B) p53, and Procaspase-9 protein expression in A549 cells treated with 8-HOA and cisplatin for 48 h. Relative protein expressions were normalized with β-actin. Data represent mean ± SEM for n=6. (C) BAX protein expression in A549 cells after treatment (n=3). The ratio of expression of BAX to Bcl-2 was normalized with the vehicle group. $^{***}P<0.01$, $^{**}P<0.01$, $^{*}P<0.05$ *vs* Vehicle group; $^{\&\&}P<0.01$, $^{\&}P<0.05$ *vs* 8-HOA+ Cisplatin group.

3.4. 8-HOA Suppressed the HDAC Activity and YAP1/TAZ pathway in A549 Lung Cancer Cells

In our previous studies, we have demonstrated that 8-HOA could inhibit acetyl-histone H3 protein expression [81], which is the major substrate of HDAC. The interrelationship and relevance of 8-HOA and HDAC may build up the molecular basis of 8-HOA on lung cancer therapy. In the current study, we observed that 8-HOA could inhibit HDAC activity of A549 lung cancer cells during 48 h treatment (Fig. 8). The IC50 of 8-HOA to HDAC activity is about 0.5 μM. Notably, 8-HOA shares a partial structure as the classical HDAC inhibitor, valproic acid. Therefore, 8-HOA may regulate lung cancer cell growth and apoptosis via inhibiting HDAC activity. It has been demonstrated that classical HDAC inhibitors could affect cancer proliferation by acting on YAP1/TAZ pathway [106]. YAP1/TAZ pathway is the downstream effector of the Hippo pathway, which is responsible for controlling cancer cell growth, metastasis, and survival [107]. To elucidate the effect of 8-HOA on the YAP1/TAZ pathway, we determined the protein expression of YAP1, TAZ, and the downstream molecule of the YAP1/TAZ pathway, CTGF in A549 cells treated with 1 μM 8-HOA at different time points (Fig. 9). The protein expression of YAP1 was significantly inhibited by 8-HOA at 6 h ($p<0.05$, Fig. 9) but returned to the initial level after 12 h of treatment. Analogous to YAP1, the protein expression of TAZ was significantly reduced in A549 cells treated with 8-HOA for 3 h ($p<0.05$) and 6 h ($p<0.05$, Fig. 9), indicating that the 8-HOA could downregulate YAP1/TAZ pathway in a short period. However, the protein expression of CTGF was significantly inhibited by 8-HOA in A549 cells after 48 h and 72 h of treatment ($p<0.05$, Fig. 9). Although the effect of 8-HOA on the YAP1/TAZ pathway occurs in the early phase of treatment, the prolonged effect of 8-HOA on downstream molecules of the YAP1/TAZ pathway,

such as CTGF, can be observed after 48 h. This phenomenon may also explain why we observed the anti-cancer effect of 8-HOA on A549 cells after 48 h of treatment in Figures 1 to 7.

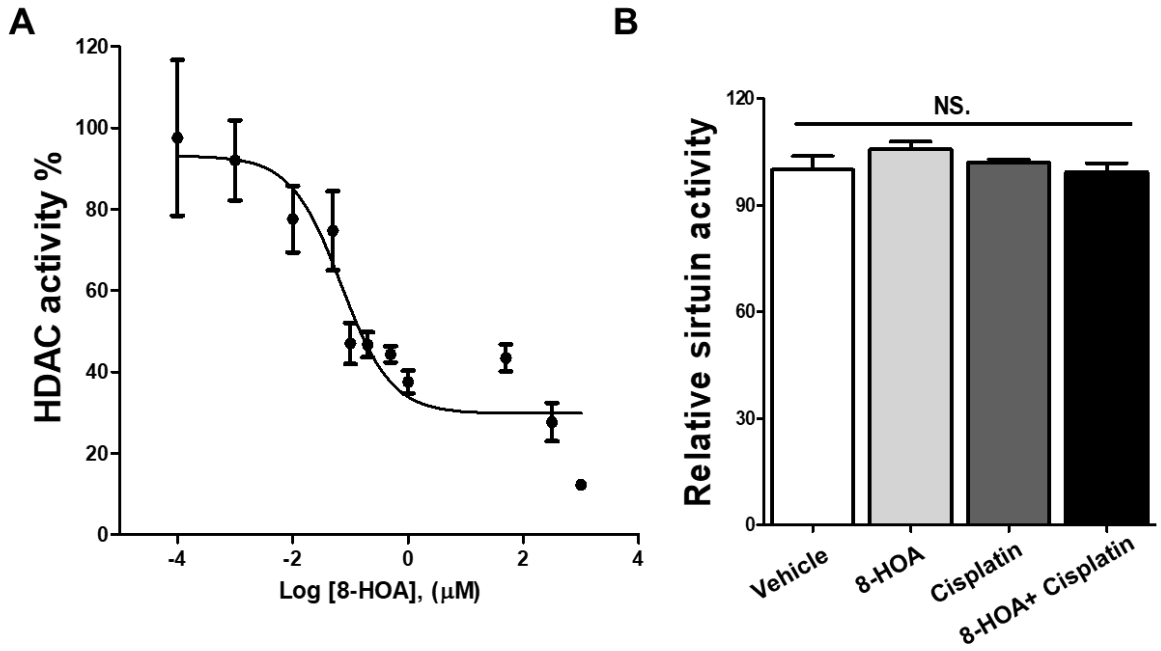

Figure 8. 8-HOA inhibited HDAC activity of A549 lung cancer cells. (A) Dose-response curve of HDAC activity to 8-HOA treatment in A549 cells. A549 cells were treated with different concentrations of 8-HOA for 48 h. The HDAC activity was normalized with the vehicle group. HDAC activity versus Log [8-HOA] was generated from GraphPad. (B) Relative sirtuin activity of A549 lung cancer cells. Cells were treated with 1 μM 8-HOA and/or 1.5 μM cisplatin for 48 h. The sirtuin activity was normalized with the vehicle group. NS. not significant.

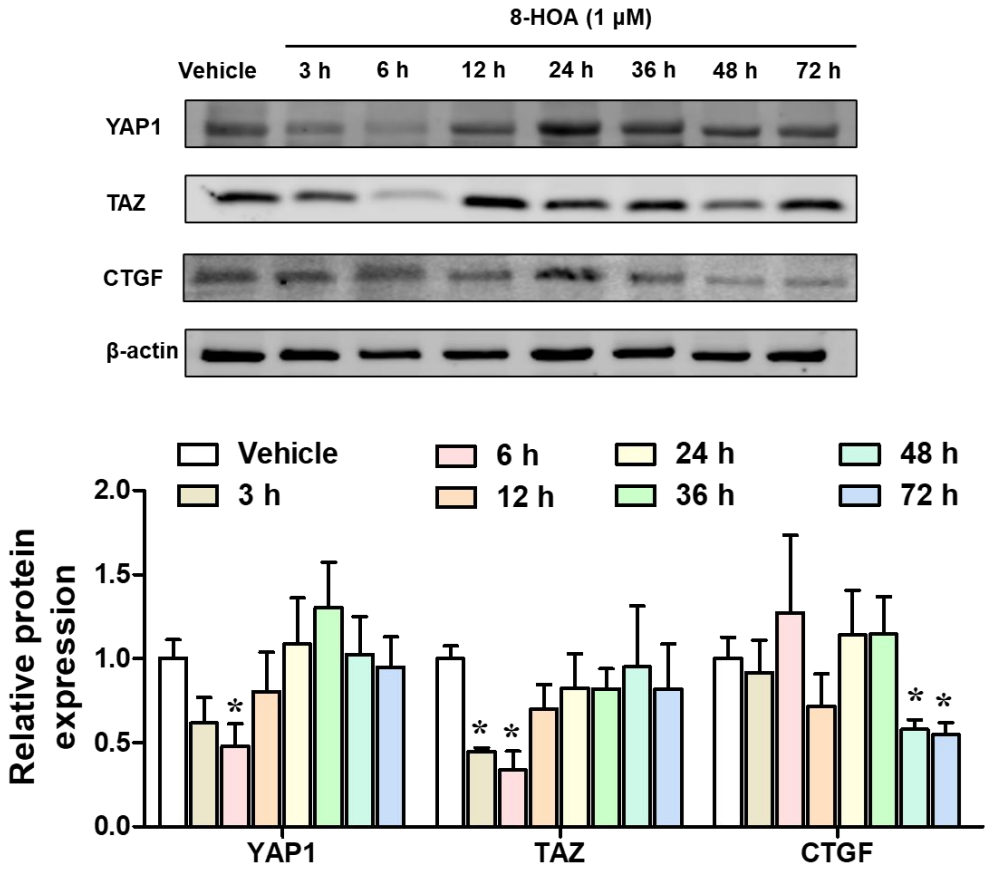

Figure 9. 8-HOA inhibited YAP1/TAZ pathway in A549 lung cancer cells. (A) YAP1, TAZ, and CTGF protein expression in A549 cells treated with 8-HOA for 3, 6, 12, 24, 36, 48, and 72 h. Relative protein expressions were normalized with β-actin. Data represent mean ± SEM for n=3. $^{*}P<0.05$ *vs* Vehicle group.

3.5. Effect of 8-HOA on BEAS-2B Normal Lung Epithelial Cells

Although 8-HOA significantly suppressed lung cancer cell growth, we are still unclear the role of 8-HOA in noncancerous cells. To confirm the effect of 8-HOA on normal lung epithelial cells, we investigated the cell proliferation and survival of BEAS-2B normal lung epithelial cells by measuring the cell viability and LDH activity of BEAS-2B cells treated with 8-HOA followed with MTT assay and LDH cytotoxicity assay (Fig. 10). The cell viability of BEAS-2B cells was significantly suppressed by 8-HOA (1 μM, 48 h) ($p<0.001$, Fig. 10A). The cytotoxicity assay suggested that 8-HOA could significantly promote the release of LDH from the cytoplasm to

extracellular space (p<0.001, Fig. 10B), indicating that the cell membrane was broken by 8-HOA. Therefore, 8-HOA may serve as a broad-spectrum cytotoxic reagent for both lung cancer and lung epithelial cells, implicating the importance of developing the treatment to specifically promote 8-HOA generation within lung cancer cells.

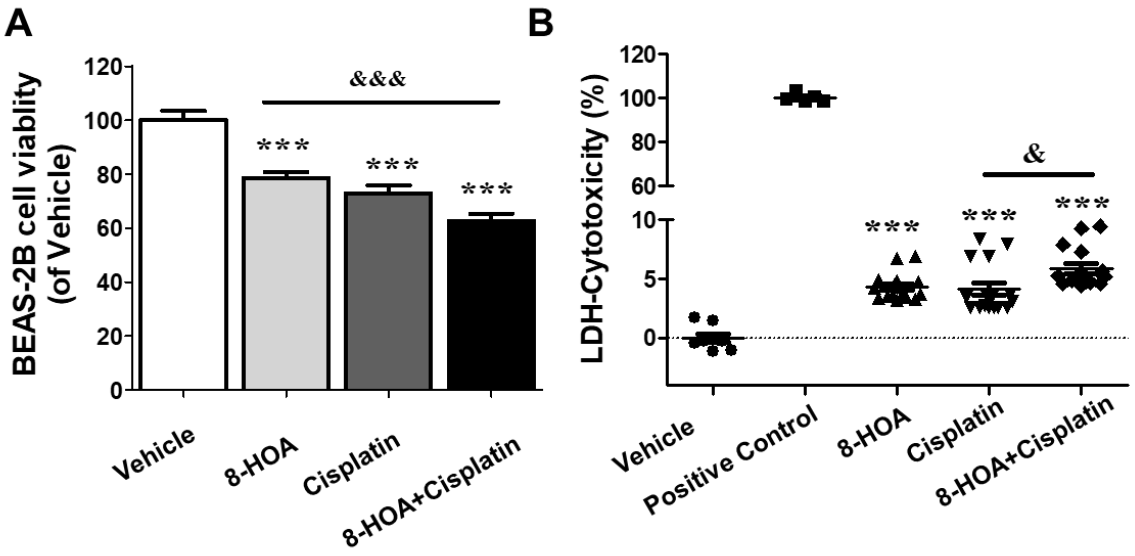

Figure 10. 8-HOA inhibited the growth of BEAS-2B normal lung epithelial cells. (A) The cell viability of BEAS-2B cells was normalized by vehicle group. BEAS-2B cells were treated with 1 μM 8-HOA and/or 1.5 μM cisplatin for 48 h. n=6 (B) Lactate dehydrogenase (LDH) cytotoxicity of BEAS-2B cells treated with 1 μM 8-HOA and/or 1.5 μM cisplatin. Data represent mean ± SEM for n=12. $^{***}P$<0.001 *vs* Vehicle group; $^{\&\&\&}P$<0.001, $^{\&}P$<0.05 *vs* 8-HOA+ Cisplatin group.

3.6. Conclusion and Discussion

In our previous studies, we have identified 8-HOA as a distinct anti-cancer free radical byproduct from COX-2 catalyzed DGLA peroxidation [76,77]. The exogenous 8-HOA could inhibit the growth of colon and pancreatic cancer via regulating proliferation, migration, cell cycle, invasion, and apoptosis [11,13]. Although lung cancer cells (especially NSCLC) are highly expressing COX-2 [73], we are still unclear whether 8-HOA could suppress lung cancer cells. We investigated the effect of exogenous 8-HOA on lung cancer cells by assessing various aspects of tumorigenesis, including proliferation, migration, apoptosis, survival in A549 and H1299 lung

cancer cells. Moreover, the effect of 8-HOA on normal lung epithelial cells also have been examined.

COX-2 is a bi-functional (cyclooxygenase activity and peroxidase activity) membrane-bound enzyme [108]. In the traditional concept, COX-2 is the key enzyme to catalyze AA to form downstream PGs, including PGE_2 [109]. The AA/PGE_2 axis has been widely studied in cancer and many metabolic diseases [110,111]. PGE_2 triggers proliferation, invasion, EMT, stemness, and angiogenesis through an autocrine and paracrine effect. Additionally, PGE_2 plays a key role in TME, resulting in immunosuppression [52]. On a positive note, however, we have found that COX-2 also could catalyze DGLA to produce 8-HOA for cancer inhibition [13,77]. We investigated the effect and molecular mechanisms of 8-HOA on lung cancer, which is also overexpressing COX-2 [73]. The proliferation and survival of A549 and H1299 lung cancer cells were suppressed by 8-HOA. While the apoptosis was activated by 8-HOA in lung cancer cells. Moreover, we have examined the interrelationship between 8-HOA and cisplatin in lung cancer cells by using two different mathematical models, the “one-belt, one-line” model and HAS model. Both models could help us to determine the synergistic, antagonistic, and additive effects of the combination of 8-HOA and cisplatin. The judgment criteria of the “one-belt, one-line” model are, $CI_{d1}>1$ and $CI_{d2}>1$ synergy, $CI_{d1}\leq 1\leq CI_{d2}$ addition, $CI_{d1}<1$ and $CI_{d2}<1$ antagonism [100]. In this model, we observed that all CIds of 8-HOA and cisplatin on survival fraction were higher than 1, implicating that the observed efficacy of 8-HOA+ cisplatin is greater than the value domain range of the expected effect of 8-HOA plus the expected effect of cisplatin. Another model we used to evaluate the synergy effect is HAS model. The synergy score was generated under the Combenefit platform. The judgment criteria of the HSA model are, score>10 synergy, 0≤score≤10 addition, score<0 antagonism [112]. In HAS model, the additional effect of 8-HOA and cisplatin is over the

higher single drug, either 8-HOA or cisplatin, on the cell viability of A549 cells. Given the fact that cisplatin is a DNA damage reagent [113], 8-HOA may also suppress lung cancer by affecting gene transcription and translation. Indeed, we observed that 8-HOA could inhibit HDAC activity in lung cancer cells. HDAC is the key enzyme to remove the acetyl group from histone, resulting in a tighter structure of histone and preventing the DNA transcription [114]. HDAC could promote cancer cell proliferation by inhibiting tumor suppressor gene activity [115,116]. Moreover, cancer cells with high HDAC activity appear less chance of apoptosis [117]. Therefore, it is plausible that the synergy effect between 8-HOA and cisplatin on lung cancer is contributed by their co-effect on gene transcription. Apoptosis is one of the most significant changes in cells after treatment of DNA damage reagents [118]. The pSIVA probe allowed us to monitor the apoptosis of lung cancer cells in real-time [119,120]. Interestingly, most of the apoptotic A549 cells occurred during 24 h to 48 h of the post-treatment period, indicating that 8-HOA may induce apoptosis via regulating other signaling pathways during the first 24 h. This phenomenon is consistent with our observation, in which 8-HOA suppressed the YAP1 and TAZ protein expression at 6 h and 12 h. Since YAP1/TAZ is overexpressed in lung cancer and suppresses apoptosis, the activation of apoptosis may be caused by the 8-HOA induced down-regulation of the YAP1/TAZ pathway in lung cancer cells.

We demonstrated that exogenous 8-HOA could inhibit lung cancer cell growth. To further improve the effectiveness of 8-HOA, instead of using exogenous 8-HOA, we would induce DGLA-derived endogenous 8-HOA in lung cancer cells. Indeed, we observed that exogenous 8-HOA only resulted in about a 20% reduction of cell viability and survival fraction in A549 cells, possibly due to exogenous 8-HOA is not in free radical form. Although the existence of free radical form 8-HOA is instantaneous, endogenous 8-HOA may damage cancer cells more effectively than

exogenous 8-HOA ($C_8H_{16}O_3$). Therefore, we would investigate the role of endogenous 8-HOA in lung cancer cells via redirecting the DGLA peroxidation pattern by D5D knockdown as demonstrating in the next chapter.

4. INHIBITION OF LUNG CANCER CELL GROWTH VIA PROMOTING THE FORMATION OF 8-HOA VIA COX-2-CATALYZED DGLA PEROXIDATION BY KNOCKING DOWN D5D EXPRESSION

In cellular condition, DGLA could be catalyzed by D5D to produce AA, which is the precursor of PGE_2, resulting in cancer progression [21]. However, under D5D inhibition, we have previously identified that 8-HOA is the distinct byproduct of COX-2-catalyzed DGLA peroxidation [77,80,93]. 8-HOA suppresses the development of colon and pancreatic cancers [80,92,93]. Analogously, we also observed that exogenous 8-HOA suppressed lung cancer cell growth via regulating proliferation, migration, and apoptosis. However, as we discussed in chapter 3, DGLA-derived endogenous 8-HOA may be more effective in lung cancer therapy, since endogenous 8-HOA is in free radical form upon producing from DGLA [76,77]. To promote the generation of endogenous 8-HOA, we would inhibit the expression or activity of D5D in lung cancer cells. We hypothesis that suppression of D5D could redirect COX-2 catalyzed DGLA peroxidation, rebalancing the AA and 8-HOA levels in cancer cells. By using D5D siRNA transfection, we investigated the effect of DGLA-derived endogenous 8-HOA on lung cancer cells.

RNAi (miRNA and siRNA) is one of the most remarkable technological breakthroughs in modern biology, allowing us to knock down specific genes in the mammalian system directly by taking advantage of natural machinery in the cell [121]. Inhibitory antisense oligonucleotides (ASOs), microRNA (miRNA), and siRNA are the major categories of gene therapy for triggering gene inhibition [122]. Compared to ASOs and miRNA, siRNA could silence genes more efficiently and specifically [123]. Since the discovery of siRNA in plants and *Caenorhabditis elegans*, it has been given high expectations on pharmaceutical usage [124]. The function of siRNA is depending on the Watson-Crick base pairing with the corresponding miRNA [123]. On

the contrary, the traditional small molecule or peptide drugs need to bind to a certain protein in a distinct spatial conformation. Therefore, the precise crystal structure of D5D is essential for developing small molecule or peptide D5D inhibitors. Unfortunately, we have not yet obtained the precise crystal structure of D5D and still ongoing reserach. Additionally, it is still a challenge to synthesize or isolate the D5D enzyme with high purity and activity, which is indispensable for studying enzyme kinetics. While RNAi technology can be employed to study the function of a certain protein without the knowledge of the accurate structure of this protein [125]. Moreover, siRNA knocking down can silence any gene in a shorter span [19]. Thus, knocking down D5D by RNAi technology may be an accessible and robust strategy for investigating the role of D5D in COX-2 catalyzed DGLA peroxidation in lung cancer cells.

The siRNA is a typical double-strand short RNA sequence, which is consisting of ~21 nucleotides [122]. The siRNA contains a sense strand, which is an mRNA sequence, and an antisense strand, which is the complement of mRNA [126]. The first step of RNAi is cleaving and processing the double-strand RNA to siRNA by Dicer, which is the RNase III-like enzyme. The RNA-induced silencing component (RISC) could be assembled by conjugating one strand of siRNA. RISC further binds to mRNA under the guidance of antisense siRNA sequence, resulting in the cleavage of mRNA. The degradation of mRNA ultimately leads to the stop of corresponding protein production [122,124,127].

In our previous studies, we have successfully knocked down D5D expression in several cancer cell linesby RNAi technology [12,16]. D5D controls the rate-limiting step during ω-6 metabolism. It efficiently converts DGLA to AA in cells, thereby restricting DGLA's growth inhibitory effects. We have observed that knocking down D5D (via siRNA transfection) in colon cancer cells (HCA-7 and HT-29) and pancreatic cancer cells (BxPC-3) resulted in the

accumulation of 8-HOA, which elicited DGLA's growth inhibitory effects [10,11,15,81]. Not only promoting the formation of 8-HOA, but the D5D inhibition can also limit the production of AA and the downstream cancer inducer PGE_2. By the D5D inhibition, the DGLA supplementation (precursor of 8-HOA) and COX-2 overexpression in cancer (enzyme to produce 8-HOA) is likely to trigger the cancer self-destruction [10,11,13,15]. However, it is still unclear whether the D5D knocking down can promote the 8-HOA formation in lung cancer. Additionally, the role of DGLA-derived 8-HOA in lung cancer cells is still underexplored, especially in the condition of D5D inhibition.

4.1. Inhibition D5D Redirected COX-2 Catalyzed DGLA Peroxidation Pattern in Lung Cancer Cells

To promote the DGLA-derived endogenous 8-HOA production, we used D5D siRNA to transfect A549 lung cancer cells. In our previous studies, we have investigated the effect of D5D siRNA transfection on colon and pancreatic cancer cells [11,81]. However, the effect of D5D siRNA transfection on lung cancer cells is still unknown. To suppress D5D expression, we transfected A549 lung cancer cells with D5D siRNA for 6 h with lipofectamine. A549 cells were incubated in the fresh DMEM medium for another 12, 24, or 48 h. The vehicle group was treated with negative control siRNA (*NC-si*) without D5D inhibition capability. At each time point, cells were collected for analyzing D5D expression by using Western blot. We observed that the protein expression of D5D was significantly decreased after 12 h ($p<0.05$), 24 h ($p<0.01$), or 48 h ($p<0.01$) of D5D siRNA transfection in a time-dependent manner (Fig. 11).

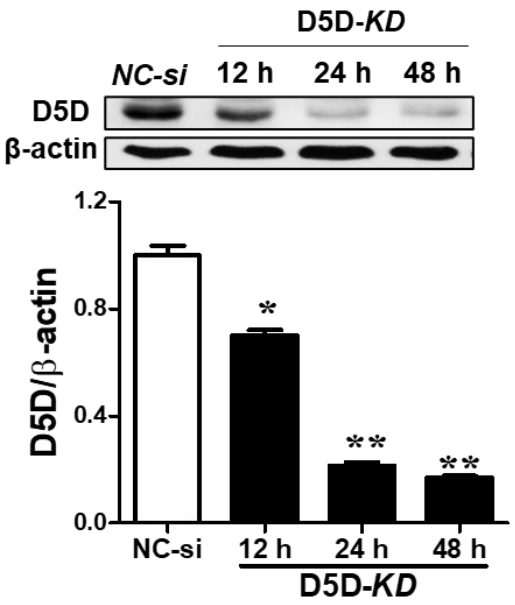

Figure 11. D5D siRNA transfection suppressed the protein expression of D5D in A549 lung cancer cells. A549 cells were treated with D5D siRNA (D5D-*KD*) or negative control siRNA (*NC-si*) for 6 h. The D5D protein expression in A549 cells was measured after 12, 24, and 48 h of transfection. Relative protein expressions were normalized with β-actin. Data represent mean ± SEM for n=3. $^{**}P<0.01$, $^{*}P<0.05$ *vs NC-si* group.

To evaluate the role of D5D inhibition in the COX-2 catalyzed DGLA peroxidation pattern, we further quantified the concentration of two substrates of COX-2, DGLA and AA, in A549 cells after siRNA transfection. By LC-MS analysis, we found that the ratio of DGLA to AA in A549 cells did not significantly change after D5D siRNA transfection ($p>0.05$, Fig. 12A), indicating that DGLA peroxidation could remain stable in the first 12 h of D5D siRNA transfection. However, a significant increase of DGLA to AA ratio was observed in A549 cells after 24 h and 48 h D5D siRNA transfection ($p<0.05$, Fig. 12A), suggesting that D5D siRNA could trigger A549 cells to generate more DGLA and less AA at 24 and 48 h. The change of the DGLA/AA ratio is also consistent with the decrease of D5D protein expression that we have observed in Figure 11. To assess the free radical byproduct of DGLA, we measured the 8-HOA level in A549 cells transfected with *NC-si* or D5D siRNA along with 100 μM DGLA supplementation. The GC-MS

results suggested that the 8-HOA level was significantly improved from ~0.1 μM/1*10^6 cells to more than 0.6 μM/1*10^6 cells (p<0.01, Fig. 12B), indicating that the 8-HOA generation could be triggered by D5D siRNA transfection.

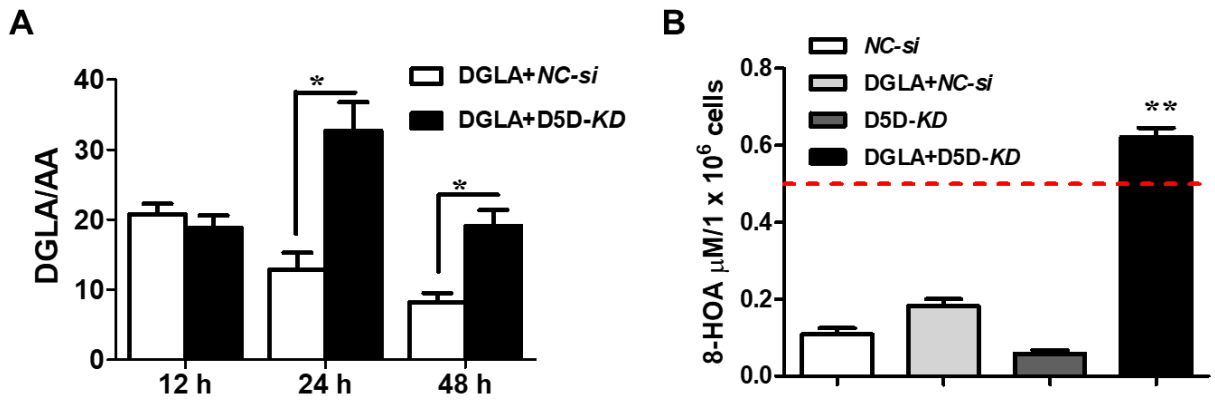

Figure 12. D5D siRNA transfection redirected the DGLA peroxidation pattern of A549 lung cancer cells. (A) The DGLA to AA ratio in lung cancer cells. The DGLA and AA concentration was measured by LC/MS after 12, 24, and 48 h treatment. (B) GC/MS quantification of 8-HOA from cell medium containing 1.0 × 10^6 D5D siRNA transfected A549 cells or *NC-si* transfected cells after 100 μM DGLA treatment for 48 h. The dash line indicated the desirable threshold of 8-HOA for displaying the anti-cancer effect. Data represent mean ± SEM for n=3. $^{**}P$<0.01, $^{*}P$<0.05 *vs* DGLA+ D5D-*KD* group.

4.2. D5D siRNA Transfection Suppressed the Survival and Migration of A549 Lung Cancer Cells

We have previously found that 0.5 μM is the *in vitro* threshold of endogenous 8-HOA for displaying inhibitory effect on colon and pancreatic cancer cells [11,80]. Because the combination of DGLA and D5D siRNA promoted the generation of ~0.6 μM of 8-HOA, we hypothesis that D5D siRNA transfection is also effective enough to inhibit lung cancer cell growth via inducing 8-HOA production from DGLA. To evaluate the growth of A549 lung cancer cells, we performed the colony formation assay on A549 cells to assess the survival fraction. We observed that D5D siRNA alone or the combination of D5D siRNA and DGLA could significantly reduce the survival fraction of A549 cells (p<0.05, Fig. 13), indicating that the lung cancer cells growth was

suppressed by D5D siRNA. Additionally, we observed that A549 cells treated with the combination of D5D siRNA and DGLA have a significantly lower survival fraction (~6%) than cells treated with D5D siRNA alone (~23%) (p<0.05, Fig. 13).

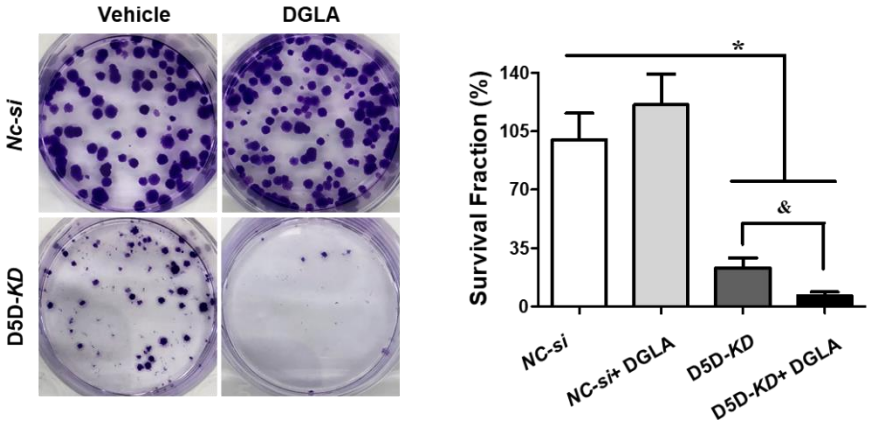

Figure 13. D5D siRNA transfection suppressed the growth of A549 lung cancer cells. Colony formation of A549 lung cancer cells treated with DGLA (100 μM) +*NC-si* or D5D siRNA. The survival fraction (%) of A549 cells was normalized by vehicle group. Data represent mean ± SEM for n=3. $^{*}P$<0.05 *vs NC-si* group; $^{\&}P$<0.05 *vs* D5D-*KD*+ DGLA group.

To investigate the effect of D5D inhibition on lung cancer cell migration, we measured the relative migration rate and wound healing rate of A549 lung cancer cells by transwell migration assay and wound healing assay, respectively. In the transwell migration assay, we observed that the relative migration rate was significantly suppressed in the group where A549 cells were treated with the combination of D5D siRNA and DGLA supplementation (p<0.001, Fig. 14). The migration rate of this group (~9.1%) is even significantly lower than cells treated with the DGLA alone (~77%) (p<0.01, Fig. 14). Moreover, the cancer cell migration was monitored by wound healing assay during 48 h of DGLA treatment. We found that the *NC-si* transfected A549 cells have a faster wound healing rate than other groups. This smaller wound area of the *NC-si* group at 48 h implicated the high migration ability of A549 lung cancer cells without treatment. However, larger wounds have been observed in cells treated with the combination of DGLA and D5D siRNA

after 24 and 48 h (Fig. 15). The wound healing rate of cells transfected with *NC-si* versus the combination of DGLA and D5D siRNA was ~78.5 to ~100.8% at 24 h and ~69.1 to ~98.9% at 48 h (p<0.05, Fig. 15), suggesting that D5D knockdown could trigger the effect of DGLA on suppressing lung cancer cells migration.

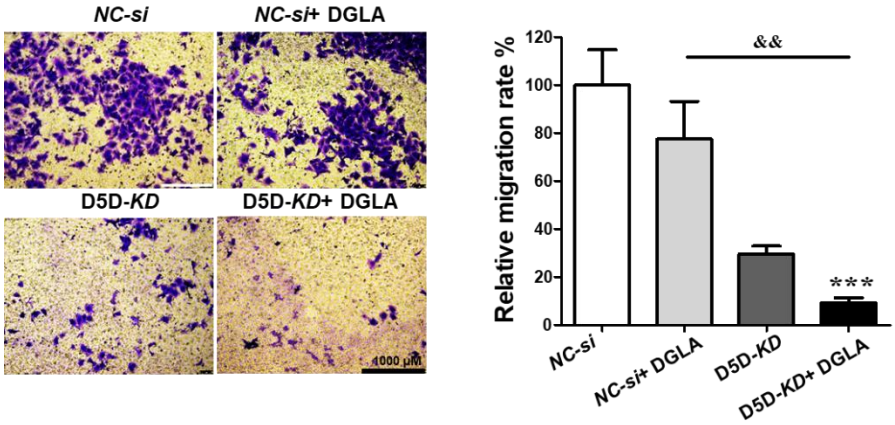

Figure 14. D5D siRNA transfection suppressed the migration rate of A549 lung cancer cells. Transwell migration assay of A549 lung cancer cells treated with DGLA (100 μM) + *NC-si* or D5D siRNA. The relative migration rate (%) of A549 cells was normalized by the *NC-si* group. Data represent mean ± SEM for n=3. $^{***}P$<0.001 *vs NC-si* group; $^{\&\&}P$<0.01 *vs* D5D-*KD*+ DGLA group.

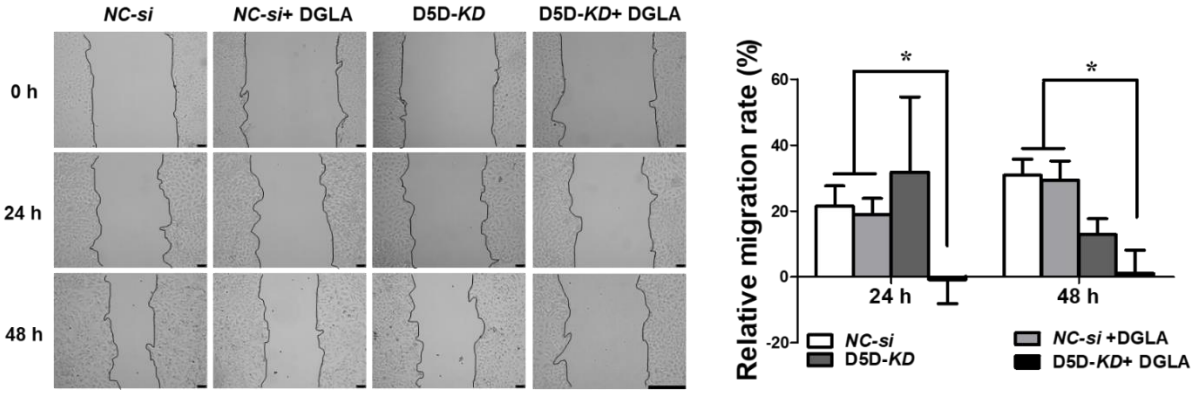

Figure 15. D5D siRNA transfection suppressed the migration of A549 lung cancer cells. Wound healing assay of A549 lung cancer cells treated with DGLA (100 μM) + *NC-si* or D5D siRNA. The relative migration rate (%) of A549 cells was normalized by the *NC-si* group. Data represent mean ± SEM for n=3. $^{*}P$<0.05 *vs* D5D-*KD*+ DGLA group.

4.3. D5D siRNA Transfection Induced Apoptosis in Lung Cancer Cells

We have demonstrated in previous studies and chapter 3 that exogenous 8-HOA could trigger apoptosis in the colon [81], pancreatic [11], and lung cancer cells. Given the fact that 8-HOA could be produced from DGLA in D5D knocked down lung cancer cells, we hypothesize that the endogenous 8-HOA, which is directly derived from DGLA, also could activate apoptosis in lung cancer cells. To evaluate the apoptosis level, we quantified the percentage of the positive apoptotic A549 lung cancer cells via flow cytometry with Annexin V-FITC/PI double staining. A549 cells were transfected with D5D siRNA and administrated with DGLA for 48 h before subjecting to flow cytometry analysis. We observed that the percentage of apoptotic A549 cells significantly increased from 7.5% to more than 14.9% by the treatment of D5D siRNA transfection and DGLA supplementation (p<0.01, Fig. 16), suggesting that inhibition of D5D could elicit the effect of DGLA on inducing apoptosis.

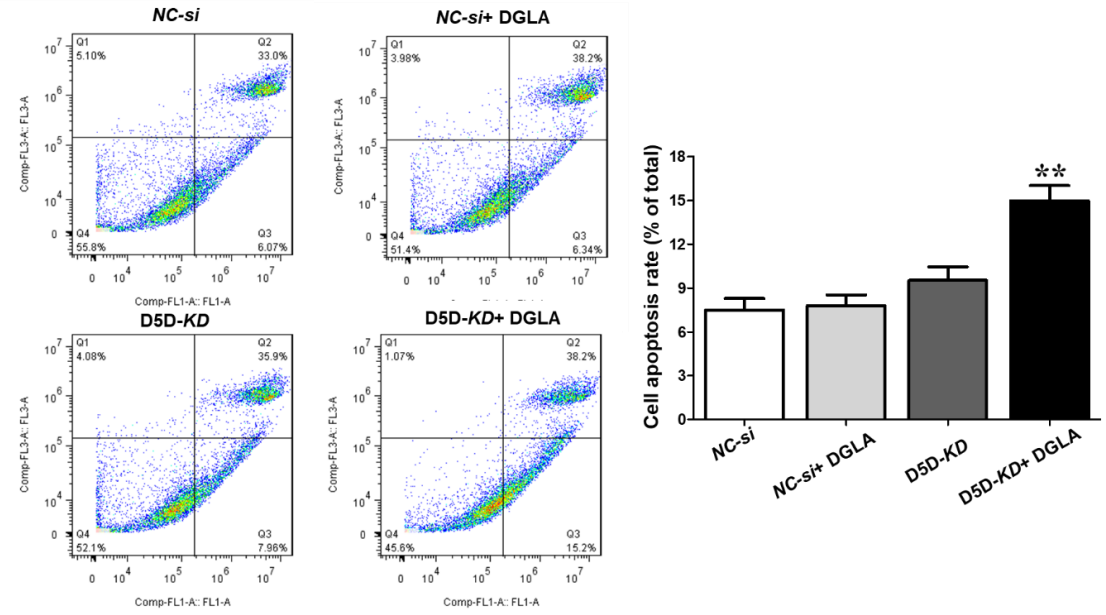

Figure 16. D5D siRNA transfection induced the apoptosis of A549 lung cancer cells. Apoptosis was determined by flow cytometry on A549 cells in staining of Annexin V-FITC/PI. A549 lung cancer cells were treated with DGLA (100 μM) + *NC-si* or D5D siRNA. Cell apoptosis rate (%) of A549 cells was determined by analyzing the percentage of Q3 gated cells. Data represent mean ± SEM for n=3. $^{**}P$<0.01 *vs NC-si* group.

Since 8-HOA generation is catalyzed by COX-2, maintaining the high COX-2 expression level in lung cancer cells may be essential to maximize 8-HOA production. To ensure the overexpression of COX-2 in lung cancer cells, we measured the protein expression of COX-2 in A549 cells treated with D5D siRNA and /or DGLA. Interestingly, the high COX-2 expression cannot be changed by either DGLA or D5D siRNA ($p>0.05$, Fig. 17A). This stable COX-2 expression in A549 cells allowed the continuous 8-HOA production from DGLA peroxidation after D5D knockdown. The production of endogenous 8-HOA could further promote apoptosis in lung cancer cells. Indeed, the pre-apoptosis protein BAX expression was significantly increased in A549 cells treated with the combination of DGLA and D5D siRNA ($p<0.001$, Fig. 17A). To investigate the molecular mechanism of D5D inhibition triggered apoptosis, we tested the protein expression of p53, procaspase-9, and procaspase-3 in A549 lung cancer cells by Western analysis. We found that the protein expression of p53 was significantly improved by DGLA and D5D siRNA transfection in A549 cells ($p<0.01$, Fig. 17B). However, the protein expression of procaspase-3 ($p<0.01$) and procaspase-9 ($p<0.05$) was significantly decreased in D5D siRNA transfected A549 cells with DGLA supplementation (Fig. 17B). We may conclude that D5D suppression could induce p53 dependent intrinsic apoptosis pathway through redirecting COX-2 catalyzed DGLA peroxidation.

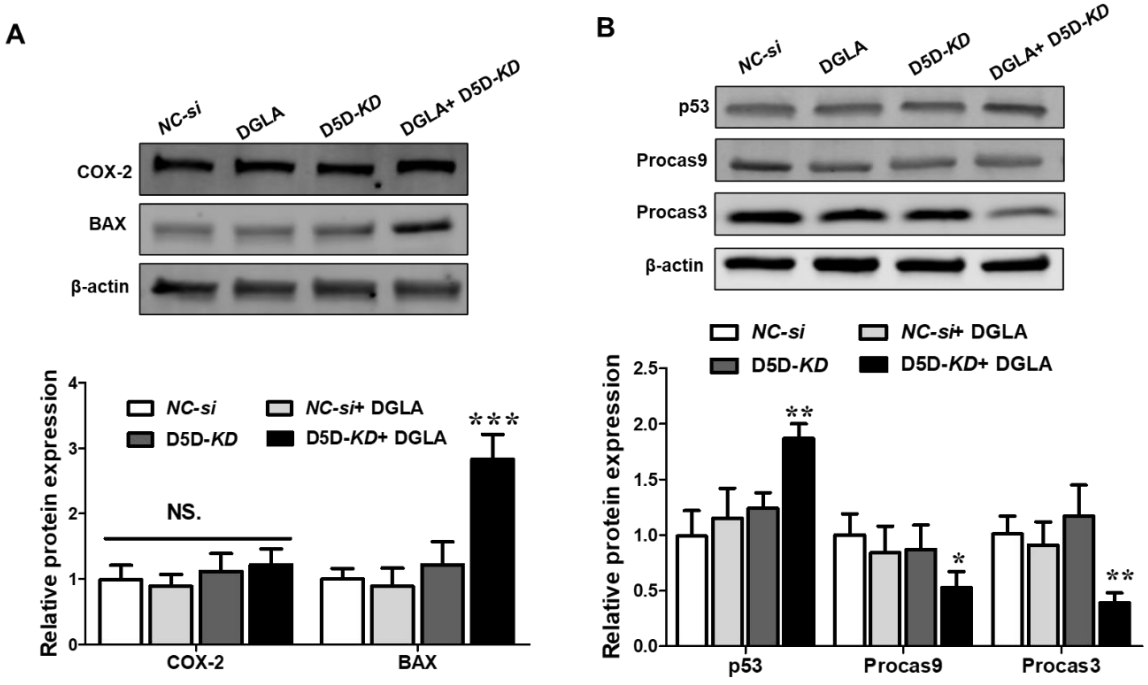

Figure 17. D5D siRNA transfection activated p53 dependent apoptosis in A549 lung cancer cells. A549 cells were transfected with D5D siRNA (D5D-*KD*) or negative control siRNA (*NC-si*) for 6 h. A549 cells were treated with DGLA (100 μM) for 48 h before Western analysis. (A) COX-2 and BAX protein expression was measured after 48 h of DGLA supplementation. (B) p53, procaspase-9 (Procas9), and procaspase-3 (Procas3) protein expression was measured after 48 h of DGLA supplementation. The protein expression was normalized with β-actin. Data represent mean ± SEM for n=3. $^{***}P<0.001$, $^{**}P<0.01$, $^{*}P<0.05$ *vs NC-si* group. NS. not significant.

4.4. DGLA Supplementation and D5D Inhibition Suppressed HDAC Activity and the YAP1/TAZ Pathway

Given that 8-HOA is a potential HDAC inhibitor, it is plausible that D5D inhibition also could suppress HDAC activity and the YAP1/TAZ pathway in lung cancer cells. To investigate the effect of D5D siRNA transfection on HDAC activity, we assessed the HDAC activity in A549 lung cancer cells transfected with D5D siRNA with or without DGLA supplementation by measuring the protein expression of the substrate of HDAC, acetyl-histone H3K9 (AcH3K9). The HDAC could remove the acetyl group from AcH3K9 [128]. Thus, the high protein expression of AcH3K9 is an indicator of low cellular HDAC activity. We observed that the protein expression

of AcH3K9 was significantly increased in the A549 cells treated with D5D siRNA and DGLA (p<0.01, Fig. 18), implicating a decrease in HDAC activity. This phenomenon is consistent with the effect of exogenous 8-HOA on HDAC as we demonstrated in chapter 3. Therefore, the inhibition of HDAC activity in D5D knocked down lung cancer cells may be attributed to the generation of endogenous 8-HOA from COX-2 catalyzed DGLA peroxidation. However, we did not observe any significant change in the protein expression of total Histone H3 in lung cancer cells by DGLA or D5D siRNA treatment (Fig. 18). Thus, the D5D inhibition may only inhibit the HDAC activity, not overall histone protein expression in lung cancer cells.

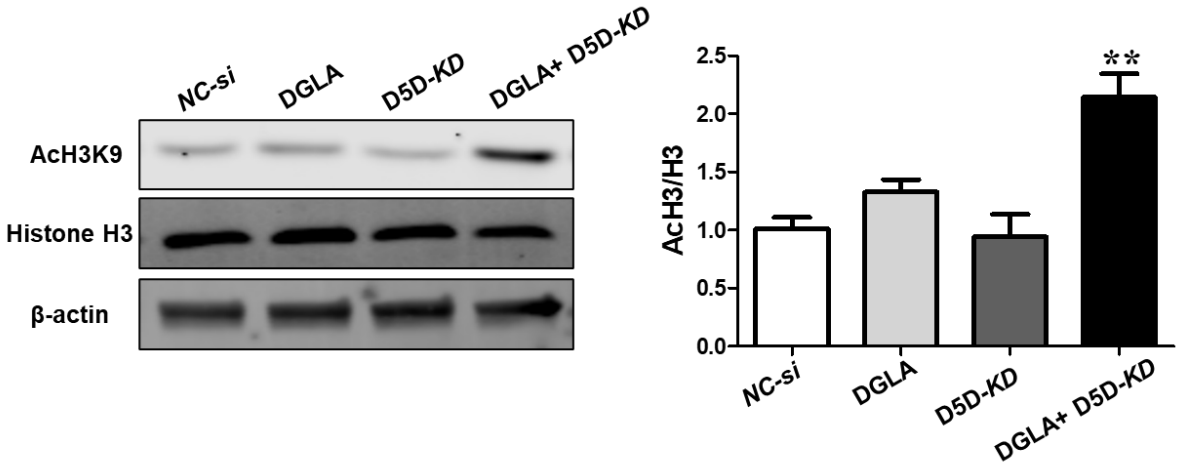

Figure 18. D5D siRNA transfection suppressed HDAC activity in A549 lung cancer cells. A549 cells were treated with D5D siRNA (D5D-*KD*) or negative control siRNA (*NC-si*) for 6 h. The acetyl-Histone H3 (AcH3K9) and Histone H3 protein expression were measured after 48 h of DGLA supplementation. The protein expression of AcH3K9 and Histone H3 were normalized with β-actin. The ratio of AcH3 to H3 was normalized with the *NC-si* group. Data represent mean ± SEM for n=3. $^{**}P$<0.01 *vs NC-si* group.

We have observed that exogenous 8-HOA could inhibit the YAP1/TAZ pathway in lung cancer cells as demonstrated in chapter 3. However, the effect of DGLA-derived endogenous 8-HOA on the YAP1/TAZ pathway is still unknown. To further explore the role of D5D in the YAP1/TAZ pathway, we measured the protein expression of YAP1, TAZ, and CTGF in A549 cells transfected with D5D siRNA and DGLA supplementation by Western analysis. We found

that the combination of DGLA and D5D siRNA could significantly inhibit YAP1 (p<0.01), TAZ (p<0.05), and CTGF (p<0.01) protein expression in A549 lung cancer cells (Fig. 19), indicating that DGLA-derived 8-HOA also could suppress the YAP1/TAZ pathway.

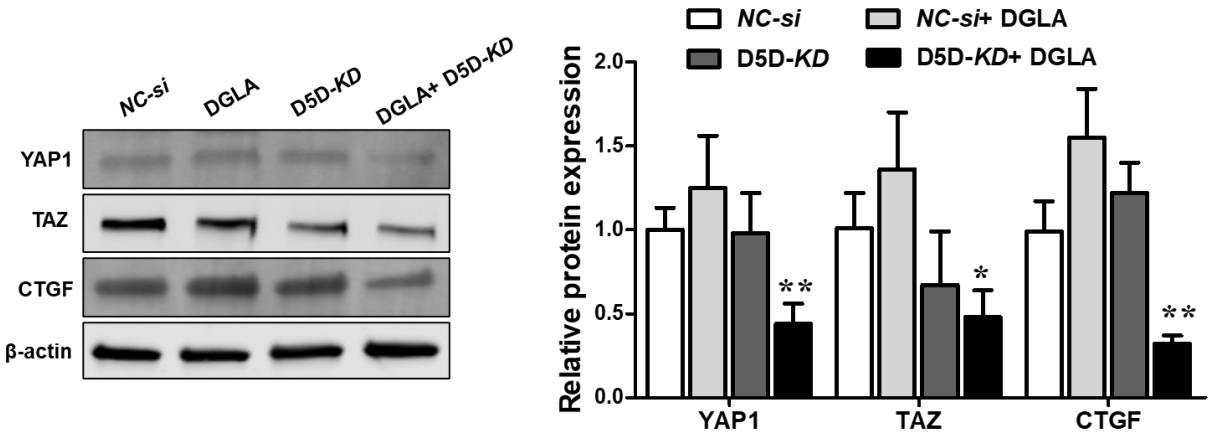

Figure 19. D5D siRNA transfection suppressed YAP1/TAZ pathway in A549 lung cancer cells. A549 cells were treated with D5D siRNA (D5D-*KD*) or negative control siRNA (*NC-si*) for 6 h. YAP1, TAZ, and CTGF protein expressions were measured after 48 h of DGLA supplementation. The protein expression was normalized with β-actin. Data represent mean ± SEM for n=3. $^{**}P$<0.01, $^{*}P$<0.05 *vs NC-si* group.

4.5. Conclusion and Discussion

We have demonstrated in chapter 3 that exogenous 8-HOA could inhibit lung cancer cell proliferation, survival, migration, and induce apoptosis. However, the effect of exogenous 8-HOA on lung cancer cells is modest. Theoretically, the endogenous 8-HOA is derived from DGLA as a free radical form, $^{\bullet}C_8H_{15}O_3$, which may have better efficacy on cancer inhibition than exogenous 8-HOA, $C_8H_{16}O_3$ [76,77]. To improve the effectiveness of the 8-HOA, we knocked down D5D in A549 lung cancer cells by siRNA transfection to promote the generation of DGLA-derived endogenous 8-HOA ($^{\bullet}C_8H_{15}O_3$). The siRNA treatment belongs to gene therapy, which is a developing platform for targeting many diseases in a gene-specific manner. Other molecules used for gene therapy include miRNA and ASOs. The siRNA silencing technique could direct the

degradation of target mRNA in high specificity [122,123]. Few siRNA drugs have been approved by the United States Food and Drug Administration (FDA), such as GIVLAARI™ for acute hepatic porphyria and ONPATTRO® for hereditary amyloidogenic transthyretin [129–131].

We found that siRNA transfection could shift the COX-2 catalyzed DGLA peroxidation pattern in lung cancer cells, resulting in more production of 8-HOA. However, D5D siRNA transfection without DGLA supplementation cannot significantly promote 8-HOA generation, implicating that DGLA may serve as the essential substrate of COX-2 for synthesizing 8-HOA in cancer cells. Notably, we observed that D5D siRNA transfection alone could suppress the survival fraction and transwell migration rate of lung cancer cells. Therefore, we believe that inhibition of D5D could suppress lung cancer progression in multiple mechanisms. Indeed, another study has demonstrated that suppression of D5D expression could inhibit the migration, invasion, and proliferation of laryngeal squamous cell carcinoma cells. The overexpression of D5D in cancer cells is one of the factors for activating the AKT/mTOR pathway, which is a critical pathway in cancer development [28]. Although D5D knockdown inhibited survival and migration of lung cancer cells, we demonstrated that the effect of the combination of D5D siRNA and DGLA on lung cancer cells was better than D5D siRNA alone, indicating that 8-HOA is also a crucial downstream functional molecule of COX-2 catalyzed DGLA peroxidation. Additionally, D5D knockdown without DGLA did not induce apoptosis in lung cancer cells. However, the significant activation of apoptosis has been found in D5D silenced lung cancer cells when supplementation of DGLA. Therefore, the effect of D5D inhibition on apoptosis may primarily depend on the 8-HOA generation from COX-2 catalyzed DGLA peroxidation.

Despite the accessibility and high efficiency of D5D siRNA, the clinical application of therapeutic siRNA still faces many challenges [125]. The stability of unmodified siRNA is

generally lower than small molecule inhibitors or peptide drugs in the serum. The poor pharmacokinetic behavior of siRNA also weighs down the siRNA drug development. The off-target effect of siRNA may cause anticipated and unanticipated side effects by affecting the normal physiological function of the target gene [132]. Since siRNA needs to compete with other double-strand RNAs on the same RNA machinery, the siRNA may trigger the innate immune system by recognizing Toll-like receptors 3 and 7 (TLR3 and TLR7) and retinoic acid-inducible gene I protein (DDX58), leading to inflammation and secretion of interferon [133–135]. Additionally, naked siRNA is struggling to enter the cytoplasm because of the large size and negative charge of siRNA. After injection, most of the siRNA molecules could be eliminated by the kidney rather than staying in the target tissues and cells [136]. To ensure the efficiency of siRNA knockdown, researchers tend to administrate a high concentration of siRNA to animals or patients, raising more safety concerns [137]. It is important to develop an active and targeted delivery system for 1) protecting D5D siRNA from degradation by RNase, 2) concentrating siRNA in targeted cancer cells, 3) avoiding toxicity and off-target effect.

5. THERAPEUTIC OUTCOMES OF DGLA SUPPLEMENTATION AND 3WJ-RNA NANOPARTICLES ON LUNG CANCER

The advance of siRNA technology holds a great promise in cancer therapy since siRNA could be designed to specifically knockdown any targeted gene [123]. Although, we demonstrated that D5D siRNA efficiently suppressed the protein expression of D5D in lung cancer cells, it is still a challenge to directly apply naked siRNA to patients due to various disadvantages, such as off-target effect, poor pharmacokinetic profile, and low stability [125,137]. To expand the clinical benefit of the D5D inhibition-based strategy to cancer patients, we would take advantage of the RNA nanoparticle system to stabilize and deliver the D5D siRNA to the cancer cells. Therapeutically siRNA could be delivered by different methods, including lipid nanoparticles (LNPs), peptide-based system, polymers, RNA nanoparticles, and N-Acetylgalactosamine (GalNAc) conjugates, of which RNA nanoparticle is one of the state-of-the-art delivery systems for siRNA therapy [123,136].

RNA nanoparticles can be fabricated with a level of simplicity characteristic of DNA [138,139]. Additionally, RNA nanoparticles have versatile tertiary structures and catalytic functions that mimic proteins. The RNA molecule is unique in comparison to DNA molecule by its high thermodynamic stability and the capability of forming both canonical and noncanonical base pairings as well as base stacking. RNA tertiary motifs can be encoded at the level of the RNA sequence for 3D architectures that exhibit helices, loops, bulges, stems, hairpins, and pseudoknots. Single-stranded RNA loops are suitable for inter-/intra-molecular interactions and self-assembling RNA nanoparticles [140,141].

The feasibility of RNA nanotechnology in cancer therapy is exemplified by the bacteriophage phi29 pRNA system, which naturally forms dimers and hexamers *via* hand-in-hand

interactions between right- and left-interlocking loops [20,142,143]. The crystal structure of the pRNA-3-Way Junction (3WJ) motif held at the center of the pRNA monomer was recently reported, allowing the construction of ultra-stable and self-assembling nanoparticles with very high affinity [138,144]. The pRNA-3WJ is also thermodynamically stable. For instance, this RNA structure is resistant to denaturation *via* 8M urea [145]. Moreover, 3WJ RNA nanoparticles are less likely to be dissociated at ultra-low concentrations *in vitro* and *in vivo* [146]. Varieties of RNA nanoparticles using a pRNA-3WJ motif (3-WJ core for harboring functional therapeutic modules) as scaffolds have already been successfully constructed [94,142]. Importantly, all modules in the RNA nanoparticle could retain their original foldings and functionalities (*e.g.*, specific cell binding, cell entry, gene silencing, catalytic function, and cancer targeting) both *in vitro* and *in vivo* [146–151]. Besides, the 2'-F modified 3WJ nanoparticles display favorable pharmacological profiles of biodistribution and pharmacokinetics (*e.g.*, stability, half-life, and clearance rate), and also appropriate immune responses [141]. Various targeting modules have been tested successfully with the pRNA-3WJ nanoparticle to specifically target cancers [141,147,148,152,153]. In this study, to improve the efficiency and tumor selectivity of D5D siRNA, we added EpCAM aptamer to the 3WJ RNA nanoparticle as a targeting module for directing D5D siRNA to the lung cancer cells. Given the fact that EpCAM is overexpressing in lung cancer cells [154,155], by conjugating EpCAM aptamer to RNA nanoparticles, 3WJ-RNA nanoparticles with D5D siRNA may specifically bind and enter EpCAM- positive lung cancer cells.

5.1. Lung Cancer Cells Internalized 3WJ-EpCAM RNA Nanoparticle

To direct D5D siRNA to the lung cancer cells, we designed and synthesized the 3WJ-EpCAM-D5D siRNA nanoparticle as shown in Fig. 20A. This RNA nanoparticle was assembled with three RNA single strands, 3WJ-a, 3WJ-b, and 3WJ-c. The multi-function of 3WJ RNA

nanoparticles is attributed to three RNA arms, H1, H2, and H3. To construct all functional parts in one nanostructure, we designed the 3WJ RNA nanoparticle, in which H1 harbored the D5D siRNA as a therapeutic module; H2 harbored the Alexa 647 as an imaging module; H3 harbored the EpCAM aptamer as a targeting module. To test the binding efficiency of nanoparticles, we evaluated the intensity of Alexa 647 in A549 cells via flow cytometry analysis. A549 cells were treated with 3WJ-EpCAM-Alexa 647 RNA nanoparticles before analysis. We observed that 3WJ-EpCAM-Alexa 647 RNA nanoparticles could shift the population of A549 cells to the right (Fig. 20B), suggesting that A549 cells can efficiently recognize 3WJ-EpCAM RNA nanoparticles. However, binding does not guarantee nanoparticle uptake, which is the most crucial barrier of siRNA-based therapy. To investigate the internalization of RNA nanoparticles, we assessed the cellular distribution of 3WJ-EpCAM-Alexa 647 RNA nanoparticles in A549 lung cancer cells by confocal microscope. Since RNA nanoparticles conjugated with Alexa 647, we can monitor the distribution of 3WJ RNA nanoparticles without other antibodies. After 4 h of incubation of RNA nanoparticles, we found a substantial amount of 3WJ RNA nanoparticles in the cytoplasm of A549 cells (Fig. 21), indicating that 3WJ-EpCAM RNA nanoparticles could efficiently pass through the cell membrane of lung cancer cells.

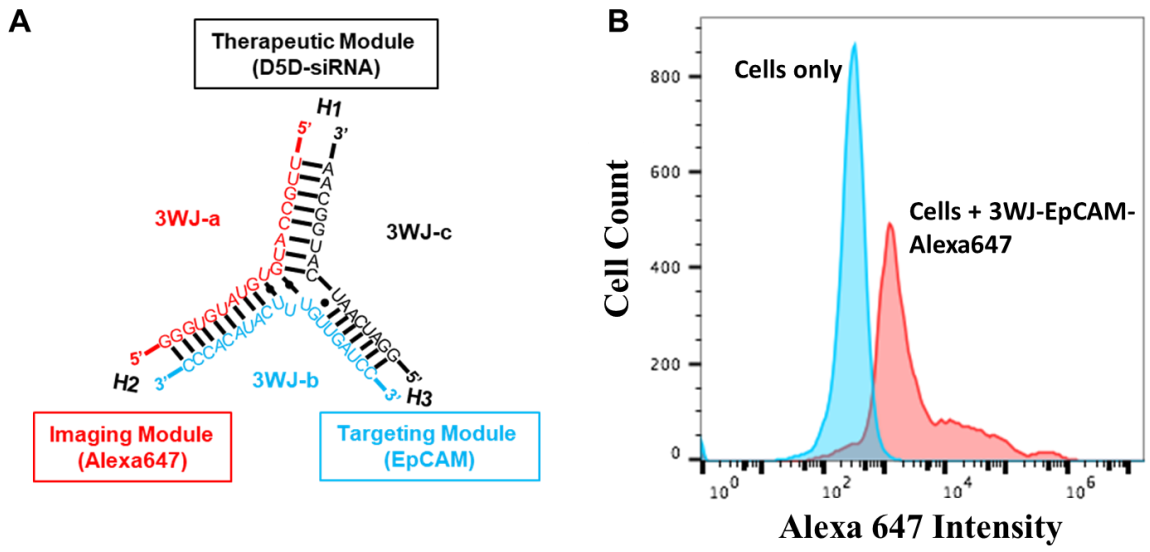

Figure 20. Structure of 3-way junction (3WJ)-epithelial cell adhesion molecule (EpCAM)-RNA nanoparticle. (A) Schematic presentation of the 3WJ-RNA nanoparticle structure. (B) Flow cytometry for RNA nanoparticle binding in A549 lung cancer cells. Red: A549 cells treated with 3WJ-EpCAM-Alexa 647; Blue: A549 cells treated with PBS. The Alexa 647 intensity was measured by the flow cytometer (n=6).

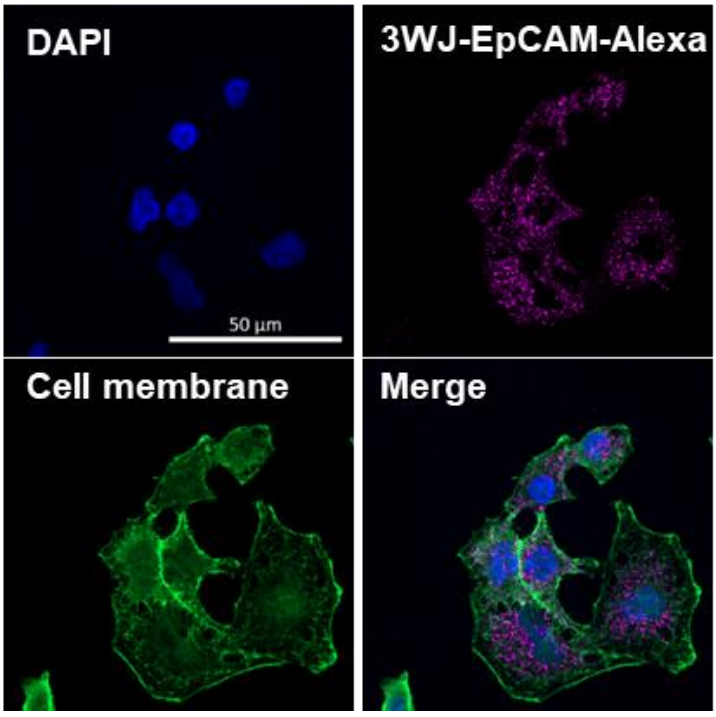

Figure 21. Distribution of 3WJ RNA nanoparticles (violet) in A549 cells via confocal microscope (n=6). F-actin was labeled with phalloidin (Alexa 488, green) and cell nuclei with DAPI.

5.2. 3WJ-EpCAM-D5D siRNA Nanoparticle Suppressed the D5D Expression in Lung Cancer Cells

To evaluate the *in vitro* effect of the 3WJ-EpCAM-D5D siRNA nanoparticle on lung cancer, we measured the protein and gene expression of D5D in A549 lung cancer cells via Western analysis, immunofluorescence analysis, and qPCR. A549 lung cancer cells were treated with 3WJ-EpCAM-D5D siRNA nanoparticle or 3WJ-EpCAM RNA nanoparticle (as the vehicle) for 48 h. The expression of D5D in A549 cells was significantly decreased in the 3WJ-EpCAM-D5D siRNA nanoparticle group ($p<0.01$, Fig. 22A and B). We observed that the effect of 3WJ-EpCAM-D5D siRNA nanoparticles on D5D expression is similar to the effect of naked D5D siRNA on A549 cells (Fig. 22B), suggesting that the 3WJ RNA nanoparticle may not impede the knocking down the efficiency of D5D siRNA. On the contrary, the 3WJ-EpCAM RNA nanoparticle (without D5D siRNA) did not decrease the protein expression of D5D in lung cancer cells (Fig. 22B). Moreover, we found that 3WJ-EpCAM-D5D siRNA nanoparticles could significantly reduce the mRNA expression of *FADS1* (gene of D5D) in A549 lung cancer cells after 24 h of incubation ($p<0.05$, Fig. 22C). Thus, we believe that 3WJ-EpCAM-D5D siRNA nanoparticles may cause mRNA degradation of D5D, leading to suppression of D5D protein translation in lung cancer cells.

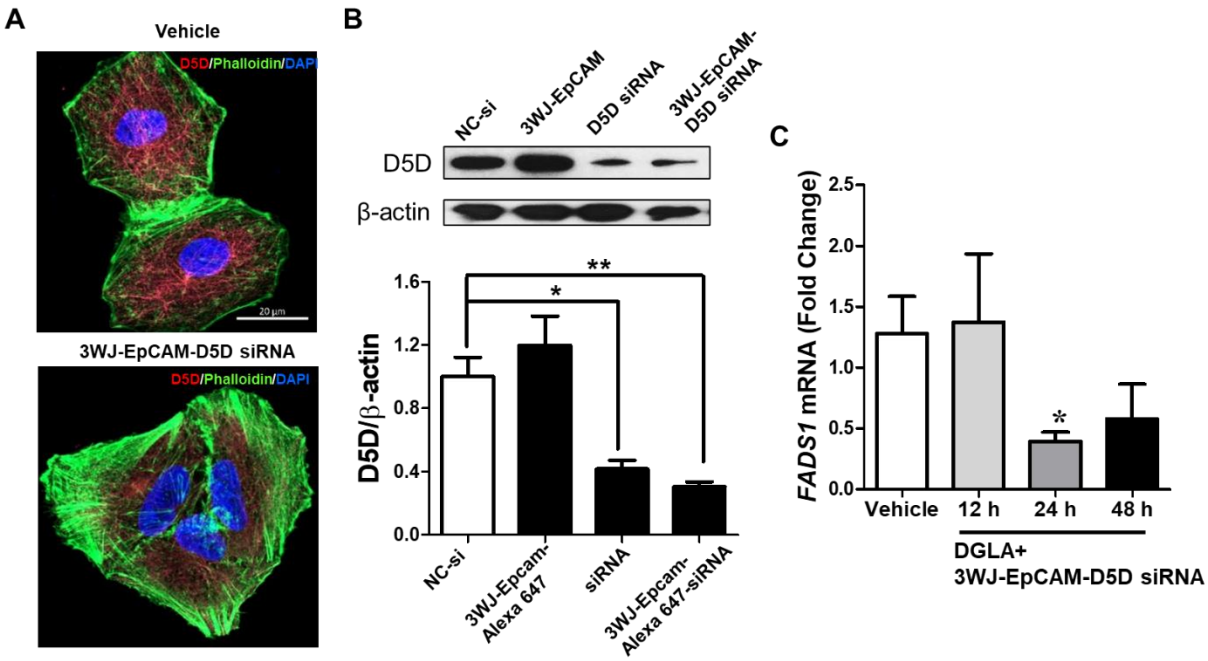

Figure 22. 3WJ-EpCAM-D5D siRNA nanoparticle suppressed the expression of D5D in A549 lung cancer cells. (A) D5D protein expression in A549 cells. Cells treated with 3WJ-EpCAM-D5D siRNA nanoparticle. Images were captured by the confocal microscope. (B) Relative protein expression of D5D in A549 cells treated with 3WJ-EpCAM-D5D siRNA nanoparticle. The relative expression of D5D to β-actin in the Vehicle group was normalized to 1. (C) D5D mRNA (*FADS1*) expression in A549 cells. Cells were treated with DGLA and 3WJ-EpCAM-D5D siRNA nanoparticle for different periods (12, 24, and 48 h). Data represent mean ± SEM for n=3. $^{**}P<0.01$, $^{*}P<0.05$ *vs NC-si* (B) or Vehicle group (A and C).

However, the role of 3WJ-EpCAM-D5D siRNA nanoparticles in 8-HOA production has not yet been analyzed. To understand how 3WJ-EpCAM-D5D siRNA nanoparticles regulate the COX-2-catalyzed DGLA peroxidation, we determined the 8-HOA concentration in A549 lung cancer cells treated with DGLA and/or 3WJ-EpCAM-D5D siRNA nanoparticle by GC-MS. We found that the 8-HOA level in cells treated with the combination of DGLA and 3WJ-EpCAM-D5D siRNA nanoparticles was significantly higher than other groups ($p<0.01$, Fig. 23), suggesting that 3WJ-EpCAM-D5D siRNA nanoparticle could shift the DGLA peroxidation pattern in lung cancer cells. Consequently, the accumulated DGLA could be converted to 8-HOA by COX-2 in lung cancer cells.

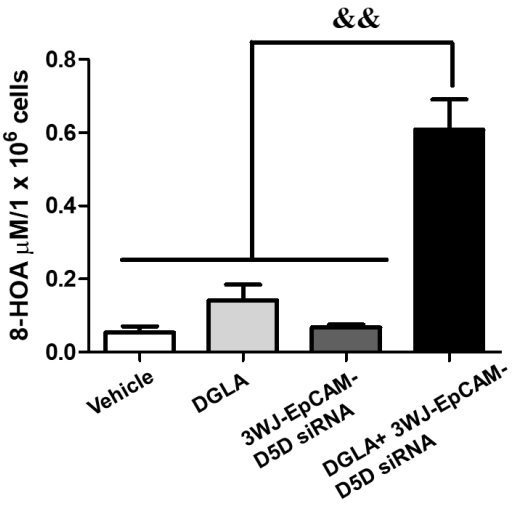

Figure 23. 8-HOA level in A549 cells was measured by GC-MS. A549 cells treated with DGLA and 3WJ-EpCAM-D5D siRNA nanoparticles. Data represent mean ± SEM for n=6. $^{\&\&}P<0.01$ *vs* DGLA+ 3WJ-EpCAM-D5D siRNA group.

5.3. 3WJ-EpCAM-D5D siRNA Nanoparticle Inhibited Proliferation of Lung Cancer Cells

To investigate the effect of the 3WJ-EpCAM-D5D siRNA nanoparticle on lung cancer, we evaluated the cell viability of A549 lung cancer cells by MTT assay. We observed that the combination of DGLA (100 μM) and 3WJ-EpCAM-D5D siRNA nanoparticle (100 and 1000 μM) could significantly decrease the cell viability of A549 cells ($p<0.01$, Fig. 24A). However, the inhibitory effect of DGLA or 3WJ-EpCAM-D5D siRNA nanoparticles alone on lung cancer is relatively less significant (Fig. 24A), implicating that the effect of 3WJ-EpCAM-D5D siRNA nanoparticles is relying on COX-2-catalyzed DGLA peroxidation. To further determine the survival and proliferation of lung cancer cells, we measured the LDH activity in A549 cells by LDH-cytotoxicity assay. Interestingly, both 3WJ-EpCAM-D5D siRNA nanoparticle alone and the combination of DGLA and 3WJ-EpCAM-D5D siRNA nanoparticle groups displayed significantly higher LDH activity than the vehicle group ($p<0.001$, Fig. 24B), indicating that 3WJ-EpCAM-D5D siRNA nanoparticle could trigger the release of LDH from dead lung cancer cells.

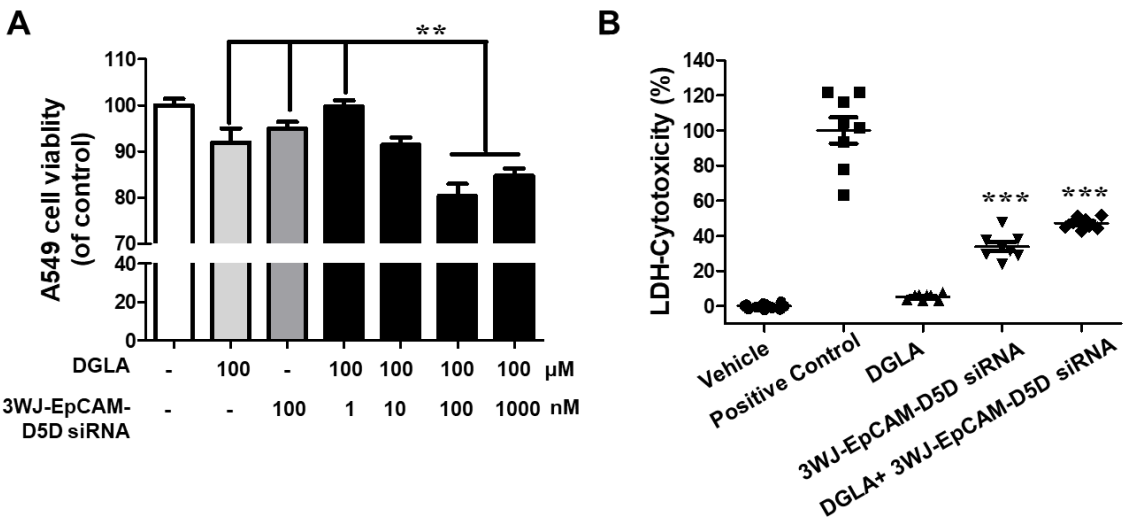

Figure 24. DGLA and 3WJ-EpCAM-D5D siRNA inhibited the proliferation of A549 lung cancer cells. (A) Cell viability of A549 cells after treatment of DGLA (100 μM) and different concentrations of 3WJ-EpCAM-D5D siRNA for 48 h. (B) LDH cytotoxicity assay of A549 cells. Cells were treated with DGLA and/or 3WJ-EpCAM-D5D siRNA for 48 h. Data represent mean ± SEM for n=8. $^{***}P<0.001$, $^{**}P<0.01$ *vs* Vehicle group.

To confirm the effect of 3WJ-EpCAM-D5D siRNA nanoparticles on the proliferation of lung cancer cells, we further detected the Ki-67 expression in A549 lung cancer cells treated with DGLA and/or 3WJ-EpCAM-D5D siRNA nanoparticle by immunofluorescence analysis. We observed that DGLA or 3WJ-EpCAM-D5D siRNA nanoparticle alone has limited effect on the protein expression of Ki-67 in A549 cells (Fig. 25), indicating that the single agent, either DGLA or 3WJ-EpCAM-D5D siRNA nanoparticle, is not enough to stop the proliferation of lung cancer cells. However, the combination of DGLA and 3WJ-EpCAM-D5D siRNA nanoparticle significantly suppressed the Ki-67 expression in A549 cells ($p<0.05$, Fig. 25), suggesting the extra inhibitory effect and benefits of the drug combination (DGLA+ 3WJ-EpCAM-D5D siRNA nanoparticle).

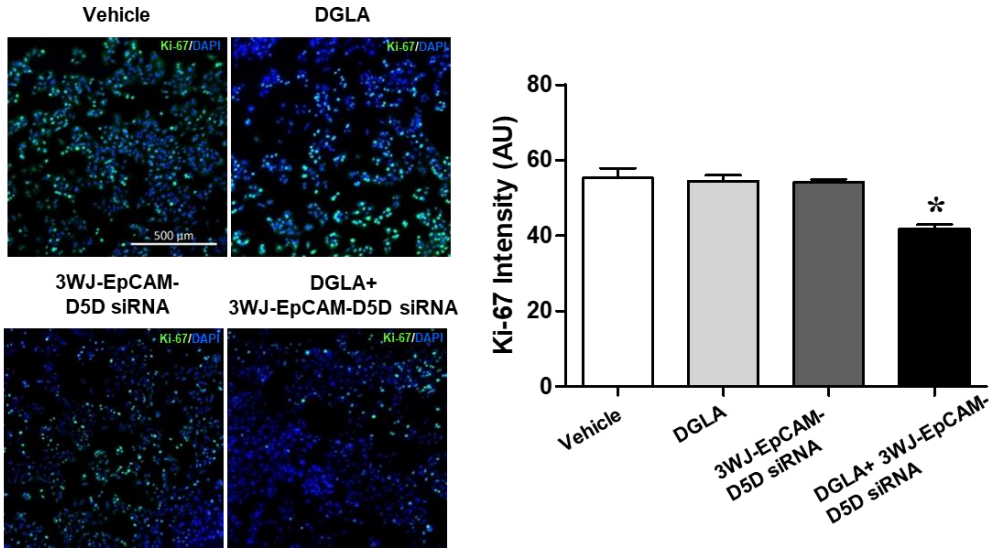

Figure 25. Immunofluorescence images and quantification of ki-67 relative intensity in A549 cells by confocal microscopy. Expression of ki-67 was stained in green, and cell nuclei were counter-stained with DAPI. Data represent mean ± SEM for n=6. $^{*}P<0.05$ *vs* Vehicle group.

5.4. DGLA and 3WJ-EpCAM-D5D siRNA Nanoparticle Suppressed the HDAC Activity and YAP1/TAZ pathway in Lung Cancer Cells

As a free radical by-product, 8-HOA suppresses lung cancer cell growth via regulating cell proliferation and apoptosis, which is highly relevant to HDAC and YAP1/TAZ pathway. We demonstrated that exogenous 8-HOA could inhibit HDAC activity in lung cancer cells in a dose-dependent pattern. Additionally, the protein expression of YAP1, TAZ, and downstream effector CTGF in lung cancer cells could be inhibited by exogenous 8-HOA. To explore the mechanism of DGLA-derived 8-HOA on lung cancer, we would investigate the role of endogenous 8-HOA on HDAC and YAP1/TAZ pathway in lung cancer cells treated with 3WJ-EpCAM-D5D siRNA nanoparticles. We observed that the combination of DGLA and 3WJ-EpCAM-D5D siRNA nanoparticle significantly decreased the HDAC activity to less than 40% in A549 lung cancer cells ($p<0.05$, Fig. 26), suggesting that 3WJ-EpCAM-D5D siRNA nanoparticle also could suppress HDAC activity via inducing the production of DGLA-derived 8-HOA. However, the mechanism

of the 3WJ-EpCAM-D5D siRNA nanoparticle on HDAC activity in lung cancer cells is still unclear. The acetylation of histone could be regulated by HAT and HDAC, which contains several subtypes, including HDAC I, II, IV (Zinc dependent), and HDAC III (sirtuins, NAD+ dependent) [114,116]. To investigate the effect of 3WJ-EpCAM-D5D siRNA nanoparticles on HAT and sirtuins, we measured the activity of HAT and sirtuins in A549 cells treated with DGLA and/or 3WJ-EpCAM-D5D siRNA nanoparticle by enzyme activity colorimetric assays with different substrates. However, we did not observe any remarkable change of HAT and sirtuins activity in A549 cells after the addition of DGLA and RNA nanoparticle ($p>0.05$, Fig. 26B and C), suggesting the specificity of DGLA-derived 8-HOA on HDAC, possibly HDAC I, II, and IV. Moreover, we examined the protein expression of HDAC1 and HAT1 in A549 cells treated with DGLA and 3WJ-EpCAM-D5D siRNA nanoparticles by Western analysis. We found that neither DGLA nor 3WJ-EpCAM-D5D siRNA nanoparticles could significantly affect the protein expression of HDAC1 and HAT1 in lung cancer cells ($p>0.05$, Fig. 26D). Taken together, 3WJ-EpCAM-D5D siRNA nanoparticles could redirect COX-2-catalyzed DGLA peroxidation, leading to the generation of 8-HOA. The DGLA-derived endogenous 8-HOA could specifically inhibit HDAC activity without influence either the activity of HAT and sirtuins or the protein expression of HDAC1 and HAT1.

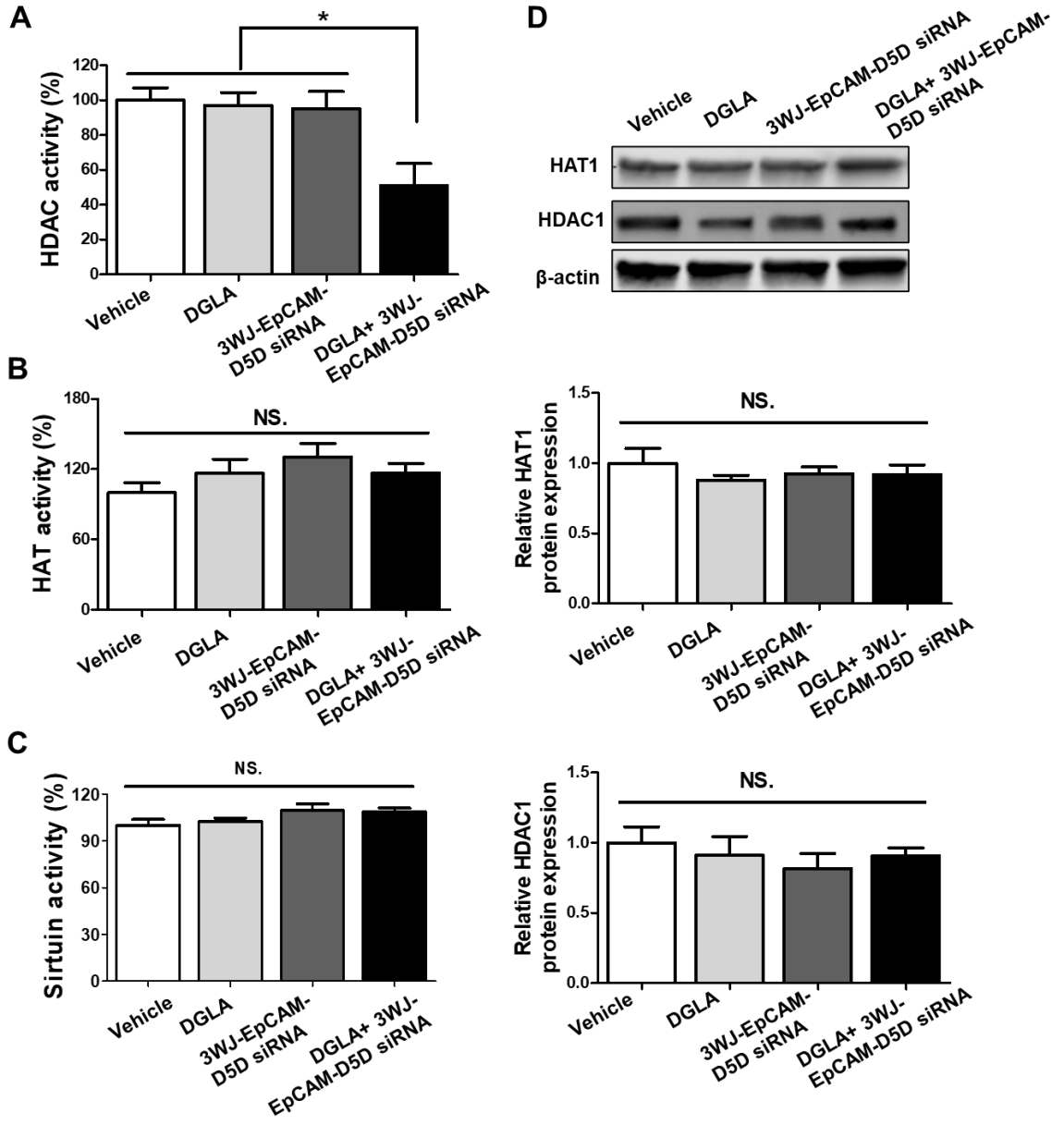

Figure 26. DGLA and 3WJ-EpCAM-D5D siRNA nanoparticles inhibited the HDAC activity of A549 cells. Cells were treated with DGLA and 3WJ-EpCAM-D5D siRNA nanoparticles for 48 h. Enzymatic assays were used to determine (A) HDAC activity, (B) HAT activity, and (C) sirtuins activity in A549 cells. (D) Relative protein expression of HAT1 and HDAC1 in A549 cells treated with 3WJ-EpCAM-D5D siRNA nanoparticle. The relative expression of D5D to β-actin in the Vehicle group was normalized to 1. Data represent mean ± SEM for n=3. $^{*}P<0.05$ *vs* DGLA + 3WJ-EpCAM-D5D siRNA nanoparticle group. NS. not significant.

Given the critical role of HDAC in the YAP1/TAZ pathway, we determined the cellular location and expression of YAP1 and TAZ in A549 lung cancer cells via immunofluorescence

analysis under confocal microscopy. The YAP1 and TAZ are commonly expressed in the cytoplasm. However, when the Hippo pathway is off, YAP1/TAZ pathway can be activated by transporting YAP1 and TAZ from the cytoplasm to nuclear, resulting in the proliferation of cancer cells. We found that most of the YAP1 and TAZ proteins are expressed in the nuclear of A549 lung cancer cells (Fig. 27 and 28), indicating the overactivation of the YAP1/TAZ pathway in lung cancer cells. However, the combination of DGLA and 3WJ-EpCAM-D5D siRNA nanoparticle significantly suppressed the nuclear translocation of YAP1 and TAZ in A549 cells (Fig. 27 and 28). This phenomenon is consistent with our previous observation, in which the combination of DGLA and D5D siRNA transfection suppressed the YAP1/TAZ pathway in lung cancer cells.

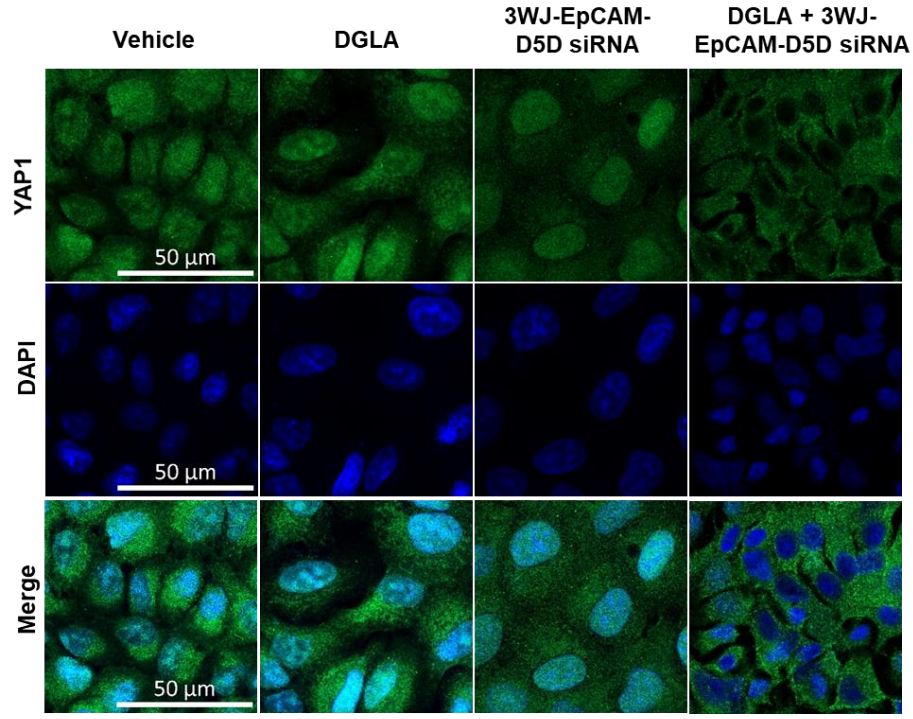

Figure 27. Immunofluorescence images of YAP1 expression in A549 cells. Expression of YAP1 was stained in green, and cell nuclei were counter-stained with DAPI (n=6).

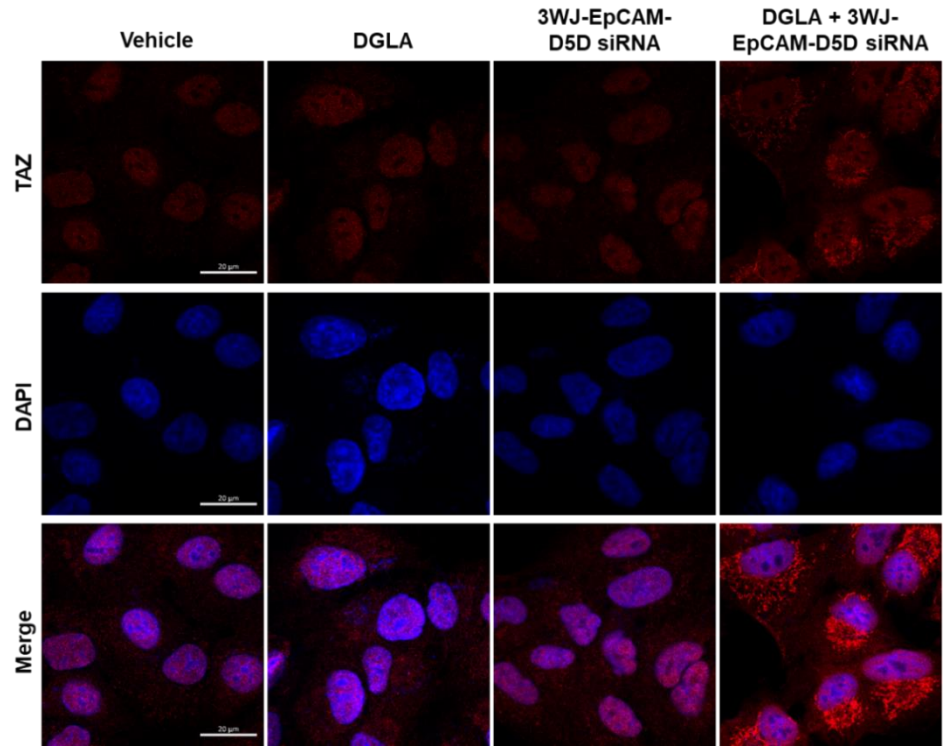

Figure 28. Immunofluorescence images of TAZ expression in A549 cells. Expression of TAZ was stained in red, and cell nuclei were counter-stained with DAPI (n=6).

5.5. COX-2 and EpCAM are Essential for Eliciting the Effect of 3WJ-EpCAM-D5D siRNA Nanoparticle on Lung Cancer

We demonstrated that the combination of DGLA and 3WJ-EpCAM-D5D siRNA nanoparticles could successfully suppress the growth of A549 lung cancer cells *in vitro*. To elucidate the mechanism of the 3WJ-EpCAM-D5D siRNA nanoparticle on lung cancer, we also enrolled another two cell lines, H1299 lung cancer cells and BEAS-2B normal lung epithelial cells into this study. We firstly profiled the COX-2 and EpCAM protein expression of A549, H1299, and BEAS-2B cells by using Western analysis. We observed that A549 lung cancer cells have the highest COX-2 and EpCAM expression; H1299 lung cancer cells have high EpCAM expression and low COX-2 expression; BEAS-2B normal lung epithelial cells have low to no expression of both COX-2 and EpCAM (p<0.001, Fig. 29). To investigate the targeting efficiency of 3WJ-

EpCAM-RNA nanoparticles in different cells, we assessed the cellular distribution of 3WJ-EpCAM-Alexa 647 RNA nanoparticles in H1299 and BEAS-2B cells by confocal microscope. We observed that 3WJ-EpCAM-Alexa 647 RNA nanoparticles could be internalized into H1299 lung cancer cells (Fig. 30). While the distribution of 3WJ-EpCAM-Alexa 647 RNA nanoparticles in BEAS-2B normal lung epithelial cells is relatively less than it in A549 and H1299 lung cancer cells (Fig. 30). The relatively low amount of 3WJ RNA nanoparticle internalization in BEAS-2B cells may be due to less expression of EpCAM in normal lung epithelial cells. Therefore, we may conclude that conjugation of EpCAM aptamer in RNA nanoparticles could allow 3WJ RNA nanoparticles to specifically target lung cancer cells with high EpCAM expression, whereas avoiding binding to normal lung epithelial cells with low EpCAM expression.

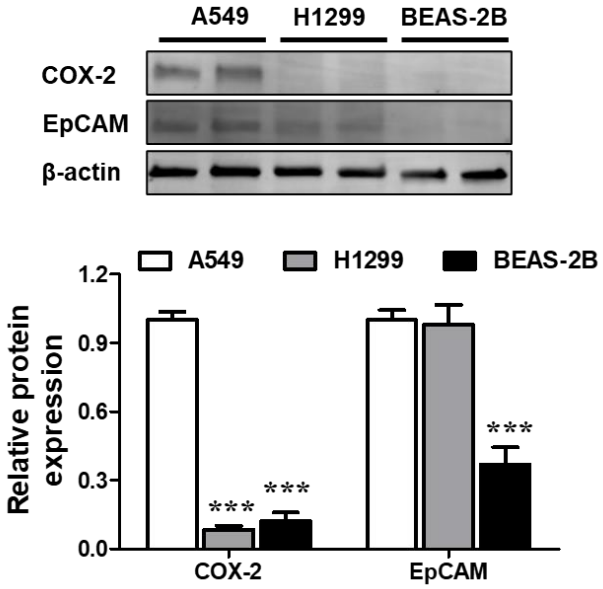

Figure 29. Relative protein expression of COX-2 and EpCAM in A549 and H1299 lung cancer cells and BEAS-2B normal lung epithelial cells. The relative expression of COX-2 and EpCAM to β-actin in the Vehicle group was normalized to 1. Data represent mean ± SEM for n=3. $^{***}P<0.001$ *vs* A549 cells.

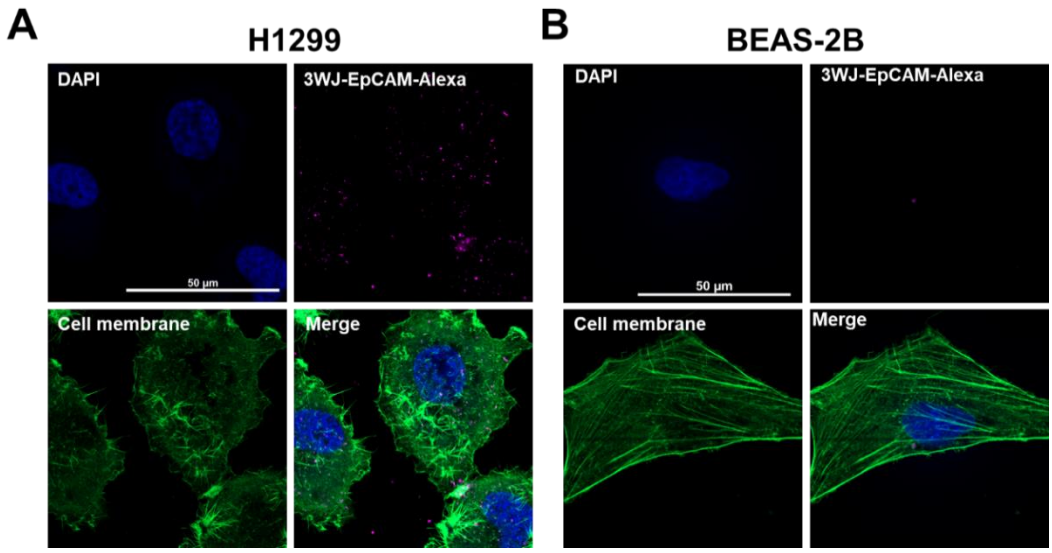

Figure 30. Distribution of 3WJ RNA nanoparticles (violet) in H1299 lung cancer cells and BEAS-2B normal lung epithelial cells. Images were captured via a confocal microscope (n=6). F-actin was labeled with phalloidin (Alexa 488, green) and cell nuclei with DAPI.

Although 3WJ RNA nanoparticles cannot be efficiently recognized by BEAS-2B cells, the normal lung epithelial cells may still be influenced by 3WJ-EpCAM-D5D siRNA nanoparticles due to possible off-target effects. To evaluate cytotoxicity and the off-target effect of 3WJ-EpCAM-D5D siRNA nanoparticles, we measured the 8-HOA concentration in BEAS-2B cells by GC-MS. However, unlike A549 cells, the 8-HOA level in BEAS-2B cells was not significantly changed by either DGLA or 3WJ-EpCAM-D5D siRNA nanoparticle (p>0.05, Fig. 31A), implicating that 3WJ RNA nanoparticle with D5D siRNA could not shift the COX-2 catalyzed DGLA peroxidation in normal lung epithelial cells. This phenomenon can be explained by the low COX-2 expression in BEAS-2B cells (Fig. 29). Since COX-2 is the essential enzyme for 8-HOA production, BEAS-2B cells may not efficiently convert DGLA to 8-HOA even in the condition of D5D inhibition. However, besides triggering 8-HOA generation, 3WJ-EpCAM-D5D siRNA nanoparticles may also affect lung cancer cells growth via regulating alternative pathways. To evaluate the mechanical basis of the 3WJ-EpCAM-D5D siRNA nanoparticle, we investigated the

effect of 3WJ-EpCAM-D5D siRNA nanoparticle on proliferation and survival of BEASE-2B cells by MTT assay, LDH cytotoxicity assay, and colony formation assay. The cell viability, LDH activity, and survival fraction of BEAS-2B cells could not be significantly changed by DGLA and 3WJ-EpCAM-D5D siRNA nanoparticle (p>0.05, Fig. 31B-D), implicating that 3WJ-EpCAM-D5D siRNA nanoparticle may avoid damage to normal lung epithelial cells with negative COX-2 and EpCAM expression.

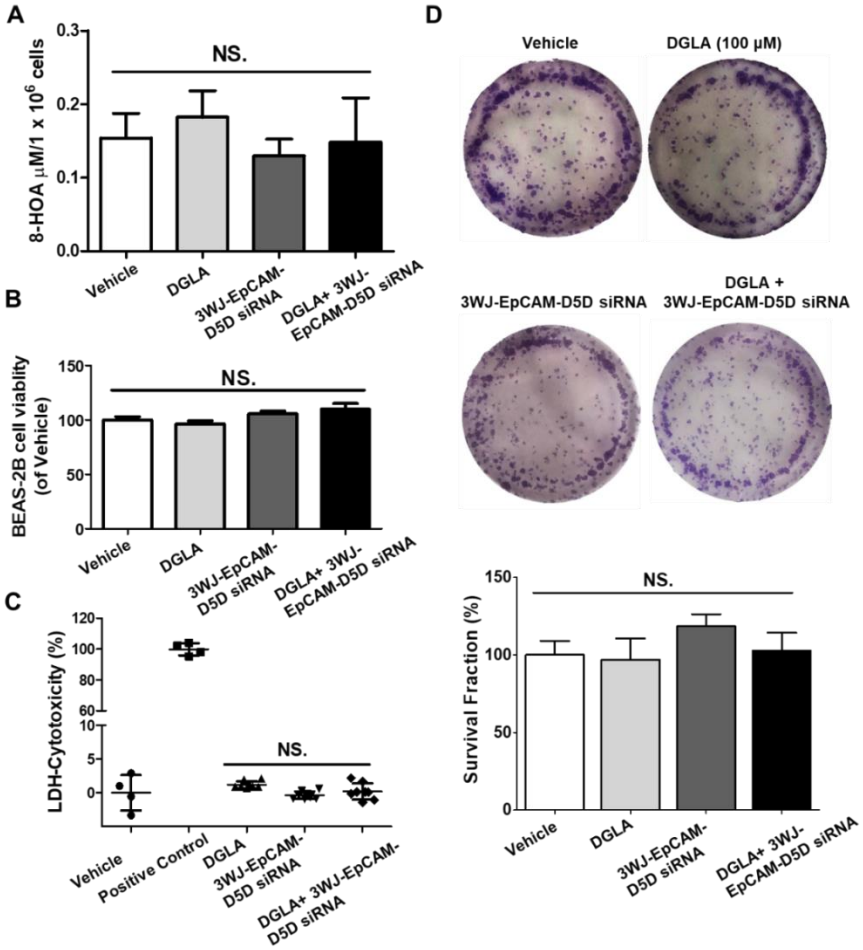

Figure 31. Effect of 3WJ-EpCAM-D5D siRNA nanoparticles on BEAS-2B normal lung epithelial cells. (A) 8-HOA content in BEAS-2B cells was determined by GC-MS. (B) The cell viability of BEAS-2B cells was measured by MTT assay. BEAS-2B cells were treated with DGLA and 3WJ-EpCAM-D5D siRNA nanoparticles. (C) LDH activity of BEAS-2B cells. Positive Control: BEAS-2B treated with Triton X-100. (D) Colony formation of BEAS-2B cells treated with DGLA and 3WJ-EpCAM-D5D siRNA nanoparticle. The survival fraction of BEAS-2B cells was normalized by the number of colonies in the Vehicle group. Data represent mean ± SEM for n=4-8. NS. Not Significant.

5.6. TNF-α Provoked the Effect of 3WJ-EpCAM-D5D siRNA Nanoparticle on H1299 Lung Cancer Cells by Promoting COX-2 Expression

Since 3WJ-EpCAM-D5D siRNA nanoparticle has no cytotoxicity on normal lung epithelial cells, we are wondering whether the D5D inhibition could affect lung cancer cells with low COX-2 expression. We evaluated the effect of the combination of DGLA and normal lung epithelial cells on H1299 lung cancer cells by MTT assay and colony formation assay. Compared to A549 lung cancer cells, H1299 cells have relatively lower COX-2 expression (Fig. 29). However, EpCAM expression in H1299 cells is sufficient to attract 3WJ-EpCAM-D5D siRNA nanoparticles (Fig. 30). Although 3WJ RNA nanoparticles can be internalized into H1299 lung cancer cells, we observed that neither DGLA nor 3WJ-EpCAM-D5D siRNA nanoparticles could significantly decrease the cell viability and survival fraction of H1299 lung cancer cells (p>0.05, Fig. 32), indicating that the effect of 3WJ-EpCAM-D5D siRNA nanoparticles on COX-2 negative lung cancer cells is limited.

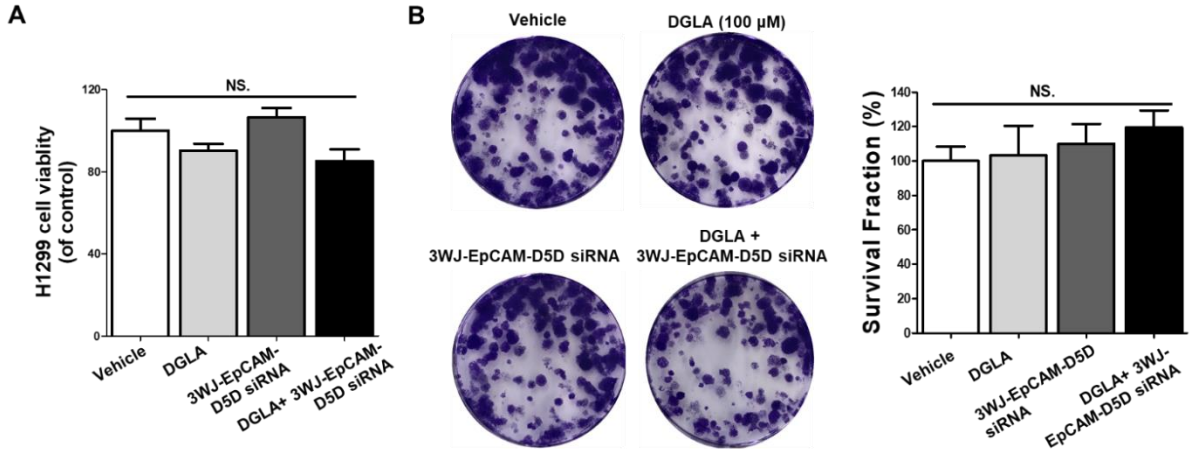

Figure 32. Effect of 3WJ-EpCAM-D5D siRNA nanoparticles on H1299 lung cancer cells. (A) The cell viability of H1299 cells was determined by MTT assay. (B) The survival fraction of H1299 lung cancer cells was determined by colony formation assay. H1299 cells were treated with DGLA and 3WJ-EpCAM-D5D siRNA nanoparticles. Data represent mean ± SEM for n=3. NS. Not Significant.

To elucidate the role of COX-2 in D5D inhibition-based anti-cancer strategy, we used TNF-α to induce COX-2 expression in H1299 lung cancer cells. H1299 cells were treated with different concentrations of TNF-α for 3, 6, and 24 h. The COX-2 protein expression was determined by Western analysis. We found that 80 and 100 ng/mL TNF-α for 24 h could significantly provoke COX-2 expression in H1299 lung cancer cells (p<0.05, Fig. 33). We administrated DGLA and 3WJ-EpCAM-D5D siRNA nanoparticle into TNF-α (100 ng/mL for 24 h) pre-treated H1299 cells for another 48 h. Notably, pre-treatment of TNF-α significantly improved the effectiveness of the combination of DGLA and 3WJ-EpCAM-D5D siRNA nanoparticle on H1299 lung cancer cells (p<0.05, Fig. 34), indicating that COX-2 is essential for eliciting the inhibitory effect of 3WJ-EpCAM-D5D siRNA nanoparticle on lung cancer. On the contrary, we did not find any significant inhibitory effect of 3WJ-EpCAM-D5D siRNA nanoparticles on H1299 lung cancer cells without co-treatment of TNF-α (Fig. 34).

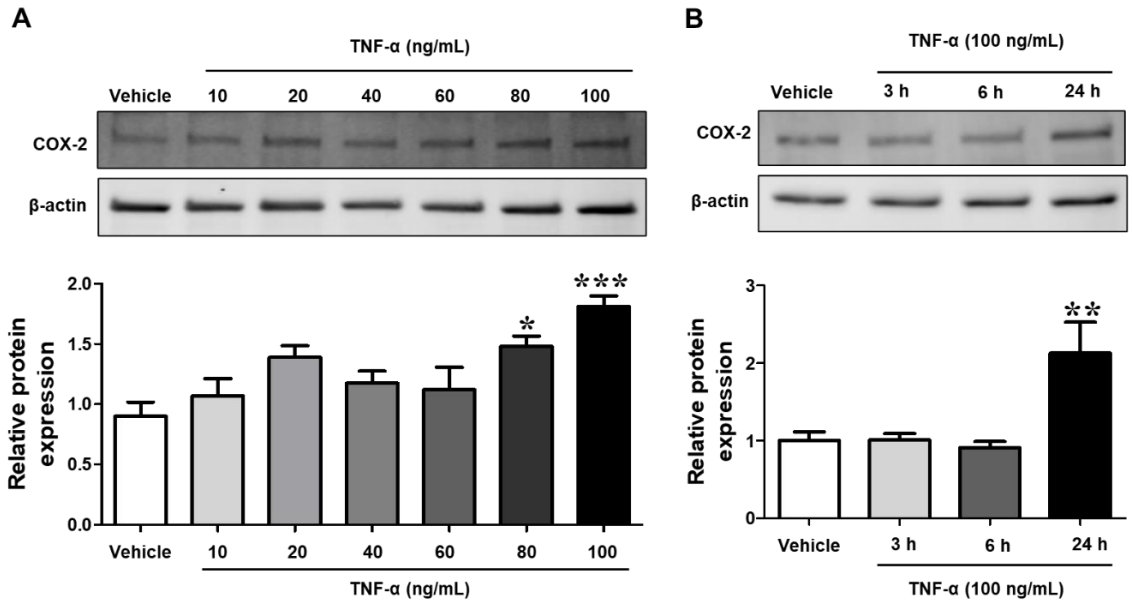

Figure 33. TNF-α induced COX-2 expression in H1299 lung cancer cells. Relative protein expression of COX-2 in H1299 lung cancer cells. H1299 cells were treated with (A) different concentrations of TNF-α for 24 h or (B) 100 ng/mL TNF-α for the different periods. The relative expression of COX-2 to β-actin in the Vehicle group was normalized to 1. Data represent mean ± SEM for n=3. $^{*}P$<0.05, $^{**}P$<0.01, $^{***}P$<0.001 *vs* Vehicle group.

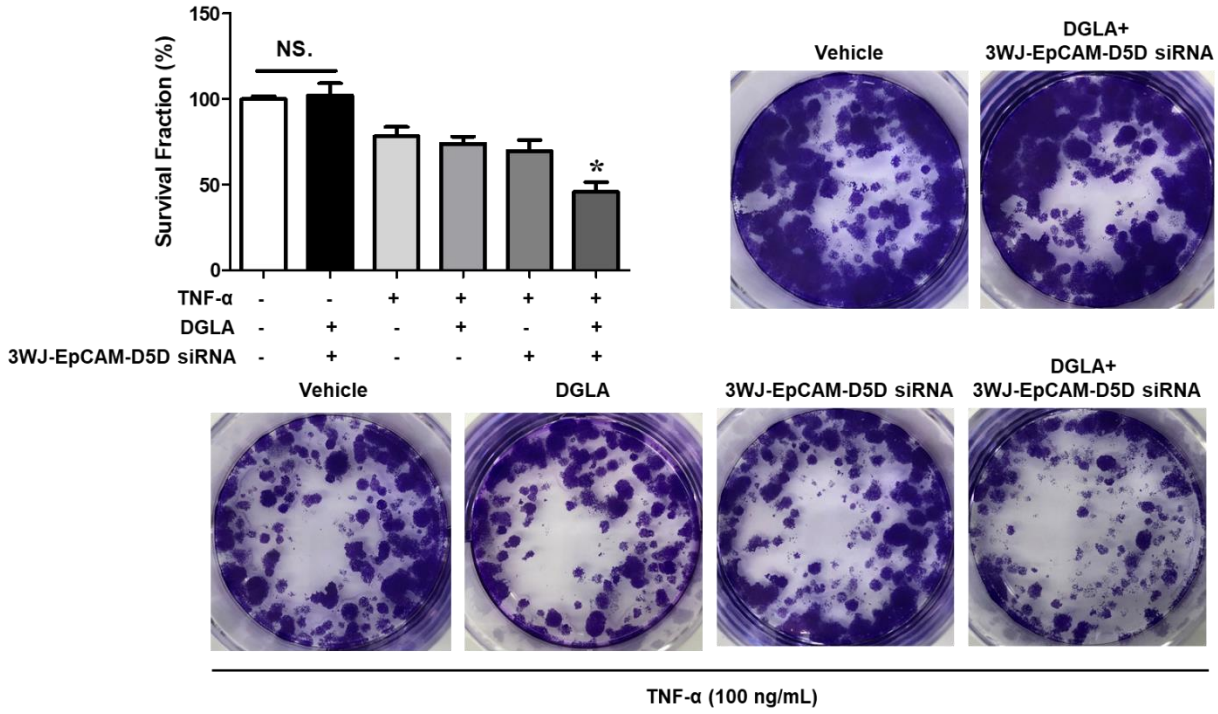

Figure 34. The inhibitory effect of 3WJ-EpCAM-D5D siRNA nanoparticles on TNF-α stimulated H1299 lung cancer cells. The survival fraction of H1299 lung cancer cells was determined by colony formation assay. H1299 cells (TNF-α pre-treated) were treated with DGLA and 3WJ-EpCAM-D5D siRNA nanoparticles. Data represent mean ± SEM for n=3. $^{*}P<0.05$ *vs* Vehicle group. NS. Not Significant *vs* Vehicle group.

5.7. 3WJ-EpCAM RNA Nanoparticle Specifically Targeted to Lung Tumor *in vivo*

Although we demonstrated the binding efficiency and effectiveness of 3WJ-EpCAM-D5D siRNA nanoparticle *in vitro*, we still need to investigate the bio-distribution and effect of 3WJ-EpCAM-D5D siRNA nanoparticles in the animal model. Due to the importance of EpCAM expression for displaying the function of EpCAM aptamer of 3WJ-EpCAM-D5D siRNA nanoparticle, we firstly assessed the EpCAM protein expression of lung tumor tissues from nude mice treated with DGLA, 3WJ-EpCAM-D5D siRNA nanoparticle, or their combination by Western analysis. We found that none of the treatments could decrease the protein expression of EpCAM in tumor tissues ($p>0.05$, Fig. 35), suggesting EpCAM is a desirable target for 3WJ-EpCAM-D5D siRNA nanoparticles.

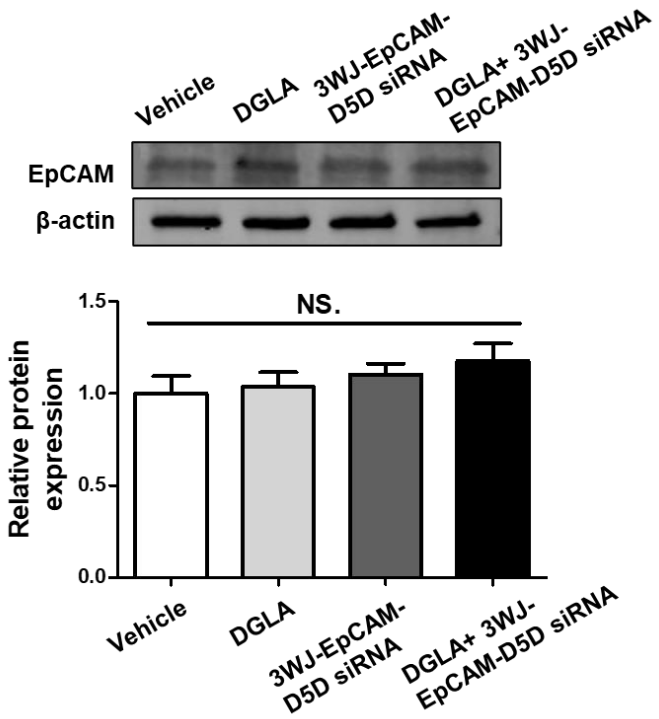

Figure 35. Relative protein expression of EpCAM in lung tumor tissues. The relative expression of EpCAM to β-actin in the Vehicle group was normalized to 1. Data represent mean ± SEM for n=3. NS. Not Significant *vs* Vehicle group.

To evaluate the targeting efficiency of the 3WJ-EpCAM RNA nanoparticle, we implanted A549 lung cancer cells into the nude mice. 3WJ-EpCAM-Alexa 647 RNA nanoparticle was injected to nude mice to determine the bio-distribution of RNA nanoparticles under the In Vivo Imaging System (IVIS) Spectrum station (Fig. 36A). We did not observe any 3WJ-EpCAM-Alexa 647 RNA nanoparticles in the organs of the vehicle group (Fig. 36B). However, a significantly higher amount of 3WJ-EpCAM-Alexa 647 RNA nanoparticles has been found in tumor tissues rather than other organs, such as the heart, liver, lung, and kidney from mice treated with 3WJ-EpCAM-Alexa 647 RNA nanoparticles (Fig. 36B), indicating the specificity of 3WJ RNA nanoparticles on lung tumors. To elucidate the dynamic distribution of 3WJ RNA nanoparticles *in vivo*, we monitored the intensity of 3WJ-EpCAM-Alexa 647 RNA nanoparticles in the whole body of nude mice for 8 h after injection. The 3WJ-EpCAM-Alexa 647 RNA nanoparticle was widely

distributed throughout the body of nude mice in the initial phase after injection (0 to 4 h). However, we only detected a remarkable amount of 3WJ-EpCAM-Alexa 647 RNA nanoparticles in the region of tumor tissues at the late stage of treatment (4 to 8 h) (Fig. 37). Therefore, we may conclude that the 3WJ RNA nanoparticle may selectively accumulate into tumor tissues in the animal model. Moreover, we did not observe the distribution of RNA nanoparticles in kidneys, suggesting that 3WJ RNA nanoparticles also protected D5D siRNA from elimination by kidneys.

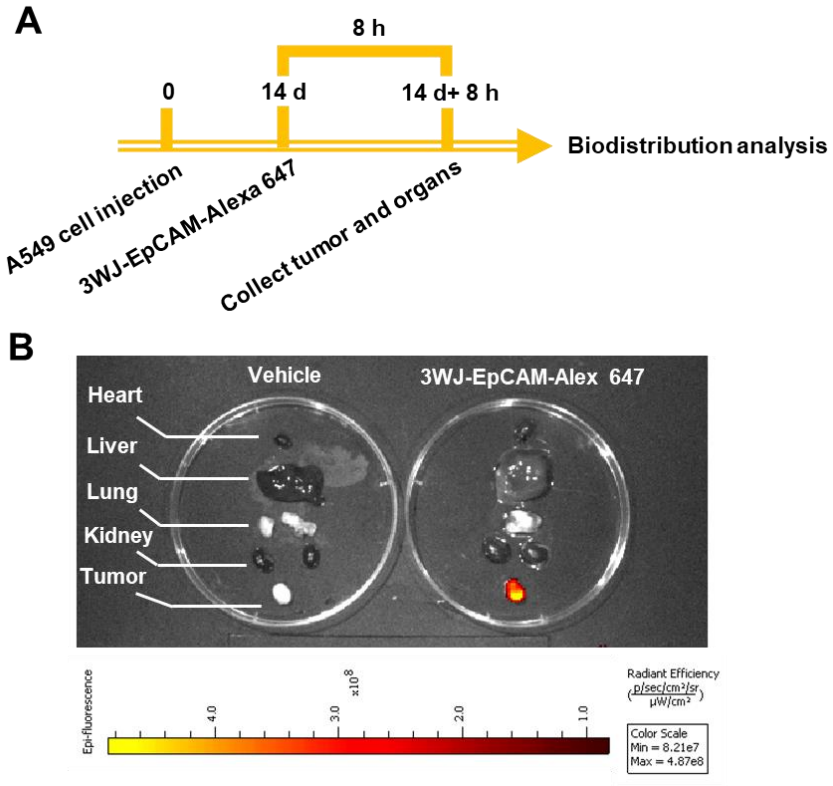

Figure 36. The distribution of nanoparticles in tumor tissues and organs from nude mice. (A) *In vivo* experiment plan for deterring the distribution of 3WJ-EpCAM-Alexa 647 nanoparticles. (B) Tumor tissues and organs were scanned under the In Vivo Imaging System (IVIS) Spectrum station (n=4).

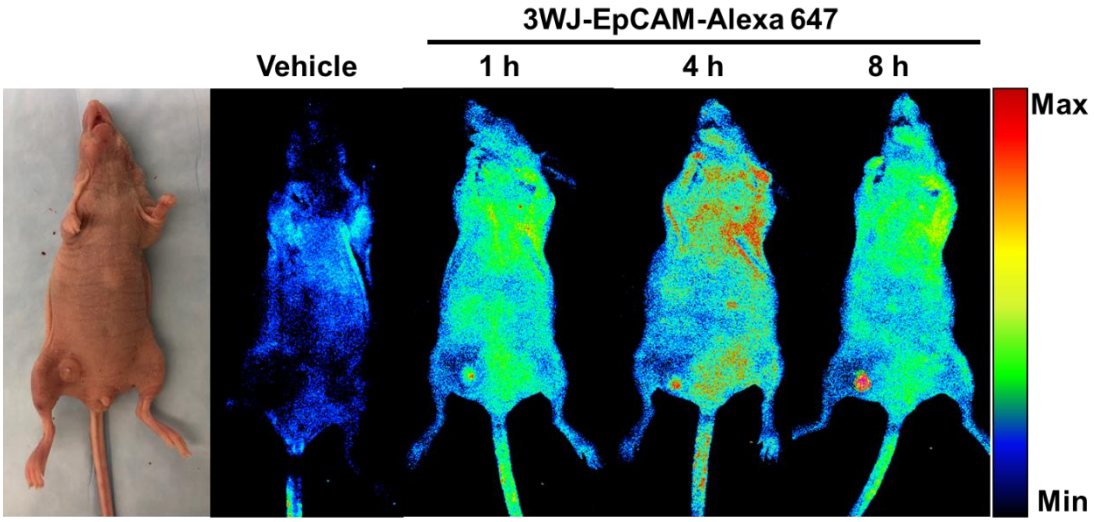

Figure 37. The whole-body distribution of nanoparticles in nude mice. Mice were treated with 3WJ-EpCAM-Alexa 647 nanoparticles. The whole-body images were captured at 1, 4, and 8 h after treatment. The intensity of the nanoparticle was indicated by different colors as scale bar (n=3).

5.8. 3WJ-EpCAM-D5D siRNA Nanoparticle Inhibited the Growth of Lung Tumor *in vivo*

To investigate the effectiveness of 3WJ-EpCAM-D5D siRNA nanoparticles on lung tumors *in vivo*, we established a xenograft model by injecting A549 cells into nude mice. The mice were administrated with DGLA and 3WJ-EpCAM-D5D siRNA nanoparticles for 4 weeks (Fig. 38A). We found that the tumor size dramatically increased in the vehicle group during 4 weeks of observation, especially in the last week of observation. However, compared to the vehicle group, the tumor size was significantly smaller in mice treated with the combination of DGLA and 3WJ-EpCAM-D5D siRNA nanoparticles ($p<0.01$, Fig. 38B). About 60% tumor reduction was observed in the combination of DGLA and 3WJ-EpCAM-D5D siRNA nanoparticle group at 42 days (Fig. 38B). To visualize the change of tumor volume during the treatment, we also scanned the tumor by ultrasound imaging system once a week. We found that tumors of the vehicle, DGLA, and 3WJ-EpCAM-D5D siRNA nanoparticle group, were growing expeditiously during treatment (14 to 42 days). However, the combination of DGLA and 3WJ-EpCAM-D5D siRNA nanoparticles almost

stopped the growth of lung tumors in nude mice (Fig. 39). The significantly smaller tumors of the combination of DGLA and 3WJ-EpCAM-D5D siRNA nanoparticle group were also observed at end of the treatment (Fig. 40). Thus, DGLA or 3WJ-EpCAM-D5D siRNA nanoparticles alone could not suppress the lung tumor in the animal model. While the combination of DGLA and 3WJ-EpCAM-D5D siRNA nanoparticles have a strong inhibitory effect on lung tumors *in vivo*.

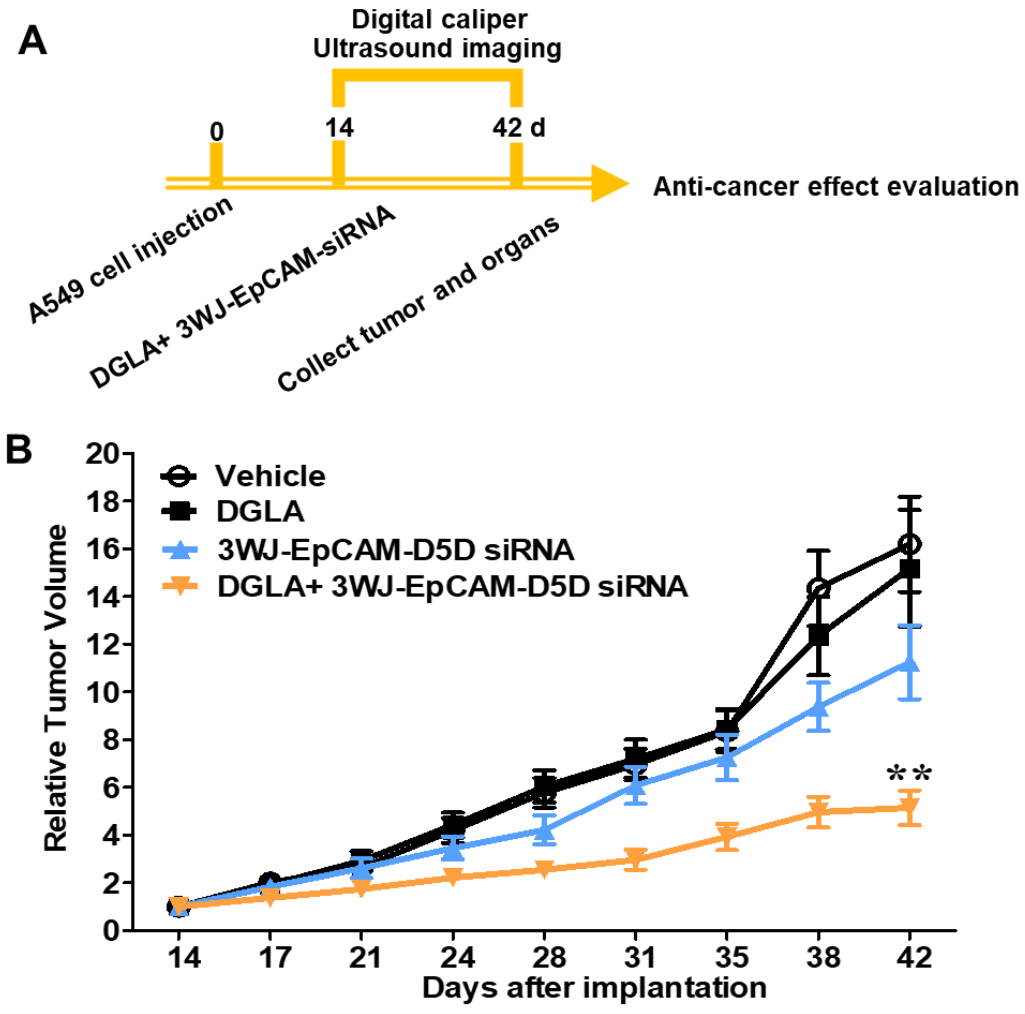

Figure 38. 3WJ-EpCAM-D5D siRNA nanoparticle suppressed the lung tumor growth in the nude mice. (A) *In vivo* experiment plan for evaluating the effect of 3WJ-EpCAM-D5D siRNA nanoparticles. (B) Tumor growth curve during 4-weeks of the treatment. The treatment starts at 14 days of tumor implantation. Data represent mean ± SEM for n=6. $^{**}P<0.01$ *vs* Vehicle group.

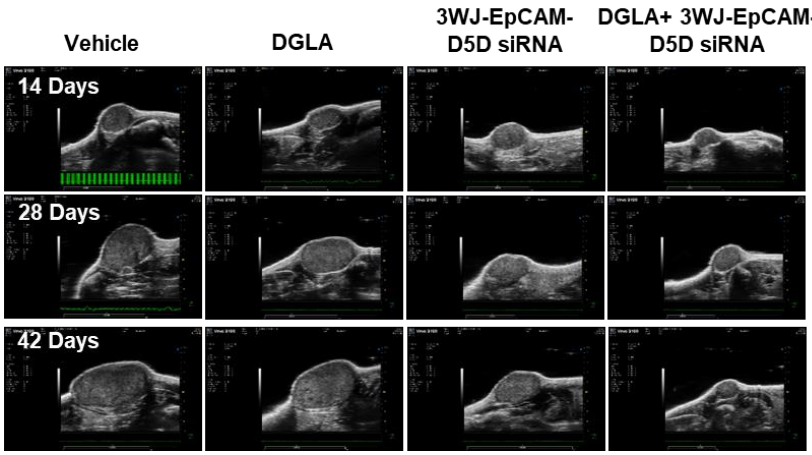

Figure 39. Ultrasound images of tumor growth in mice during 4-weeks treatments (n=6). Mice were administrated with DGLA and/or 3WJ-EpCAM-D5D siRNA. Day 14 is the first day of the treatment after cancer cell implantation.

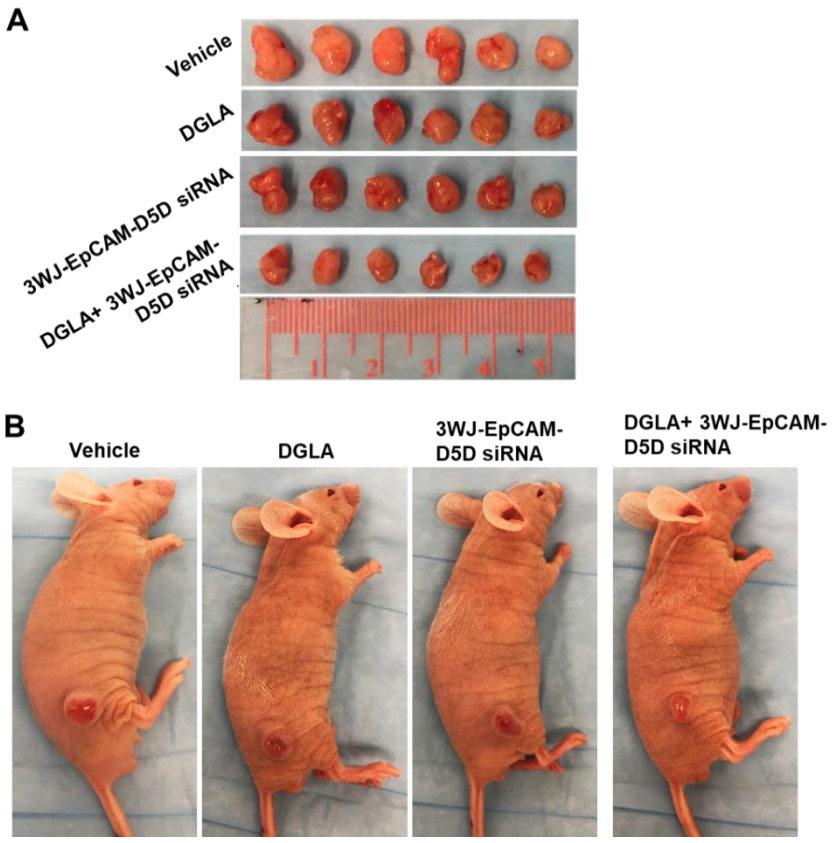

Figure 40. Effect of 3WJ-EpCAM-D5D siRNA and DGLA on nude mice with xenografted lung tumor. (A) The tumors were collected from nude mice at end of the treatment. (B) Whole-body images of nude mice at end of 4-weeks 3WJ-EpCAM-D5D siRNA nanoparticle treatment. The tumor was located at the hind flank. n=6.

5.9. 3WJ-EpCAM-D5D siRNA Nanoparticle Redirected COX-2 Catalyzed DGLA Peroxidation *in vivo*

In cellular models, we demonstrated that 3WJ-EpCAM-D5D siRNA nanoparticles could inhibit lung cancer cell growth via shifting COX-2 catalyzed DGLA peroxidation, resulting in 8-HOA production. However, the *in vivo* effect of 3WJ-EpCAM-D5D siRNA nanoparticles on DGLA peroxidation is still underexplored. To investigate the mechanism of the 3WJ-EpCAM-D5D siRNA nanoparticle, we measured the protein expression of COX-2 and D5D by Western and immunofluorescence analysis. We observed that DGLA and immunofluorescence analysis cannot alter the protein expression of COX-2 in lung tumor tissues ($p>0.05$, Fig. 41). Thus, the COX-2 may remain overexpressed in lung tumor tissues during the treatment, facilitating the production of 8-HOA. However, 3WJ-EpCAM-D5D siRNA nanoparticle significantly decreased the protein expression of D5D in tumor tissues ($p<0.05$, Fig. 41), indicating that 3WJ RNA nanoparticles could effectively protect and deliver D5D siRNA to lung tumors.

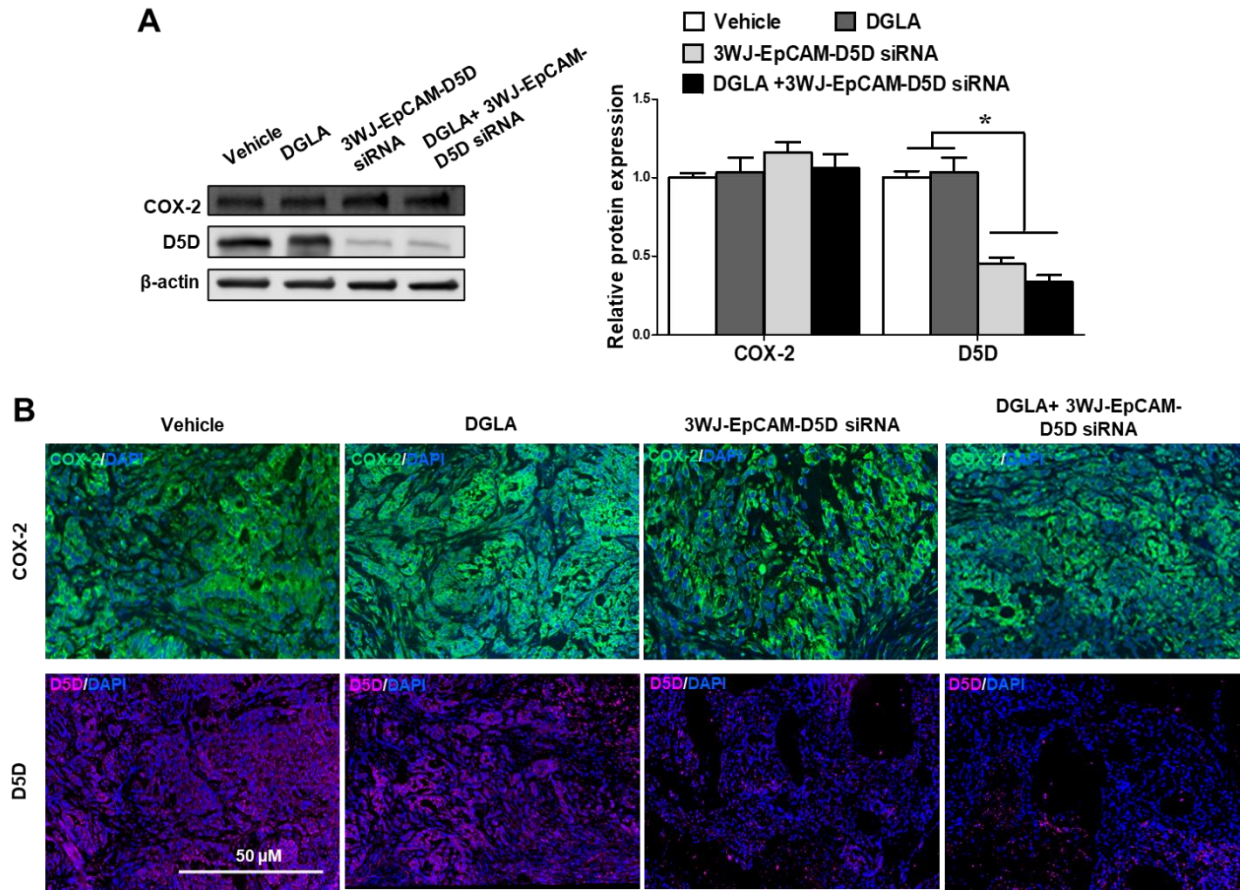

Figure 41. Effect of DGLA and 3WJ-EpCAM-D5D siRNA nanoparticle on COX-2 and D5D in tumor tissues. Relative protein expression of COX-2 and D5D in tumor tissues was determined by (A) Western analysis and (B) immunofluorescence analysis after 4 weeks of treatment of DGLA and 3WJ-EpCAM-D5D siRNA nanoparticle. Relative expression of proteins in the Western analysis was normalized by β-actin. Expression of COX-2 was stained in green, D5D in violet, and cell nuclei were counter-stained with DAPI. Data represent mean ± SEM for n=6. $^{*}P<0.05$ *vs* Vehicle and DGLA group.

To investigate the DGLA peroxidation pattern, we assessed the concentration of DGLA, AA, PGE_2, and 8-HOA in lung tumor tissues by LC-MS and GC-MS. We observed that the combination of DGLA and 3WJ-EpCAM-D5D siRNA nanoparticles could significantly improve the DGLA versus AA ratio in lung tumor tissues ($p<0.001$, Fig. 42A). However, compared with the DGLA group, the PGE_2 concentration was significantly decreased in the group treated with the combination of DGLA and 3WJ-EpCAM-D5D siRNA nanoparticle ($p<0.05$, Fig. 42B), indicating that D5D inhibition restricted the conversion of AA and PGE_2 from DGLA in lung

tumor tissues. On the contrary, we observed that the 8-HOA level was significantly improved by the combination of DGLA and 3WJ-EpCAM-D5D siRNA nanoparticle from ~0.18 to ~0.51 μg/g in lung tumor tissues from nude mice (p<0.01, Fig. 42C). To determine the specificity of the 3WJ-EpCAM-D5D siRNA nanoparticle, we also assessed the 8-HOA concentration in other vital organs, including the liver, kidneys, spleen, lung, and heart from nude mice at end of the treatment. The 8-HOA concentration is ~0.06 μg/g in the liver, ~0.08 μg/g in kidneys, ~0.04 μg/g in the spleen, ~0.17 μg/g in the lung, and ~0.17 μg/g in the heart from mice treated with the combination of DGLA and 3WJ-EpCAM-D5D siRNA nanoparticle. Notably, none of the tested tissues have a comparable level of 8-HOA as we observed in tumor tissues from nude mice. This is consistent with the bio-distribution result of the 3WJ-EpCAM-D5D siRNA nanoparticle in the mouse. 3WJ-EpCAM-D5D siRNA nanoparticles could specifically target lung tumor tissues by EpCAM aptamer. Additionally, we evaluated DGLA, AA, and 8-HOA level in the blood of nude mice. The AA level in serum was significantly suppressed by the combination of DGLA and 3WJ-EpCAM-D5D siRNA nanoparticles (p<0.01, Fig. 43A). However, DGLA (p<0.05) and 8-HOA (p<0.01) concentration in serum was improved by 3WJ-EpCAM-D5D siRNA nanoparticle with DGLA supplementation (Fig. 43). Therefore, we conclude that 1) 3WJ-EpCAM-D5D siRNA nanoparticle could efficiently cause D5D inhibition and DGLA accumulation, 2) the extra DGLA could be further converted to 8-HOA by COX-2 in lung tumor tissues and blood.

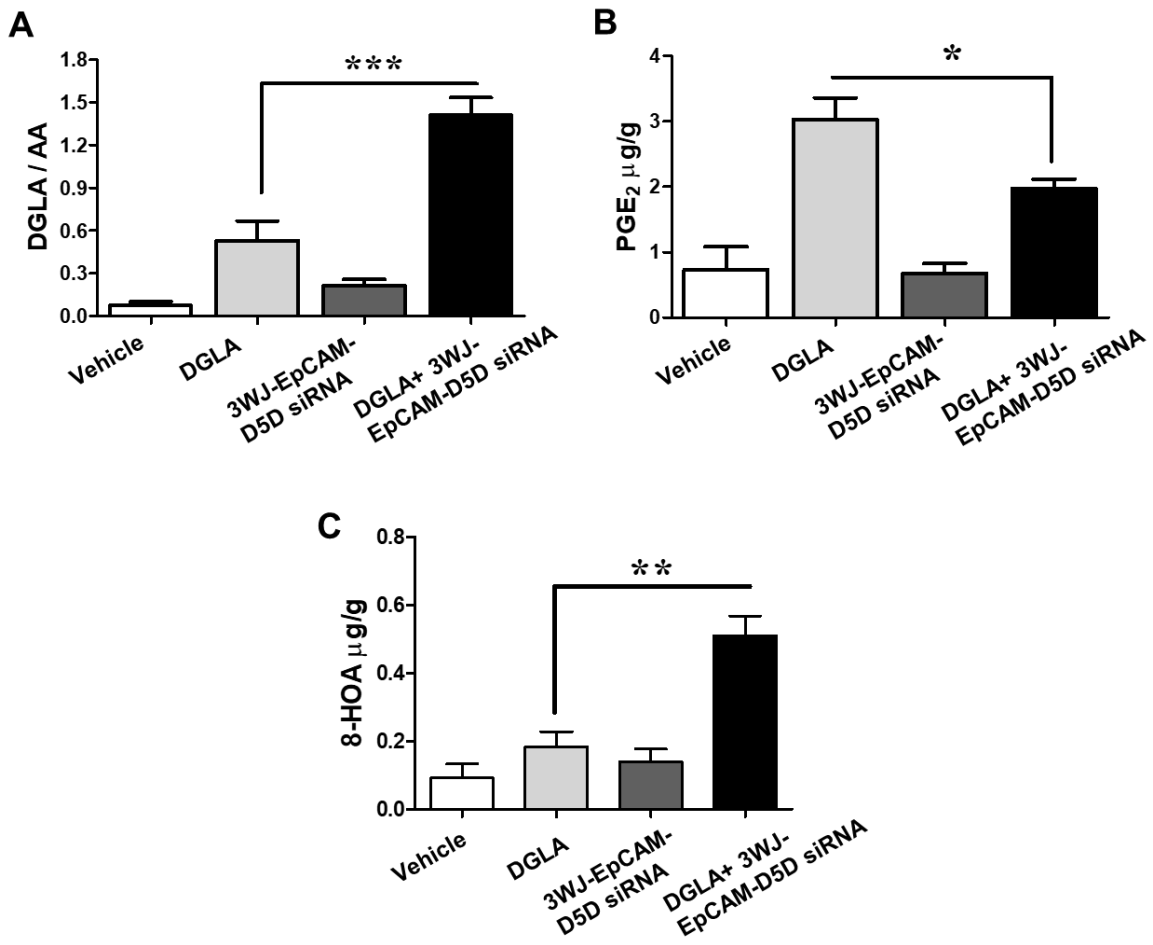

Figure 42. 3WJ-EpCAM-D5D siRNA nanoparticle shifted the COX-2-catalyzed DGLA peroxidation pattern in tumor tissues. (A) DGLA/AA level and (B) PGE_2 concentration in tumor tissues were determined by LC-MS. (C) 8-HOA concentration was measured by GC-MS. Data represent mean ± SEM for n=6. $^{*}P<0.05$, $^{**}P<0.01$, $^{***}P<0.001$ *vs* DGLA group.

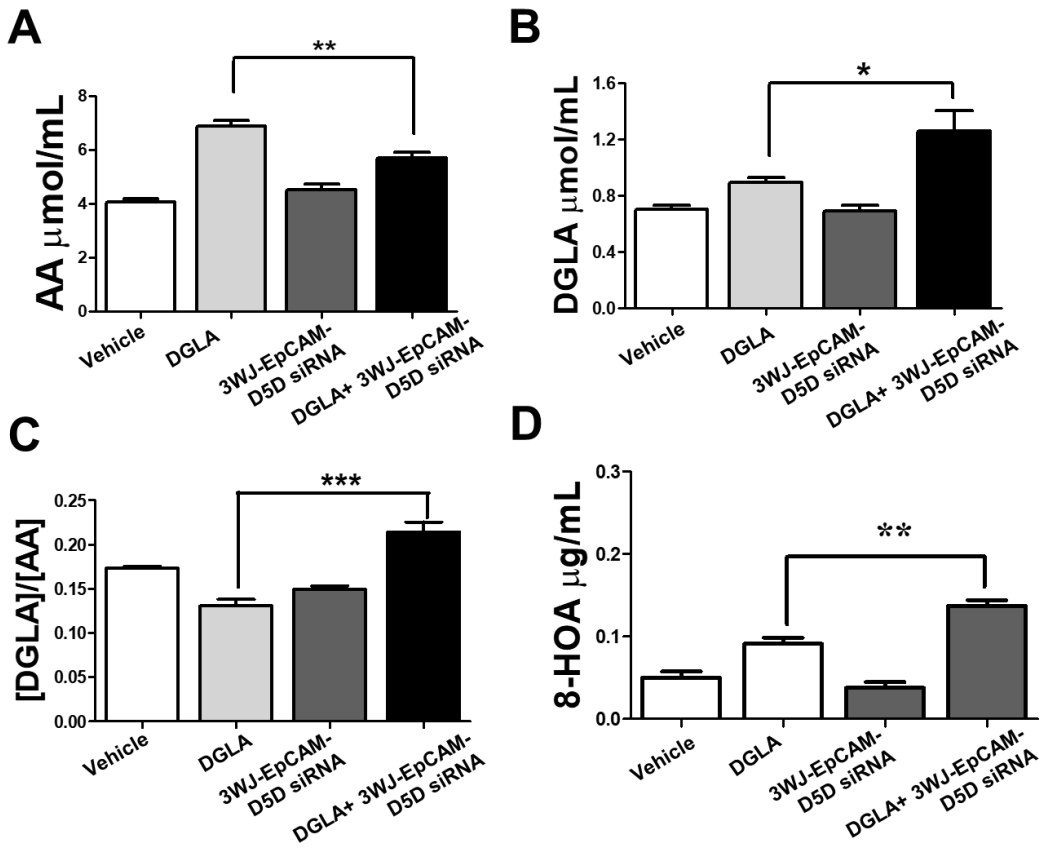

Figure 43. 3WJ-EpCAM-D5D siRNA nanoparticle shifted the COX-2-catalyzed DGLA peroxidation pattern in the serum of nude mice. (A) AA concentration, (B) DGLA concentration, (C) DGLA/AA level, and (D) 8-HOA concentration in blood were determined by GC-MS. Data represent mean ± SEM for n=6. $^{*}P<0.05$, $^{**}P<0.01$, $^{***}P<0.001$ *vs* DGLA group.

5.10. 3WJ-EpCAM-D5D siRNA Nanoparticle Inhibited HDAC and YAP1/TAZ Pathway in Lung Tumor Tissues

To investigate the *in vivo* effect of 3WJ-EpCAM-D5D siRNA nanoparticle on HDAC, we measured the HDAC, HAT, and sirtuins activity in lung tumor tissues by colorimetric assays. We found that the combination of DGLA and 3WJ-EpCAM-D5D siRNA nanoparticles could significantly decrease the HDAC activity in lung tumor tissues ($p<0.05$, Fig. 44A). However, the HAT and sirtuins activities in tumor tissues from mice treated with DGLA and 3WJ-EpCAM-D5D siRNA nanoparticles remained the same level as the activities in the vehicle group ($p>0.05$, Fig.

44B and C). Thus, 3WJ-EpCAM-D5D siRNA nanoparticles may lead to specific inhibition of HDAC activity in lung tumors without influencing the activities of HAT and sirtuins. Moreover, we observed that the protein expression of acetyl-histone H3 K9 was significantly up-regulated in tumor tissues from mice treated with DGLA and 3WJ-EpCAM-D5D siRNA nanoparticle ($p<0.01$, Fig. 45A). While the basal level of histone H3 was stable in tumor tissues from DGLA, 3WJ-EpCAM-D5D siRNA nanoparticle, and combination-treated mice (Fig. 45A). Since acetyl-histone H3 is the major substrate of HDAC, we may conclude that HDAC suppression could be induced by the combination of DGLA and 3WJ-EpCAM-D5D siRNA nanoparticles. However, treatment of DGLA or 3WJ-EpCAM-D5D siRNA nanoparticles alone cannot change the protein expression of acetyl-histone H3K9 in lung tumor tissues (Fig. 45A). This phenomenon is consistent with our *in vitro* findings, in which exogenous 8-HOA could serve as a potential HDAC inhibitor for lung cancer therapy. Furthermore, we investigated the role of 3WJ-EpCAM-D5D siRNA nanoparticles in the YAP1/TAZ pathway in tumor tissues by Western analysis. We found that 3WJ-EpCAM-D5D siRNA nanoparticle alone or combined with DGLA could significantly decrease the protein expression of YAP1 ($p<0.05$), CTGF ($p<0.01$), and Cyr61 ($p<0.05$) in lung tumor tissues from nude mice (Fig. 45). Additionally, the protein expression of TAZ was significantly inhibited by the combination of DGLA and 3WJ-EpCAM-D5D siRNA nanoparticles in lung tumor tissues ($p<0.05$, Fig. 45A). Given the key role of the YAP1/TAZ pathway in tumor development, we believe that the combination of DGLA and 3WJ-EpCAM-D5D siRNA nanoparticles could inhibit lung tumor progression via down-regulate YAP1/TAZ pathway.

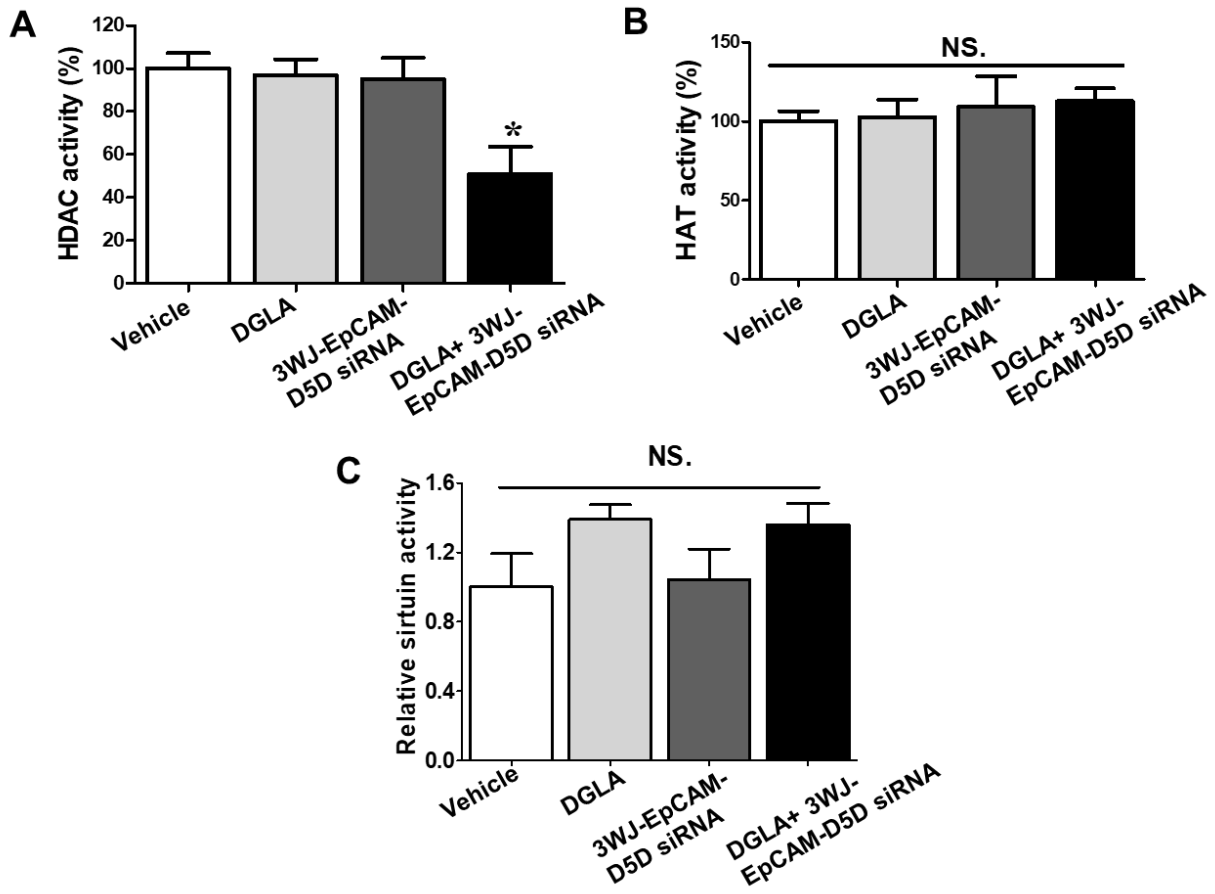

Figure 44. 3WJ-EpCAM-D5D siRNA nanoparticle inhibited HDAC activity in tumor tissues. (A) HDAC activity, (B) HAT activity, and (C) sirtuin activity in tumor tissues were determined by enzymatic assays. Data represent mean ± SEM for n=6. $^{*}P<0.05$ *vs* Vehicle group. NS. Not Significant *vs* Vehicle group.

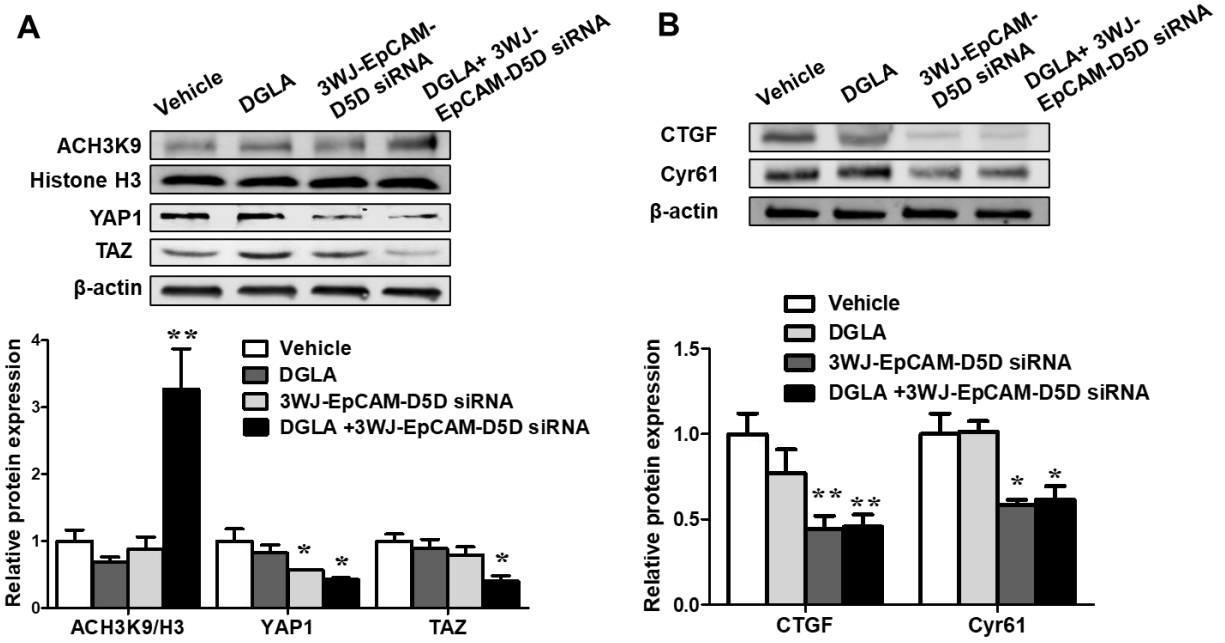

Figure 45. 3WJ-EpCAM-D5D siRNA nanoparticle inhibited HDAC and YAP1/TAZ pathway in tumor tissues. (A) Relative protein expression of ACH3K9, Histone H3, YAP1, and TAZ in lung tumor tissues. The relative protein expression to β-actin in the Vehicle group was normalized to 1. The ratio of ACH3K9 to Histone H3 was calculated. (B) Relative protein expression of CTGF and Cyr61 in lung tumor tissues. Data represent mean ± SEM for n=3. $^{*}P<0.05$, $^{**}P<0.01$ *vs* Vehicle group.

5.11. 3WJ-EpCAM-D5D siRNA Nanoparticle Regulated Apoptosis and Metastasis in Lung Tumor Tissues

To determine the effect of 3WJ-EpCAM-D5D siRNA nanoparticle on apoptosis *in vivo*, we evaluated the protein expression of procaspase-9, procaspase-3, BAX, cleaved PARP, and p53 in tumor tissues from nude mice treated DGLA and 3WJ-EpCAM-D5D siRNA nanoparticles for 4 weeks. We found that the combination of DGLA and 3WJ-EpCAM-D5D siRNA nanoparticle significantly decreased the protein expression of procaspase-3 ($p<0.001$) and procaspase-9 ($p<0.01$, Fig. 46), indicating the cleavage of caspases and activation of intrinsic apoptosis. However, the BAX ($p<0.001$), cleaved PARP ($p<0.001$), and p53 ($p<0.01$) protein expression was significantly increased in tumor tissues from nude mice treated with the combination of DGLA and 3WJ-

EpCAM-D5D siRNA nanoparticle (Fig. 46), suggesting that DNA damage and apoptosis were p53 dependent. Additionally, the significant reduction of cleaved PARP expression was also confirmed in lung tumor tissues by immunofluorescence analysis (p<0.001, Fig. 47). Interestingly, the percentage of Ki-67 positive cells was significantly decreased in tumor tissues from mice treated with DGLA and 3WJ-EpCAM-D5D siRNA nanoparticle (p<0.001, Fig. 47), implicating that D5D inhibition could decrease cell proliferation in lung tumor tissues.

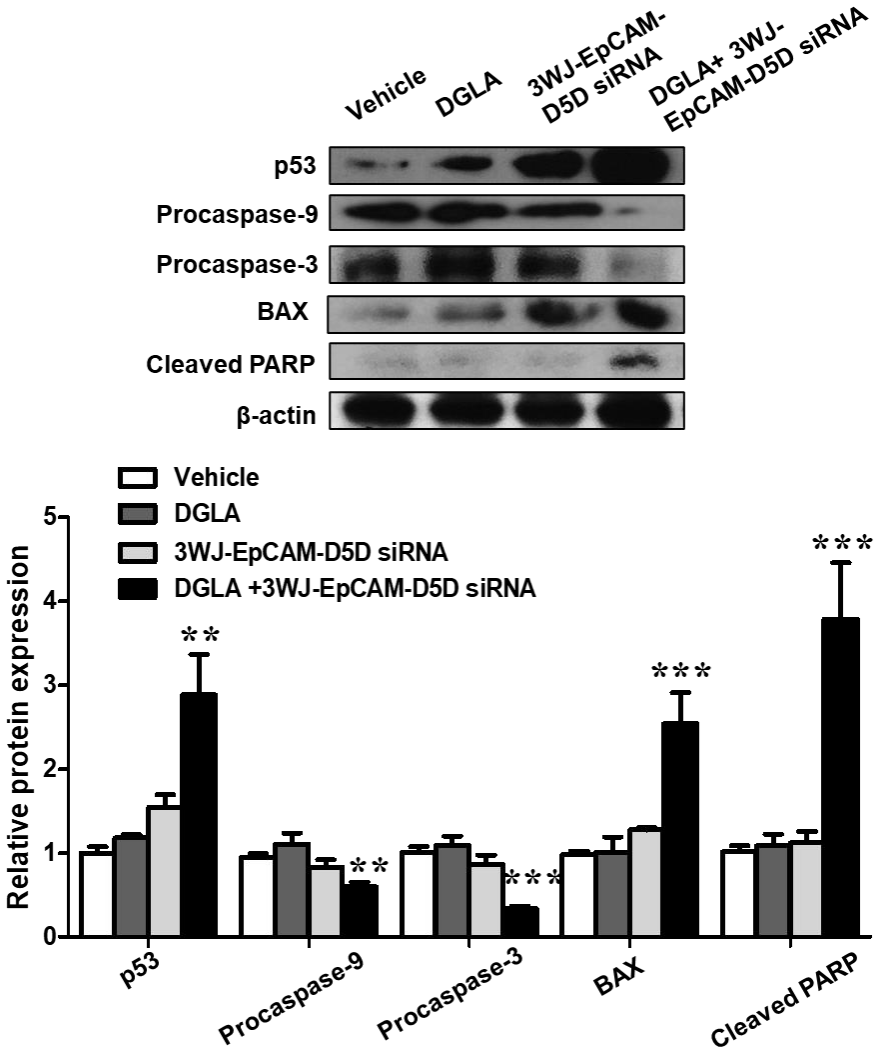

Figure 46. 3WJ-EpCAM-D5D siRNA nanoparticle-induced apoptosis in tumor tissues. Relative protein expression of p53, procaspase-9, procaspase-3, BAX, and cleaved PARP in lung tumor tissues. The relative protein expression to β-actin in the Vehicle group was normalized to 1. Data represent mean ± SEM for n=3. $^{**}P$<0.01, $^{***}P$<0.001 *vs* Vehicle group.

To investigate the effect of the 3WJ-EpCAM-D5D siRNA nanoparticle on metastasis of lung cancer cells, we determined the protein expression of MMP-2 and E-cadherin in lung tumor tissues by immunofluorescence analysis. We observed that the combination of DGLA and 3WJ-EpCAM-D5D siRNA nanoparticle significantly decreased the expression of MMP-2 in tumor tissues ($p<0.05$, Fig. 47). MMP-2 is the vital enzyme in cancer cells to degrade the extracellular matrix, facilitating the migration of cancer cells [156,157]. Thus, the reduction of MMP-2 implicated that the combination of DGLA and 3WJ-EpCAM-D5D siRNA nanoparticles could protect the extracellular matrix in tumor tissues. However, we found that the combination of DGLA and 3WJ-EpCAM-D5D siRNA nanoparticle significantly improved the protein expression of E-cadherin in lung tumor tissues ($p<0.01$, Fig. 47). Given the key role of E-cadherin in epithelial-mesenchymal transition [158,159], 3WJ-EpCAM-D5D siRNA nanoparticles may prevent lung cancer metastasis via strengthening cell-cell adhesion in tumor tissues. Furthermore, we evaluated the activity of pro-MMP-9, MMP-9, pro-MMP-2, and MMP-2 in lung tumor tissues by zymogram analysis. The combination of DGLA and 3WJ-EpCAM-D5D siRNA nanoparticle significantly inhibited the activity of MMP-9 ($p<0.05$) without influencing the activity of pro-MMP-9 (Fig. 48). While the activity of both pro-MMP-2 and MMP-2 can be significantly suppressed by 3WJ-EpCAM-D5D siRNA nanoparticle and the combination of DGLA and 3WJ-EpCAM-D5D siRNA nanoparticle ($p<0.05$, Fig. 48). Therefore, we may conclude that the 3WJ-EpCAM-D5D siRNA nanoparticle could prevent lung cancer metastasis by inhibiting the expression and activity of MMPs.

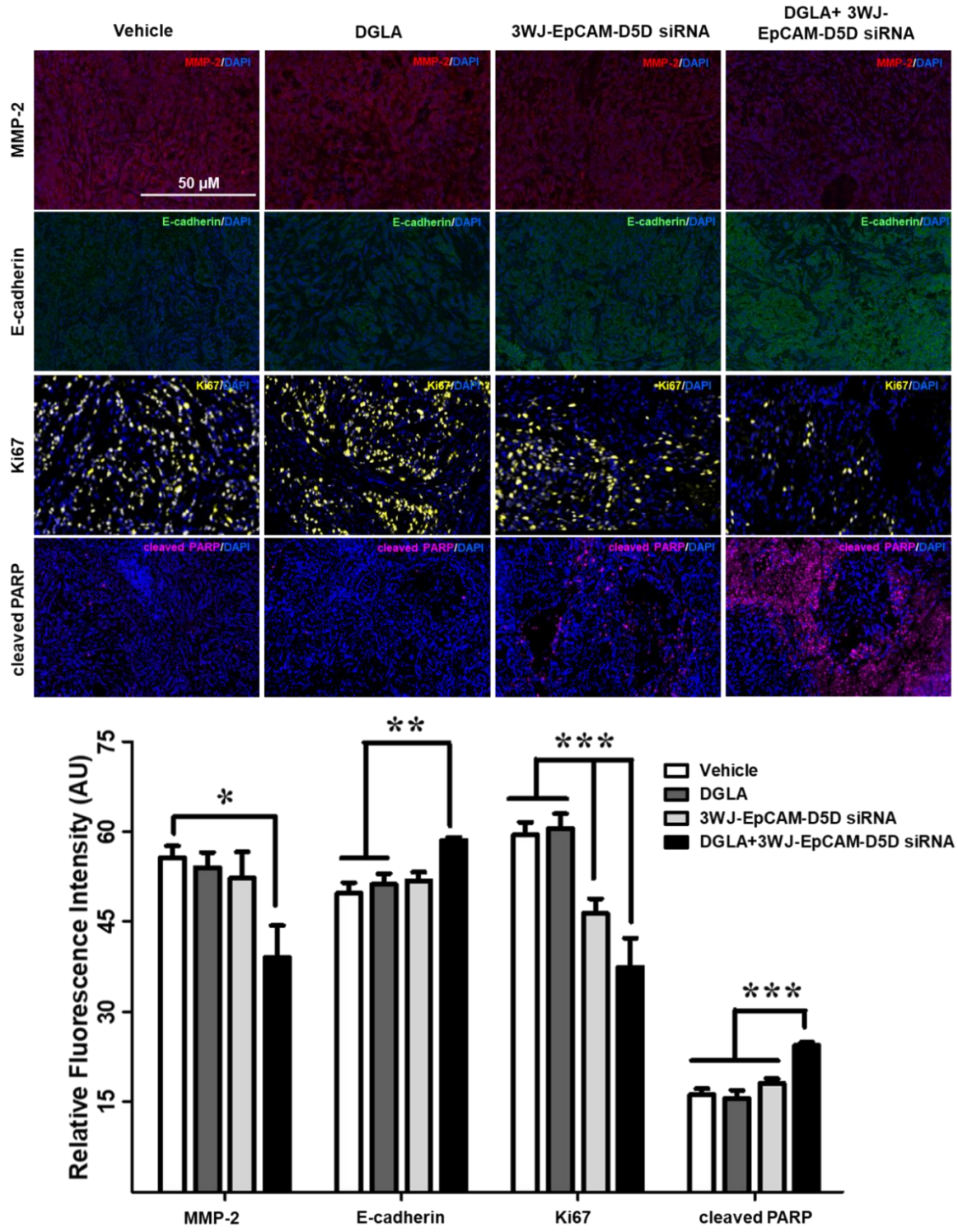

Figure 47. The expression of MMP-2, E-cadherin, Ki-67, and cleaved PARP was determined by immunofluorescence analysis. MMP-2 was stained in red, E-cadherin in green, Ki-67 in yellow, cleaved PARP in violet, and cell nuclei were counter-stained with DAPI. Data represents mean ± SEM for n=6. $^{***}P<0.001$, $^{**}P<0.01$, $^{*}P<0.05$ *vs* Vehicle group.

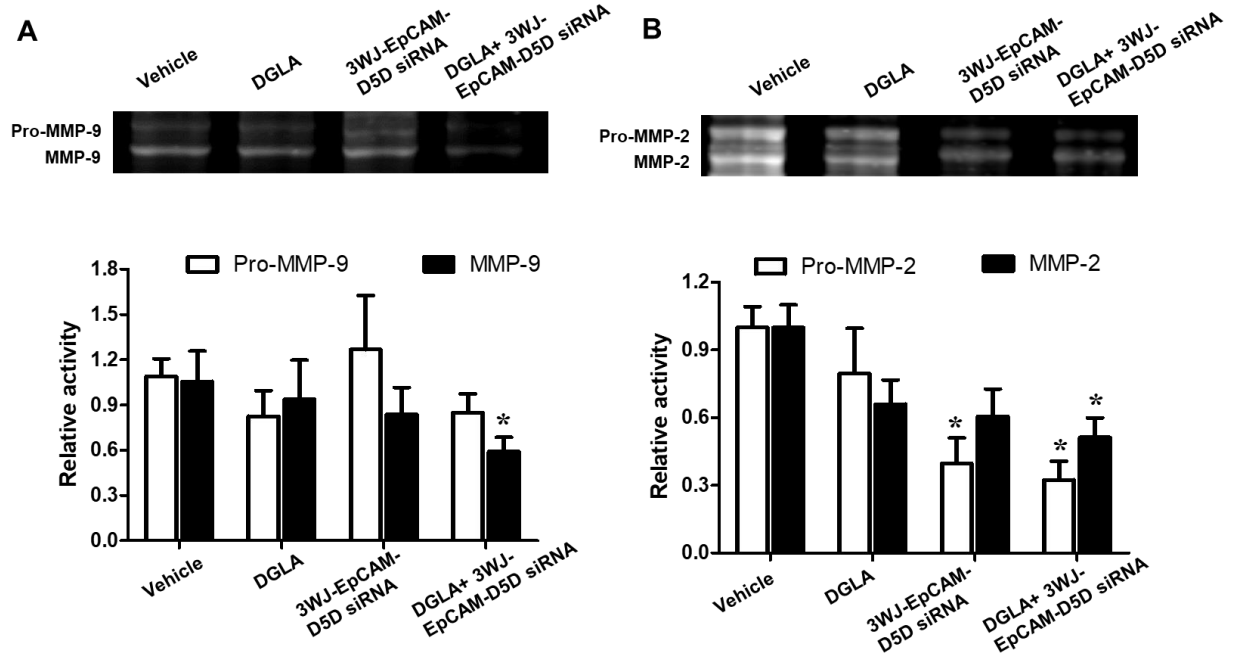

Figure 48. 3WJ-EpCAM-D5D siRNA nanoparticle suppressed the activity of MMPs in tumor tissues. The activity of (A) pro-MMP-9/MMP-9 and (B) pro-MMP-2/MMP-2 were determined by zymogram. Data represent mean ± SEM for n=6. $^{*}P<0.05$ *vs* Vehicle group.

5.12. 3WJ-EpCAM-D5D siRNA Nanoparticle Avoided to Damage Other Organs of Nude Mice

To investigate the safety of 3WJ-EpCAM-D5D siRNA nanoparticles in animals, we performed H&E staining on the major organs of nude mice, including the heart, kidneys, liver, lung, and spleen. We did not observe any remarkable pathological change in the above-listed organs from mice treated with either DGLA or 3WJ-EpCAM-D5D siRNA nanoparticle (Fig. 49). Moreover, we monitored the change of body-weight of nude mice during 4 weeks of treatment. We observed that the body-weight of nude mice was in the normal range after treatment for all the groups (Fig. 50A), suggesting no general toxicity of DGLA and 3WJ-EpCAM-D5D siRNA nanoparticle in nude mice. Furthermore, to assess the hepatotoxicity of the 3WJ-EpCAM-D5D siRNA nanoparticle, we measured the activity of ALT and AST, which are biomarkers of liver damage, in the serum of mice at end of 4 weeks of treatment. We observed that neither DGLA nor

3WJ-EpCAM-D5D siRNA nanoparticles could change the activity of ALT and AST in the blood of nude mice (Fig. 50B), suggesting no hepatotoxicity of this D5D-inhibition-based strategy in the animal model.

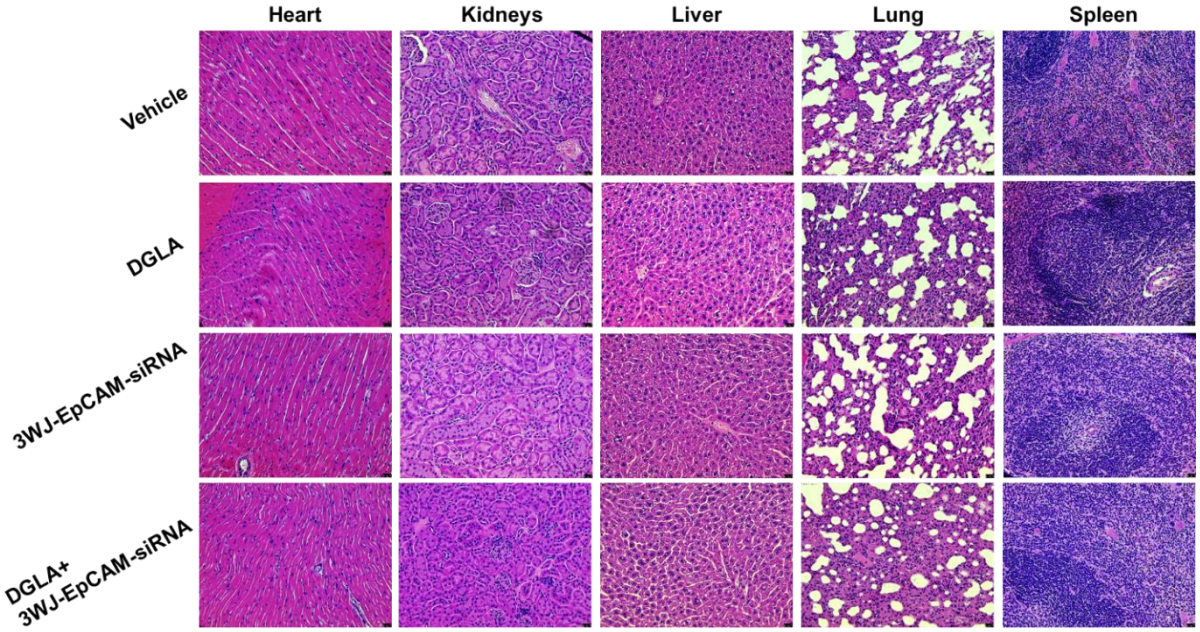

Figure 49. Hematoxylin and eosin **(**H&E) staining for organs harvested from nude mice at the end of the treatment. H&E of tissue sections of nude mice subjected to the vehicle, DGLA, and/or 3WJ-EpCAM-D5D siRNA nanoparticle treatment for 4 weeks (n=3).

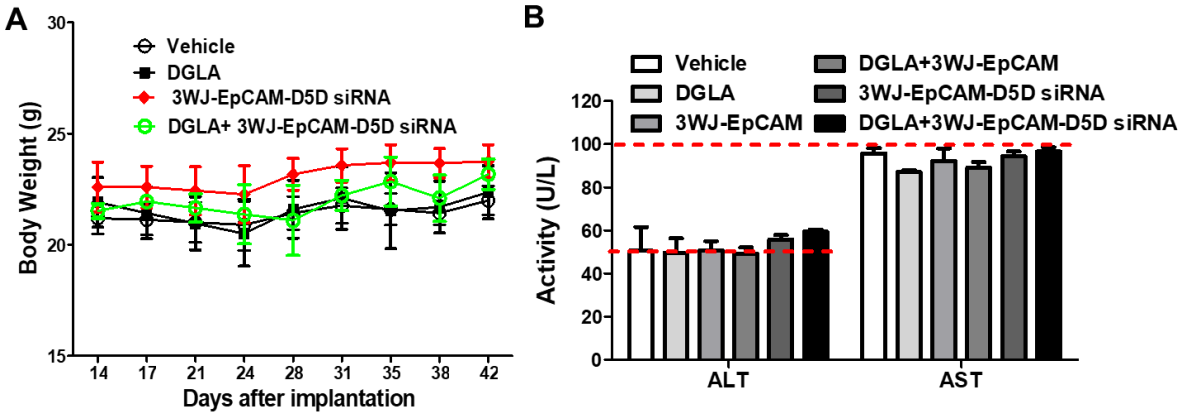

Figure 50. Toxicity test of the 3WJ-EpCAM nanoparticle. (A) Body weight of nude mice treated with 3WJ-EpCAM-D5D siRNA nanoparticles from starting of treatment (14 days) to end of treatment (42 days). (B) Alanine aminotransferase (ALT) and aspartate aminotransferase (AST) activity colorimetric assay quantification of ALT and AST level from blood. Data represent mean ± SEM, n=6.

5.13. Conclusion and Discussion

In our previous studies, we have reported that D5D siRNA transfection could slow down the development of colon and pancreatic cancer [12,16]. However, the siRNA is vulnerable to the nuclease (RNase) during *in vivo* administration, restricting the application of siRNA in clinical practice. Moreover, compared to other organs, kidneys could accommodate more siRNA molecules, resulting in a high elimination rate [160]. Thus, the siRNA-based therapy is confined by the poor bioavailability and *in vivo* efficiency [18]. Various nanoparticle-based delivery systems have been proposed to improve the *in vivo* efficiency of siRNA, such as polymer matrix, RNA/DNA nanoparticle, and liposomes for delivering siRNA to tumor tissues [125,129]. Compared to other systems, RNA nanoparticles has better biocompatibility, since they are composed of nucleotides [146]. Indeed, we did not observe major pathologic changes in organs from mice treated with DGLA and/or 3WJ-EpCAM-D5D siRNA nanoparticles for 4 weeks. It is consistent with the previous studies, in which RNA nanoparticles were assembled with different functional sequences [94]. In this study, we added D5D siRNA, EpCAM aptamer, and Alexa 647, all in one multivalent structure of RNA nanoparticles. By binding of EpCAM, 3WJ RNA nanoparticles could selectively recognize and enter lung cancer cells without disturbing surrounding normal lung epithelial cells. The internalization of the 3WJ-EpCAM-D5D siRNA nanoparticle could further trigger the generation of 8-HOA from COX-2 catalyzed DGLA peroxidation in lung cancer cells.

Diet is one of the vital factors influencing cancer progression. The recommended ratio of n-6 to n-3 PUFAs in a healthy diet is about 4 to 1 or even less. However, in most western diets, the ratio of n-6/n-3 is remarkably higher, for example, ~20 to 1 in certain diets. Unfortunately, high n-6 fatty acid uptake may cause cancer development [161]. One possible explanation is that

AA and PGE_2 can be derived from COX-2 catalyzed n-6 fatty acid (such as DGLA) peroxidation, resulting in the proliferation of cancer cells and immunosuppression via regulating TME. For instance, the PGE_2 could activate the EGFR signaling pathway, promoting cancer cell migration through activating MMPs in cancer cells [4,162]. Interestingly, we also found that the combination of DGLA and 3WJ-EpCAM-D5D siRNA nanoparticles inhibited the expression and activity of MMP-2 and MMP-9 in lung tumor tissues. The suppression of MMPs also implicated the low PGE_2 level in tumors. In addition, 8-HOA production was improved in lung cancer cells by the 3WJ-EpCAM-D5D siRNA nanoparticle. We found that D5D inhibition also could activate apoptosis but inhibit migration and proliferation via inducing 8-HOA generation in lung tumor tissues. Taking together, we established a novel treatment strategy for lung cancer by taking advantage of the high COX-2 expression in cancer cells to redirect DGLA peroxidation. Furthermore, the 3WJ-EpCAM RNA nanoparticle overcame the disadvantages of naked siRNA in cancer therapy. The excellent chemical and thermodynamical stability of the 3WJ RNA core guaranteed the functional integrity and effectiveness of D5D siRNA *in vivo* during 4 weeks of treatment. Moreover, EpCAM aptamer in 3WJ RNA nanoparticle allowed the specific internalization of D5D siRNA into lung cancer cells. Consequently, we did not observe any significant toxicity, off-target effect, and unexpected immune responses in nude mice. We believe that the safety of 3WJ-EpCAM RNA nanoparticle may be attributed to the selectively cytotoxicity of RNA nanoparticle in lung cancer cells with a double positive expression of COX-2 and EpCAM.

6. SUMMARY, DISCUSSION, AND FUTURE DIRECTION

6.1. The Role of DGLA-derived Free Radical Byproduct (8-HOA) in Lung Cancer

We have previously demonstrated that the free radical byproduct 8-HOA could be derived from DGLA by COX-2, suppressing colon and pancreatic cancer growth [10–13,15]. In this study, we expanded the benefit of 8-HOA into lung cancer, which is the second most common cancer worldwide. Although the mortality of lung cancer is decreasing due to advances in early detection and treatment, it is still the leading cause of cancer death among all types of cancers [1]. Therefore, the development of alternative strategies and supplementary treatments is urgent for lung cancer. To investigate the effect of 8-HOA on lung cancer, we assessed the survival fraction, cell viability, apoptosis rate, the migration rate of lung cancer cells *in vitro* by colony formation, MTT, PI/Annexin V double staining, transwell migration, and wound healing assay. Exogenous 8-HOA (1 μM) significantly suppressed the cell viability of A549 and H1299 lung cancer cells. Additionally, 8-HOA caused a ~40% reduction of survival fraction in H1299 and A549 cells. Not only proliferation, but the migration ability of lung cancer cells was also suppressed by 8-HOA. Additionally, we observed that 8-HOA could activate apoptosis in lung cancer cells. We monitored the real-time change of apoptosis in A549 cells treated with 8-HOA by using the pSIVA probe in a time-lapse Lionheart FX Automated Microscope. The percentage of apoptotic lung cancer cells was continuously increased by 8-HOA, indicating the long-term effectiveness of 8-HOA on inducing apoptosis in lung cancer.

To further elucidate the mechanism of 8-HOA on lung cancer, we measured the protein expression of Bcl-2, BAX, procaspase-3, procaspase-9, and p53 in A549 lung cancer cells treated with 8-HOA. Bcl-2 and BAX are belonging to the Bcl-2 family, which is the most critical gene/protein family in regulating apoptosis, especially in cancer cells [104]. However, the effect

of Bcl-2 and BAX on apoptosis is the opposite. Bcl-2 could affect mitochondrial dynamics and inhibit the pro-apoptotic proteins, such as BAX, resulting in the survival of cancer cells. Thus, the ratio of BAX to Bcl-2 is a vital standard for evaluating apoptosis in cells. The cancer cells used to have a low BAX/Bcl-2 ratio as inhibition of apoptosis [105]. However, we observed that 8-HOA could up-regulate the ratio of BAX/Bcl-2 by simultaneously increasing the protein expression of BAX and decreasing the protein expression of Bcl-2. Therefore, 8-HOA may suppress the survival of lung cancer cells via regulating molecules in the Bcl-2 family. Given the important role of Bcl-2 in mitochondrial [163], we further explored the effect of 8-HOA on intrinsic apoptosis, which is also known as the mitochondrial apoptosis pathway. Indeed, 8-HOA decreased the protein expression of procaspase-3 and procaspase-9, which are key enzymes in the intrinsic pathway. Moreover, the p53 protein expression was increased by 8-HOA, suggesting that the effect of 8-HOA on intrinsic apoptosis is p53 dependent. Additionally, we observed that 8-HOA could enhance the effect of cisplatin on apoptosis in lung cancer cells. By using "One-belt, one-line" model and HSA model, we confirmed that the effect of 8-HOA and cisplatin on cell viability and survival of lung cancer cells is synergistic. Given that cisplatin is a DNA damage reagent [99,102,113], we believe that 8-HOA may inhibit cancer growth via damaging DNA or regulating epigenetic modifications.

Since we demonstrated that 8-HOA could regulate many aspects of cancer development, such as proliferation, survival, migration, and apoptosis, we hypothesis that the effect of 8-HOA on lung cancer may be attributed to upstream epigenetic molecules, such as HDAC, which is a core enzyme for regulating cell survival and proliferation. We plotted the dose-response curve of 8-HOA to HDAC activity in lung cancer cells and calculated IC_{50} accordingly. Consequently, we identified that 8-HOA could serve as an HDAC inhibitor. Although 8-HOA does not affect the

activity of sirtuins (type III HDAC), the overall HDAC activity could be suppressed by exogenous 8-HOA. Furthermore, another upstream pathway, YAP1/TAZ pathway also could be regulated by 8-HOA in lung cancer cells. YAP1/TAZ is under the Hippo pathway, which is the main pathway that determines organ size by balancing proliferation and apoptosis [107,164–166]. The YAP1/TAZ pathway can be activated and translocated into nuclear when Hippo is off in cancer cells, resulting in proliferation and inhibition of apoptosis [68,106,167]. We found that 8-HOA could inhibit the protein expression of YAP1/TAZ in the early stage, decreasing the protein expression of a downstream molecule, CTGF in lung cancer cells. Taken together, we demonstrated that 8-HOA could inhibit lung cancer cell proliferation, migration, and promote apoptosis via regulating HDAC activity and YAP1/TAZ pathway. These findings encouraged us to continuously explore the effectiveness of DGLA-derived endogenous 8-HOA on lung cancer cells.

6.2. Inhibition of Lung Cancer Cell Growth via Promoting the Formation of 8-HOA from COX-2-catalyzed DGLA Peroxidation by Knocking Down D5D Expression

Despite the inhibitory effect of 8-HOA on lung cancer, we noticed that the effectiveness of exogenous 8-HOA is modest (≤50%) in regulating lung cancer cell proliferation, migration, and apoptosis. Notably, the exogenous 8-HOA is not the free radical form, whereas the DGLA-derived endogenous 8-HOA is generated in the free radical form in cancer cells [76,77]. Although the free radical form is transient, it may provide extra benefit than the exogenous form 8-HOA in cancer therapy. Therefore, we developed a new anti-cancer strategy to trigger the production of endogenous 8-HOA in cancer cells to kill lung cancer cells themselves. In Scheme 3, we showed that D5D could catalyze DGLA, producing AA in normal cellular conditions. In lung cancer cells, AA can be catalyzed by COX-2 to form PGs, including PGE_2, resulting in cancer progression.

However, we have found that DGLA also can be directly catalyzed by COX-2 to generate 8-HOA, which is in the free radical form [77]. To enforce the formation of 8-HOA from DGLA, we inhibited D5D expression in lung cancer cells by D5D siRNA. The D5D siRNA transfection significantly decreased the protein expression of D5D in lung cancer cells, shifting the DGLA to AA ratio from ~8.2 to ~19.1 in A549 cells. In this scenario, DGLA is unable to efficiently convert to AA in lung cancer cells, resulting in 8-HOA formation in lung cancer cells.

We observed that D5D siRNA transfection displayed better effectiveness on lung cancer *in vitro* than the exogenous 8-HOA. The D5D knockdown resulted in a ~93% reduction of survival faction in lung cancer cells, whereas exogenous 8-HOA led to a ~31% reduction; the D5D knockdown resulted in ~30% change of wound healing rate in lung cancer cells, whereas exogenous 8-HOA led to a ~28% reduction. Moreover, we found that D5D knockdown also could promote the protein expression of p53 and BAX and decrease the protein expression of procaspase-3 and procaspase-9, inducing apoptosis in lung cancer cells. To validate the mechanism of D5D inhibition in lung cancer, we also measured the protein expression of AcH3K9, YAP1, TAZ, and CTGF in A549 cells treated with D5D siRNA and DGLA by Western analysis. Consistent with the effect of exogenous 8-HOA, DGLA-derived 8-HOA also suppressed the YAP1/TAZ pathway and HDAC activity in lung cancer cells. Therefore, we may conclude that D5D inhibition could lead to the production of 8-HOA, resulting in suppression of proliferation, migration, and activation of apoptosis in lung cancer cells via down-regulating YAP1/TAZ pathway and HDAC activity.

6.3. Therapeutic Outcomes of DGLA Supplementation and 3WJ-RNA Nanoparticles on Lung Cancer

We have demonstrated the effectiveness of D5D siRNA on lung cancer *in vitro*. However, the *in vivo* application of D5D siRNA is still challenged by several disadvantages, such as off-target effect, poor pharmacokinetic profile, and low stability [125,137]. To expand the clinical benefit of the D5D inhibition-based strategy for cancer patients, we innovatively applied the RNA nanoparticle system to stabilize and deliver the D5D siRNA to the lung cancer cells. The effectiveness of D5D siRNA-loaded RNA nanoparticles has been investigated in both *in vitro* and *in vivo* models.

Due to the limitations of naked siRNA, various delivery systems and methods have been developed to facilitate siRNA-based gene therapy, such as LNPs, peptide-based systems, polymers, RNA nanoparticles, and GalNAc conjugates, of which RNA nanoparticle is one of the most advanced delivery systems for siRNA therapy [123,136]. RNA nanoparticles can be assembled by a level of simplicity characteristic of DNA [138,139]. Moreover, RNA nanoparticles have various tertiary structures and catalytic functions that mimic proteins [140,141]. 3WJ RNA nanoparticles could be resistant to denaturation in 8M urea. Additionally, the integrity of 3WJ RNA nanoparticles cannot be altered in ultra-low concentrations *in vitro* and *in vivo*, indicating the excellent chemical stability and thermodynamic stability of the 3WJ RNA nanoparticle [146].

In this study, we assembled EpCAM aptamer to the 3WJ RNA nanoparticle as a targeting module, Alexa 647 as an imaging module, and D5D siRNA as a therapeutical module. The cell binding and internalization studies suggested that 3WJ-EpCAM-D5D siRNA nanoparticles could specifically deliver D5D siRNA to lung cancer cells with high EpCAM expression, whereas it could avoid knockdown the D5D expression in normal lung epithelial cells with relatively low

EpCAM expression, protecting healthy cells from off-target effect. Consistent with the result of D5D siRNA transfection, 3WJ-EpCAM-D5D siRNA nanoparticle also redirected the COX-2-catalyzed DGLA peroxidation, leading to high production of 8-HOA and low PGE_2 in lung cancer cells. Consequently, 3WJ-EpCAM-D5D siRNA nanoparticles suppressed the proliferation and survival of lung cancer cells. Moreover, we demonstrated that both COX-2 and EpCAM are essential for eliciting the effect of 3WJ-EpCAM-D5D siRNA nanoparticles on lung cancer. EpCAM is the target for anchoring and internalizing 3WJ-EpCAM-D5D siRNA nanoparticles into lung cancer cells. While COX-2 is the core enzyme to catalyze 8-HOA formation from DGLA in lung cancer cells. Lacking either factor could impede the efficiency of 3WJ-EpCAM-D5D siRNA nanoparticles in inhibiting lung cancer. Furthermore, we investigated the *in vivo* biodistribution of 3WJ-EpCAM-D5D siRNA nanoparticles in xenograft lung tumor models in nude mice. The 3WJ-EpCAM-D5D siRNA nanoparticle could specifically be uptake by tumor tissues, whereas low to no distribution of 3WJ-EpCAM-D5D siRNA nanoparticles has been observed in other vital organs, including the heart, kidneys, lung, and liver. The high tumor selectivity of the 3WJ-EpCAM-D5D siRNA nanoparticle resulted in more 8-HOA production in tumor tissues than in other organs. The treatment of 3WJ-EpCAM-D5D siRNA nanoparticles caused a ~69% reduction of tumor size in 4 weeks. We observed that the HDAC activity and YAP1/TAZ pathway were down-regulated by 3WJ-EpCAM-D5D siRNA nanoparticle in tumor tissues, implicating that RNA nanoparticle triggered the same mechanism *in vivo* as we observed *in vitro*. Moreover, 3WJ-EpCAM-D5D siRNA nanoparticle inhibited the protein expression of MMP-2 and activity of MMP-2/MMP-9, whereas the expression of E-cadherin was increased by RNA nanoparticle, suggesting the suppression of cancer metastasis. To investigate the safety of 3WJ-EpCAM-D5D siRNA nanoparticles in animals, we performed H&E staining on major organs of nude mice, including

the heart, kidneys, liver, lung, and spleen. We did not observe any remarkable pathological change in the vital organs from mice treated with either DGLA or 3WJ-EpCAM-D5D siRNA nanoparticles. Moreover, we monitored the change of body-weight of nude mice during 4 weeks of treatment. Furthermore, we observed that neither DGLA nor 3WJ-EpCAM-D5D siRNA nanoparticles could change the activity of ALT and AST in the blood of nude mice, suggesting no hepatotoxicity of this D5D-inhibition-based strategy in the animal model.

6.4. Conclusion and Discussion

Lung cancer is the second most common cancer and the leading cause of cancer death in both men and women. About 80% to 85% of lung cancers are NSCLC. A variety of therapeutic and adjuvant approaches have so far been studied for lung cancer, including chemotherapy, targeted therapy, COX-2 inhibition, and n-3 fatty acid dietary manipulation [1,2]. Despite n-6 fatty acids are more widespread in our daily diet, n-6s-based dietary strategies in cancer treatment have not yet been well developed.

COX is a bi-functional membrane-bound enzyme that typically metabolizes AA in two steps to PGE_2. The inducible form COX-2 can readily be induced by stresses, pro-inflammatory signals, growth factors, and tumor promoters [4]. COX-2 expression is also associated with cancer invasion and has prognostic significance in tumor metastasis [73,168]. The substrate molecule PGE_2 has been reported to promote cancer invasion through the up-regulation of MMPs expression. The classic strategy is using COX-2 inhibitors to suppress the commonly high COX-2 expression in cancer cells, limiting COX-2-catalyzed AA peroxidation and subsequent PGE_2 formation [3,4]. However, many COX-2 inhibitors suffer from safety issues and limited clinical responses [5,6]. To improve the clinical management of lung cancer, there is a critical need to

advance alternative strategies addressing both the overexpression of COX-2 in cancer cells and the inevitable COX-2-catalyzed peroxidation of n-6 PUFAs.

Therefore, instead of direct COX-2 inhibition, our new concept takes advantage of overexpressed COX-2 in an entirely different way. DGLA is one of the precursors of AA. The formation of AA from DGLA is catalyzed by D5D. By blocking DGLA/AA conversion, the accumulated precursor, DGLA, can form 8-HOA by COX-2-catalyzed peroxidation. In this study, we found that exogenous 8-HOA can inhibit proliferation, survival, migration, and induce apoptosis in lung cancer cells. Additionally, exogenous 8-HOA could enhance the efficacy of cisplatin on inhibiting lung cancer cell proliferation and survival in a synergistic pattern. This new strategy considers the COX-2 overexpression as a favorable factor rather than trouble, because more COX-2 could stimulate more 8-HOA production in lung cancer cells. To activate endogenous 8-HOA formation, we supplemented DGLA to D5D knockdown lung cancer cells. The DGLA-derived 8-HOA also suppressed proliferation, survival, migration, and activated apoptosis in lung cancer cells. However, the application of RNAi-based treatment *in vivo* and in patients is limited by stability, off-target effect, and unexpected immune response. To realize D5D inhibition *in vivo*, in this study, we combined the novel COX-2 cancer biology concept with innovative 3WJ-EpCAM-D5D siRNA nanoparticles to deliver the therapeutic D5D siRNA specifically to lung tumors. 3WJ-EpCAM-D5D siRNA nanoparticles not only suppressed lung cancer development *in vivo* and *in vitro* effectively, but also avoid the side effects and off-target effects. We also explored the possible mechanism of 3WJ-EpCAM-D5D siRNA nanoparticles in lung cancer. 3WJ-EpCAM-D5D siRNA nanoparticles could specifically target lung cancer cells with high EpCAM expression, resulting in inhibition of D5D expression and the paradigm shift of COX-2 catalyzed DGLA peroxidation pattern. Consequently, the DGLA supplementation and 3WJ-EpCAM-D5D

siRNA nanoparticles successfully promoted the formation of 8-HOA in lung cancer cells, inhibiting proliferation, survival, migration, and inducing apoptosis via suppressing HDAC activity and YAP1/TAZ pathway. Given the fact that lung cancer cells not only express much higher COX-2 levels, but also have a greater need for fatty acids as nutrition during their growth, our strategy generated an effective outcome and paved the road to COX-2-based precise medicine for lung cancer therapy.

6.5. Limitation and Future Direction

6.5.1. Limitation of the Study

In this study, we evaluated the effect of 3WJ RNA nanoparticles on nude mice with xenografted lung tumors. Although subcutaneous xenograft nude mouse is the most common animal model in cancer research, it is limited by the immunocompromised murine background, and metastasis cannot be evaluated with respect to targeted therapies. To comprehensively evaluate the effect of 3WJ RNA nanoparticles on lung cancer metastasis, the tumor syngeneic animal model may need to be employed. Additionally, we only monitored the toxic responses of nude mice in 4 weeks of treatment, the long-term toxicity and true immune responses of the 3WJ RNA nanoparticle *in vivo* are still underexplored. Although we demonstrated that the 3WJ RNA nanoparticle redirected DGLA peroxidation in lung tumor tissues, resulting in 8-HOA formation, other signaling pathways may also be regulated by RNA nanoparticles, such as PI3K/Akt/mTOR pathway and ferroptosis.

6.5.2. To Design and Synthesis Specific D5D Small Molecule Inhibitor

In this study, we used D5D siRNA and 3WJ-EpCAM-D5D siRNA nanoparticles to knock down the expression of D5D in lung cancer cells *in vitro* and *in vivo.* Although 3WJ-EpCAM-D5D siRNA nanoparticles are efficient in targeting and inhibiting lung tumors in nude mice, we

are still expecting to design and synthesis a D5D small molecule inhibitor. Previous studies have reported few D5D small molecule inhibitors, including natural compounds and synthetic products. For instance, sesame, curcumin, and CP-24879 have been reported with D5D inhibition activity [82–84]. However, none of these molecules could specifically suppress D5D activity without affecting other fatty acid desaturases, such as D6D and D12D. Takeda Pharmaceutical Company recently discovered a series of specific D5D inhibitors, such as D5D-IN-326, T-3364366, and 3,5-diphenyl-4-methyl-1,3-oxazolidin-2-ones. While these molecules have only been evaluated in other disease models (such as insulin resistance, obesity, and atherosclerosis) rather than cancer [85–88]. Despite the advancement of macromolecule therapy, small molecule inhibitor is still superior in cost performance, stability, and accessibility. Therefore, the development of the specific D5D inhibitor for cancer treatment may expand the clinical benefit of the D5D-inhibition based strategy to cancer patients.

We recently identified and patented a new small molecule D5D inhibitor iminodibenzyl [89]. Our *in vivo* and *in vitro* preliminary study has demonstrated that the combination of iminodibenzyl and DGLA could significantly suppress tumor growth via regulating cancer cell proliferation, survival, migration, and apoptosis [79,169]. However, the PK profile, long-term toxicity, metabolism, and enzyme kinetics of iminodibenzyl are still unexplored. To understand the enzyme kinetics of iminodibenzyl, we may need to purify the D5D enzyme with high activity. Additionally, the poor solubility of iminodibenzyl limited the route of administration and application of iminodibenzyl in animal study. Therefore, we may synthesis a series of D5D inhibitors based on the basic structure of iminodibenzyl to maximum the strength of the D5D inhibition and improve the solubility of the D5D inhibitor.

6.5.3. To Investigate the Effect of 3WJ-EpCAM-D5D siRNA Nanoparticles on Patient-derived Xenografts (PDX) and Syngeneic Models

We evaluated the *in vivo* effect of 3WJ-EpCAM-D5D siRNA nanoparticles on lung cancer in xenograft lung tumor models in nude mice. In our future study, we may further investigate the effectiveness of 3WJ-EpCAM-D5D siRNA nanoparticles in the PDX model. PDX with early passages maintains cellular and genetic heterogenicity correlating to the patient and provides enough numbers of live tumor-bearing mice, allowing rapid study and faster decision-making [170,171]. Thus, PDX models are reliable preclinical models to test the effect of 3WJ-EpCAM-D5D siRNA nanoparticles on lung cancer. We propose to purchase patient-derived triple-negative PDX mouse models from Jackson Laboratories for the initial propagation and expansion of mice at the stage of ~ F1-F3. We will validate the expression of our target protein EpCAM in this PDX model tumor tissue before the expansion phase (F4-F6). The tumor size could be monitored by using a digital caliper and ultrasound imaging system.

To investigate the effect of 3WJ-EpCAM-D5D siRNA nanoparticles on lung cancer metastasis, we may employ the Lewis lung carcinoma (LLC)-based syngeneic model. LLC cells are derived from C57BL/6 mice. The subcutaneous injection of LLC cells could result in lung metastasis in C57BL/6 mice [172]. The LLC model may allow us to examine the effect and mechanism of 3WJ-EpCAM-D5D siRNA nanoparticles in animals with immunocompetent backgrounds and true immune and toxicity responses.

6.5.4. To Determine the PK Profile and Long-term Toxicity of 3WJ-EpCAM-D5D siRNA Nanoparticles

Although we demonstrated that 3WJ-EpCAM-D5D siRNA nanoparticles could inhibit lung tumor progression *in vivo*, we are still unclear about the PK profile and long-term toxicity of

3WJ-EpCAM-D5D siRNA nanoparticles. In future studies, we may investigate how 3WJ-EpCAM-D5D siRNA nanoparticles are internalized into cancer cells. For instance, the RNA nanoparticle may be transported into the cytoplasm by EpCAM recycling/internalization or non-receptor-mediated endocytosis [173]. The metabolism of RNA nanoparticles also needs to be explored. We may mark RNA nanoparticles with isotope and track the elimination parameters of 3WJ-EpCAM-D5D siRNA nanoparticles in animal models. Furthermore, the long-term toxicity of RNA nanoparticles needs to be investigated in future studies. Despite we did not observe toxicity and body-weight loss in nude mice during 4 weeks of the administration of 3WJ-EpCAM-D5D siRNA nanoparticles, we are still unclear about the long-term toxicity of RNA nanoparticles *in vivo*. Therefore, we may monitor the immune and toxicity responses of wild-type mice treating 3WJ-EpCAM-D5D siRNA nanoparticles for more than 6 months to profile the comprehensive toxicity data in animal.

6.5.5. To Further Explore Molecular Mechanism of D5D-inhibition-based Strategy in Cancer

In the current study, we investigated the mechanism of D5D-inhibition-based anti-cancer strategy in lung cancer in cell and animal models. 3WJ-EpCAM-D5D siRNA nanoparticles inhibited D5D expression and redirected the COX-2-catalyzed DGLA peroxidation pattern, resulting in 8-HOA production. 8-HOA could serve as an HDAC inhibitor and block the expression and nuclear translocation of YAP1 and TAZ, leading to down-regulate CTGF and Cyr61 in lung cancer cells. Given YAP1/TAZ are the primary downstream effectors of the Hippo pathway [165], we hypothesis that D5D inhibition may directly affect upstream molecules in the Hippo pathway, such as MST1/2, LAST1/2, and MOB1A/B. Additionally, YAP1/TAZ may also

be regulated by angiomotin, PTPN14 (protein tyrosine phosphatase non-receptor type 14), α-catenin, and scribble planar cell polarity protein (SCRIB) [174].

Furthermore, the effect of 3WJ-EpCAM-D5D siRNA nanoparticles on lung cancer may not exclusively depend on 8-HOA generation. A recent study suggested that D5D knockdown (without DGLA supplementation) could inhibit the proliferation, migration, and invasion of laryngeal squamous cell carcinoma cells via regulating the AKT/mTOR pathway [28]. Thus, we may also investigate the effect of 3WJ-EpCAM-D5D siRNA nanoparticles on the AKT/mTOR pathway in lung cancer cells. Moreover, to elucidate the alternative mechanisms of 3WJ-EpCAM-D5D siRNA nanoparticles, we may use POBN to capture and remove the DGLA-derived 8-HOA and other free radical products in lung cancer cells. This will allow us to identify the effect of 3WJ-EpCAM-D5D siRNA nanoparticles on other signaling pathways beyond 8-HOA. Additionally, the binding and inhibiting mechanism of 8-HOA to HDAC also needs to be explored. In this study, we demonstrated that 8-HOA may inhibit HDAC I, II, and IV activity in lung cancer cells. However, it is still unclear which specific subtype of HDAC is the primary substrate of 8-HOA. Therefore, we may test the inhibitory effect of 8-HOA on different HDAC substrate to evaluate the specificity of 8-HOA. The binding mechanism and interrelationship between 8-HOA and HDAC also can be determined by AutoDockTools, machine-learning systems, and transformative artificial intelligence (AI) tools, such as AlphaFold.

REFERENCES

[1] N. Howlader, A.M. Noone, M. Krapcho, D. Miller, A. Brest, M. Yu, J. Ruhl, Z. Tatalovich, A. Mariotto, D.R. Lewis, SEER Cancer Statistics Review, 1975-2016, National Cancer Institute. Bethesda, MD, National Cancer Institute. Bethesda, MD, 2019.

[2] Non-Small Cell Lung Cancer Treatment (PDQ®)–Health Professional Version, National Cancer Institute. (2019). https://www.cancer.gov/types/lung/hp/non-small-cell-lung-treatment-pdq (accessed January 13, 2020).

[3] J.-B. Méric, S. Rottey, K. Olaussen, J.-C. Soria, D. Khayat, O. Rixe, J.-P. Spano, Cyclooxygenase-2 as a target for anticancer drug development, Critical Reviews in Oncology/Hematology. 59 (2006) 51–64.

[4] K. Subbaramaiah, A.J. Dannenberg, Cyclooxygenase 2: a molecular target for cancer prevention and treatment, Trends in Pharmacological Sciences. 24 (2003) 96–102.

[5] H.J. Groen, H. Sietsma, A. Vincent, M.M. Hochstenbag, J.W. van Putten, A. van den Berg, O. Dalesio, B. Biesma, H.J. Smit, A. Termeer, Randomized, placebo-controlled phase III study of docetaxel plus carboplatin with celecoxib and cyclooxygenase-2 expression as a biomarker for patients with advanced non–small-cell lung cancer: the NVALT-4 study, Oncology. (2009).

[6] S.D. Solomon, J.J. McMurray, M.A. Pfeffer, J. Wittes, R. Fowler, P. Finn, W.F. Anderson, A. Zauber, E. Hawk, M. Bertagnolli, Cardiovascular risk associated with celecoxib in a clinical trial for colorectal adenoma prevention, New England Journal of Medicine. 352 (2005) 1071–1080.

[7] M.T. Nakamura, T.Y. Nara, Structure, function, and dietary regulation of δ6, δ5, and δ9 desaturases, Annu. Rev. Nutr. 24 (2004) 345–376.

[8] M. Matsuda, T. Kawamoto, R. Tamura, Predictive value of serum dihomo-γ-linolenic acid level and estimated Δ-5 desaturase activity in patients with hepatic steatosis, Obes Res Clin Pract. 11 (2017) 34–43. https://doi.org/10.1016/j.orcp.2016.02.004.

[9] V. Lamantia, S. Bissonnette, V. Provost, M. Devaux, Y. Cyr, C. Daneault, C.D. Rosiers, M. Faraj, The Association of Polyunsaturated Fatty Acid δ-5-Desaturase Activity with Risk Factors for Type 2 Diabetes Is Dependent on Plasma ApoB-Lipoproteins in Overweight and Obese Adults, J Nutr. 149 (2019) 57–67. https://doi.org/10.1093/jn/nxy238.

[10] Y. Xu, X. Yang, D. Gao, L. Yang, K. Miskimins, S.Y. Qian, Dihomo-γ-linolenic acid inhibits xenograft tumor growth in mice bearing shRNA-transfected HCA-7 cells targeting delta-5-desaturase, BMC Cancer. 18 (2018) 1268.

[11] X. Yang, Y. Xu, T. Wang, D. Shu, P. Guo, K. Miskimins, S.Y. Qian, Inhibition of cancer migration and invasion by knocking down delta-5-desaturase in COX-2 overexpressed cancer cells, Redox Biology. 11 (2017) 653–662.

[12] Y. Xu, X. Yang, P. Zhao, Z. Yang, C. Yan, B. Guo, S.Y. Qian, Knockdown of delta-5-desaturase promotes the anti-cancer activity of dihomo-γ-linolenic acid and enhances the efficacy of chemotherapy in colon cancer cells expressing COX-2, Free Radical Biology and Medicine. 96 (2016) 67–77.

[13] Y. Xu, J. Qi, X. Yang, E. Wu, S.Y. Qian, Free radical derivatives formed from cyclooxygenase-catalyzed dihomo-γ-linolenic acid peroxidation can attenuate colon cancer cell growth and enhance 5-fluorouracil′ s cytotoxicity, Redox Biology. 2 (2014) 610–618.

[14] Y. Xu, X. Yang, D. Gao, K. Miskimins, S. Qian, Suppressing Colon Cancer Growth in Xenograft Tumors via Knocking Down Delta-5-Desaturase and Exploiting High COX-2 Expression Levels in Cancer, Free Radical Biology and Medicine. 100 (2016) S133.

[15] Y. Xu, X. Yang, T. Wang, L. Yang, Y.-Y. He, K. Miskimins, S.Y. Qian, Knockdown delta-5-desaturase in breast cancer cells that overexpress COX-2 results in inhibition of growth, migration and invasion via a dihomo-γ-linolenic acid peroxidation dependent mechanism, BMC Cancer. 18 (2018) 330.

[16] X. Yang, Y. Xu, A. Brooks, B. Guo, K.W. Miskimins, S.Y. Qian, Knockdown delta-5-desaturase promotes the formation of a novel free radical byproduct from COX-catalyzed $ømega$-6 peroxidation to induce apoptosis and sensitize pancreatic cancer cells to chemotherapy drugs, Free Radical Biology and Medicine. 97 (2016) 342–350.

[17] X. Yang, Y. Xu, K.W. Miskimins, S.Y. Qian, Knocking Down Delta-5 Desaturase and Exploiting High Expression Level of COX-2 to Inhibit Cancer Migration and Invasion, Free Radical Biology and Medicine. 100 (2016) S133.

[18] K. Gao, L. Huang, Achieving efficient RNAi therapy: progress and challenges, Acta Pharmaceutica Sinica B. 3 (2013) 213–225. https://doi.org/10.1016/j.apsb.2013.06.005.

[19] S.Y. Wu, G. Lopez-Berestein, G.A. Calin, A.K. Sood, RNAi Therapies: Drugging the Undruggable, Science Translational Medicine. 6 (2014) 240ps7-240ps7.

[20] P. Guo, O. Coban, N.M. Snead, J. Trebley, S. Hoeprich, S. Guo, Y. Shu, Engineering RNA for Targeted siRNA Delivery and Medical Application, Advanced Drug Delivery Reviews. 62 (2010) 650–666. https://doi.org/10.1016/j.addr.2010.03.008.

[21] F. Tosi, F. Sartori, P. Guarini, O. Olivieri, N. Martinelli, Delta-5 and delta-6 desaturases: crucial enzymes in polyunsaturated fatty acid-related pathways with pleiotropic influences in health and disease, Adv Exp Med Biol. 824 (2014) 61–81. https://doi.org/10.1007/978-3-319-07320-0_7.

[22] J.M. Lee, H. Lee, S. Kang, W.J. Park, Fatty Acid Desaturases, Polyunsaturated Fatty Acid Regulation, and Biotechnological Advances, Nutrients. 8 (2016). https://doi.org/10.3390/nu8010023.

[23] B. Koletzko, E. Reischl, C. Tanjung, I. Gonzalez-Casanova, U. Ramakrishnan, S. Meldrum, K. Simmer, J. Heinrich, H. Demmelmair, FADS1 and FADS2 Polymorphisms Modulate Fatty Acid Metabolism and Dietary Impact on Health, Annual Review of Nutrition. 39 (2019) 21–44. https://doi.org/10.1146/annurev-nutr-082018-124250.

[24] M.C. Mansilla, C.E. Banchio, D. de Mendoza, Signalling pathways controlling fatty acid desaturation, Subcell Biochem. 49 (2008) 71–99. https://doi.org/10.1007/978-1-4020-8831-5_3.

[25] M. Wolters, C. Dering, A. Siani, P. Russo, J. Kaprio, P. Risé, L.A. Moreno, S. De Henauw, K. Mehlig, T. Veidebaum, D. Molnár, M. Tornaritis, L. Iacoviello, Y. Pitsiladis, C. Galli, R. Foraita, C. Börnhorst, The role of a FADS1 polymorphism in the association of fatty acid blood levels, BMI and blood pressure in young children—Analyses based on path models, PLoS One. 12 (2017). https://doi.org/10.1371/journal.pone.0181485.

[26] V. Nobili, A. Alisi, Z. Liu, T. Liang, A. Crudele, M. Raponi, J. Lin, N.P. Chalasani, W. Liu, In a pilot study, reduced fatty acid desaturase 1 function was associated with nonalcoholic fatty liver disease and response to treatment in children, Pediatr Res. 84 (2018) 696–703. https://doi.org/10.1038/s41390-018-0132-7.

[27] F. Jiao, H. Sun, Q. Yang, H. Sun, Z. Wang, M. Liu, J. Chen, Identification of FADS1 Through Common Gene Expression Profiles for Predicting Survival in Patients with Bladder Cancer, Cancer Manag Res. 12 (2020) 8325–8339.

[28] R. Zhao, L. Tian, B. Zhao, Y. Sun, J. Cao, K. Chen, F. Li, M. Li, D. Shang, M. Liu, FADS1 promotes the progression of laryngeal squamous cell carcinoma through activating AKT/mTOR signaling, Cell Death & Disease. 11 (2020) 1–14.

[29] D.A. Los, N. Murata, Structure and expression of fatty acid desaturases, Biochimica et Biophysica Acta (BBA) - Lipids and Lipid Metabolism. 1394 (1998) 3–15.

[30] P.C. Calder, 1 - Nutritional benefits of omega-3 fatty acids, in: C. Jacobsen, N.S. Nielsen, A.F. Horn, A.-D.M. Sørensen (Eds.), Food Enrichment with Omega-3 Fatty Acids, Woodhead Publishing, 2013: pp. 3–26. https://doi.org/10.1533/9780857098863.1.3.

[31] X. Wang, H. Lin, Y. Gu, Multiple roles of dihomo-γ-linolenic acid against proliferation diseases, Lipids in Health and Disease. 11 (2012) 25. https://doi.org/10.1186/1476-511X-11-25.

[32] S. Athinarayanan, Y.-Y. Fan, X. Wang, E. Callaway, D. Cai, N. Chalasani, R.S. Chapkin, W. Liu, Fatty Acid Desaturase 1 Influences Hepatic Lipid Homeostasis by Modulating the PPARα-FGF21 Axis, Hepatology Communications. 5 (2021) 461–477.

[33] A.D. Gromovsky, R.C. Schugar, A.L. Brown, R.N. Helsley, A.C. Burrows, D. Ferguson, R. Zhang, B.E. Sansbury, R.G. Lee, R.E. Morton, D.S. Allende, J.S. Parks, M. Spite, J.M. Brown, Δ-5 Fatty Acid Desaturase FADS1 Impacts Metabolic Disease by Balancing Proinflammatory and Proresolving Lipid Mediators, Arteriosclerosis, Thrombosis, and Vascular Biology. 38 (2018) 218–231. https://doi.org/10.1161/ATVBAHA.117.309660.

[34] A.D. Gromovsky, R.C. Schugar, A.L. Brown, R.N. Helsley, A.C. Burrows, D. Ferguson, R. Zhang, B.E. Sansbury, R.G. Lee, R.E. Morton, D.S. Allende, J.S. Parks, M. Spite, J.M. Brown, The Δ-5 Fatty Acid Desaturase FADS1 Impacts Metabolic Disease by Balancing

Pro-Inflammatory and Pro-Resolving Lipid Mediators, Arterioscler Thromb Vasc Biol. 38 (2018) 218–231. https://doi.org/10.1161/ATVBAHA.117.309660.

[35] R. Daneshmand, S. Kurl, T.-P. Tuomainen, J.K. Virtanen, Associations of estimated Δ-5-desaturase and Δ-6-desaturase activities with stroke risk factors and risk of stroke: the Kuopio Ischaemic Heart Disease Risk Factor Study, Br J Nutr. 117 (2017) 582–590. https://doi.org/10.1017/S000711451700054X.

[36] I. Swenne, B. Vessby, Relationship of Δ(6) -desaturase and Δ(5) -desaturase activities with thyroid hormone status in adolescents with eating disorders and weight loss, Acta Paediatr. 102 (2013) 416–418. https://doi.org/10.1111/apa.12132.

[37] M. Xiang, M.A. Rahman, H. Ai, X. Li, L.S. Harbige, Diet and Gene Expression: Delta-5 and Delta-6 Desaturases in Healthy Chinese and European Subjects, Annals of Nutrition & Metabolism. 50 (2007) 492–498.

[38] T. Matsuzaka, H. Shimano, N. Yahagi, M. Amemiya-Kudo, T. Yoshikawa, A.H. Hasty, Y. Tamura, J. Osuga, H. Okazaki, Y. Iizuka, A. Takahashi, H. Sone, T. Gotoda, S. Ishibashi, N. Yamada, Dual regulation of mouse Delta(5)- and Delta(6)-desaturase gene expression by SREBP-1 and PPARalpha, J Lipid Res. 43 (2002) 107–114.

[39] H.S. Dashti, I. Daghlas, J.M. Lane, Y. Huang, M.S. Udler, H. Wang, H.M. Ollila, S.E. Jones, J. Kim, A.R. Wood, M.N. Weedon, S. Aslibekyan, M. Garaulet, R. Saxena, Genetic determinants of daytime napping and effects on cardiometabolic health, Nature Communications. 12 (2021) 900. https://doi.org/10.1038/s41467-020-20585-3.

[40] Y. Lu, J. Shao, X. Shu, Y. Jiang, J. Rong, Y. Lai, J. Liu, FADS1 is a Prognostic Biomarker in Bladder Cancer: A Study Based on TCGA Data, Comb Chem High Throughput Screen. (2020). https://doi.org/10.2174/1386207323666200925104911.

[41] D. Wang, Y. Lin, B. Gao, S. Yan, H. Wu, Y. Li, Q. Wu, Y. Wei, Reduced Expression of FADS1 Predicts Worse Prognosis in Non-Small-Cell Lung Cancer, J Cancer. 7 (2016) 1226–1232. https://doi.org/10.7150/jca.15403.

[42] H. Lian, P. Xie, N. Yin, J. Zhang, X. Zhang, J. Li, C. Zhang, Linc00460 promotes osteosarcoma progression via miR-1224-5p/FADS1 axis, Life Sci. 233 (2019) 116757. https://doi.org/10.1016/j.lfs.2019.116757.

[43] B. Zhang, W.-H. Jia, K. Matsuda, S.-S. Kweon, K. Matsuo, Y.-B. Xiang, A. Shin, S.H. Jee, D.-H. Kim, Q. Cai, J. Long, J. Shi, W. Wen, G. Yang, Y. Zhang, C. Li, B. Li, Y. Guo, Z. Ren, B.-T. Ji, Z.-Z. Pan, A. Takahashi, M.-H. Shin, F. Matsuda, Y.-T. Gao, J.H. Oh, S. Kim, Y.-O. Ahn, A.T. Chan, J. Chang-Claude, M.L. Slattery, S.B. Gruber, F.R. Schumacher, S.L. Stenzel, G. Casey, H.-R. Kim, J.-Y. Jeong, J.W. Park, H.-L. Li, S. Hosono, S.-H. Cho, M. Kubo, X.-O. Shu, Y.-X. Zeng, W. Zheng, Large-scale genetic study in East Asians identifies six new loci associated with colorectal cancer risk, Nature Genetics. 46 (2014) 533–542. https://doi.org/10.1038/ng.2985.

[44] X.-Y. Qin, T. Su, W. Yu, S. Kojima, Lipid desaturation-associated endoplasmic reticulum stress regulates MYCN gene expression in hepatocellular carcinoma cells, Cell Death & Disease. 11 (2020) 1–13. https://doi.org/10.1038/s41419-020-2257-y.

[45] R. Wall, R.P. Ross, G.F. Fitzgerald, C. Stanton, Fatty acids from fish: the anti-inflammatory potential of long-chain omega-3 fatty acids, Nutrition Reviews. 68 (2010) 280–289. https://doi.org/10.1111/j.1753-4887.2010.00287.x.

[46] Y. Du, S.-M. Yan, W.-Y. Gu, F. He, L.-Y. Huang, M. Li, Y. Yuan, R.-H. Chen, Q. Zhong, M.-Z. Li, Y. Li, M.-S. Zeng, Decreased Expression of FADS1 Predicts a Poor Prognosis in

Patients with Esophageal Squamous Cell Carcinoma, Asian Pac J Cancer Prev. 16 (2015) 5089–5094. https://doi.org/10.7314/apjcp.2015.16.12.5089.

[47] F. Chen, B. He, L. Yan, Y. Qiu, L. Lin, L. Cai, FADS1 rs174549 Polymorphism May Predict a Favorable Response to Chemoradiotherapy in Oral Cancer Patients, J Oral Maxillofac Surg. 75 (2017) 214–220. https://doi.org/10.1016/j.joms.2016.07.005.

[48] C. Wang, N. Qin, M. Zhu, M. Chen, K. Xie, Y. Cheng, J. Dai, J. Liu, Y. Xia, H. Ma, G. Jin, C.I. Amos, Z. Hu, D. Lin, H. Shen, Metabolome-wide association study identified the association between a circulating polyunsaturated fatty acids variant rs174548 and lung cancer, Carcinogenesis. 38 (2017) 1147–1154. https://doi.org/10.1093/carcin/bgx084.

[49] N. Song, A. Shin, J.W. Park, J. Kim, J.H. Oh, Common risk variants for colorectal cancer: an evaluation of associations with age at cancer onset, Sci Rep. 7 (2017).

[50] Q. Wei, D. Yu, M. Liu, M. Wang, M. Zhao, M. Liu, W. Jia, H. Ma, J. Fang, W. Xu, K. Chen, Z. Xu, J. Wang, L. Tian, H. Yuan, J. Chang, Z. Hu, L. Wei, Y. Huang, Y. Han, J. Liu, D. Han, H. Shen, S. Yang, H. Zheng, Q. Ji, D. Li, W. Tan, C. Wu, D. Lin, Genome-wide association study identifies three susceptibility loci for laryngeal squamous cell carcinoma in the Chinese population, Nat Genet. 46 (2014) 1110–1114.

[51] N. Koundouros, G. Poulogiannis, Reprogramming of fatty acid metabolism in cancer, British Journal of Cancer. 122 (2020) 4–22. https://doi.org/10.1038/s41416-019-0650-z.

[52] F. Finetti, C. Travelli, J. Ercoli, G. Colombo, E. Buoso, L. Trabalzini, Prostaglandin E2 and Cancer: Insight into Tumor Progression and Immunity, Biology (Basel). 9 (2020).

[53] R. Mizuno, K. Kawada, Y. Sakai, Prostaglandin E2/EP Signaling in the Tumor Microenvironment of Colorectal Cancer, Int J Mol Sci. 20 (2019). https://doi.org/10.3390/ijms20246254.

[54] J. Yin, S.S. Kim, E. Choi, Y.T. Oh, W. Lin, T.-H. Kim, J.K. Sa, J.H. Hong, S.H. Park, H.J. Kwon, X. Jin, Y. You, J.H. Kim, H. Kim, J. Son, J. Lee, D.-H. Nam, K.S. Choi, B. Shi, H.-S. Gwak, H. Yoo, A. Iavarone, J.H. Kim, J.B. Park, ARS2/MAGL signaling in glioblastoma stem cells promotes self-renewal and M2-like polarization of tumor-associated macrophages, Nature Communications. 11 (2020) 2978.

[55] A. Kock, K. Larsson, F. Bergqvist, N. Eissler, L.H.M. Elfman, J. Raouf, M. Korotkova, J.I. Johnsen, P.-J. Jakobsson, P. Kogner, Inhibition of Microsomal Prostaglandin E Synthase-1 in Cancer-Associated Fibroblasts Suppresses Neuroblastoma Tumor Growth, EBioMedicine. 32 (2018) 84–92. https://doi.org/10.1016/j.ebiom.2018.05.008.

[56] R. Salcedo, X. Zhang, H.A. Young, N. Michael, K. Wasserman, W.-H. Ma, M. Martins-Green, W.J. Murphy, J.J. Oppenheim, Angiogenic effects of prostaglandin E2 are mediated by up-regulation of CXCR4 on human microvascular endothelial cells, Blood. 102 (2003) 1966–1977. https://doi.org/10.1182/blood-2002-11-3400.

[57] F. Finetti, R. Solito, L. Morbidelli, A. Giachetti, M. Ziche, S. Donnini, Prostaglandin E2 regulates angiogenesis via activation of fibroblast growth factor receptor-1, J Biol Chem. 283 (2008) 2139–2146. https://doi.org/10.1074/jbc.M703090200.

[58] K. Osawa, M. Umemura, R. Nakakaji, R. Tanaka, R.M. Islam, A. Nagasako, T. Fujita, U. Yokoyama, T. Koizumi, K. Mitsudo, Y. Ishikawa, Prostaglandin E2 receptor EP4 regulates cell migration through Orai1, Cancer Sci. 111 (2020) 160–174.

[59] J.Y. So, N. Skrypek, H.H. Yang, A.S. Merchant, G.W. Nelson, W.-D. Chen, H. Ishii, J.M. Chen, G. Hu, B.R. Achyut, E.C. Yoon, L. Han, C. Huang, M.C. Cam, K. Zhao, M.P. Lee, L. Yang, Induction of DNMT3B by PGE2 and IL6 at Distant Metastatic Sites Promotes

Epigenetic Modification and Breast Cancer Colonization, Cancer Res. 80 (2020) 2612–2627. https://doi.org/10.1158/0008-5472.CAN-19-3339.

[60] Y. Rong, L. Huang, K. Yi, H. Chen, S. Liu, W. Zhang, C. Yuan, X. Song, F. Wang, Co-administration of sulforaphane and doxorubicin attenuates breast cancer growth by preventing the accumulation of myeloid-derived suppressor cells, Cancer Letters. 493 (2020) 189–196. https://doi.org/10.1016/j.canlet.2020.08.041.

[61] X. Zhang, K. Yan, L. Deng, J. Liang, H. Liang, D. Feng, B. Ling, Cyclooxygenase 2 Promotes Proliferation and Invasion in Ovarian Cancer Cells via the PGE2/NF-κB Pathway, Cell Transplant. 28 (2019) 1S-13S. https://doi.org/10.1177/0963689719890597.

[62] N. Komura, S. Mabuchi, K. Shimura, E. Yokoi, K. Kozasa, H. Kuroda, R. Takahashi, T. Sasano, M. Kawano, Y. Matsumoto, M. Kodama, K. Hashimoto, K. Sawada, T. Kimura, The role of myeloid-derived suppressor cells in increasing cancer stem-like cells and promoting PD-L1 expression in epithelial ovarian cancer, Cancer Immunol Immunother. 69 (2020) 2477–2499. https://doi.org/10.1007/s00262-020-02628-2.

[63] G. Yan, H. Zhao, Q. Zhang, Y. Zhou, L. Wu, J. Lei, X. Wang, J. Zhang, X. Zhang, L. Zheng, G. Du, W. Xiao, B. Tang, H. Miao, Y. Li, A RIPK3-PGE2 Circuit Mediates Myeloid-Derived Suppressor Cell-Potentiated Colorectal Carcinogenesis, Cancer Res. 78 (2018) 5586–5599. https://doi.org/10.1158/0008-5472.CAN-17-3962.

[64] B. Cen, J.D. Lang, Y. Du, J. Wei, Y. Xiong, N. Bradley, D. Wang, R.N. DuBois, Prostaglandin E2 Induces MIR675-5p to Promote Colorectal Tumor Metastasis via Modulation of p53 Expression, Gastroenterology. 158 (2020) 971-984.e10. https://doi.org/10.1053/j.gastro.2019.11.013.

[65] L. Lin, D. Wang, S. Qu, H. Zhao, Y. Lin, miR-370-3p Alleviates Ulcerative Colitis-Related Colorectal Cancer in Mice Through Inhibiting the Inflammatory Response and Epithelial-Mesenchymal Transition, Drug Des Devel Ther. 14 (2020) 1127–1141.

[66] Y.R. Park, S.Y. Seo, S.L. Kim, S.M. Zhu, S. Chun, J.-M. Oh, M.R. Lee, S.H. Kim, I.H. Kim, S.O. Lee, S.T. Lee, S.W. Kim, MiRNA-206 suppresses PGE2-induced colorectal cancer cell proliferation, migration, and invasion by targetting TM4SF1, Biosci Rep. 38 (2018). https://doi.org/10.1042/BSR20180664.

[67] K. Iwamoto, H. Takahashi, D. Okuzaki, H. Osawa, T. Ogino, N. Miyoshi, M. Uemura, C. Matsuda, H. Yamamoto, T. Mizushima, M. Mori, Y. Doki, H. Eguchi, Syntenin-1 promotes colorectal cancer stem cell expansion and chemoresistance by regulating prostaglandin E2 receptor, British Journal of Cancer. 123 (2020) 955–964. https://doi.org/10.1038/s41416-020-0965-9.

[68] H.-B. Kim, M. Kim, Y.-S. Park, I. Park, T. Kim, S.-Y. Yang, C.J. Cho, D. Hwang, J.-H. Jung, S.D. Markowitz, S.W. Hwang, S.-K. Yang, D.-S. Lim, S.-J. Myung, Prostaglandin E2 Activates YAP and a Positive-signaling Loop to Promote Colon Regeneration Following Colitis but Also Carcinogenesis in Mice, Gastroenterology. 152 (2017) 616–630.

[69] M.-J. Jiang, Y.-Y. Chen, J.-J. Dai, D.-N. Gu, Z. Mei, F.-R. Liu, Q. Huang, L. Tian, Dying tumor cell-derived exosomal miR-194-5p potentiates survival and repopulation of tumor repopulating cells upon radiotherapy in pancreatic cancer, Mol Cancer. 19 (2020) 68.

[70] V. Prima, L.N. Kaliberova, S. Kaliberov, D.T. Curiel, S. Kusmartsev, COX2/mPGES1/PGE2 pathway regulates PD-L1 expression in tumor-associated macrophages and myeloid-derived suppressor cells, PNAS. 114 (2017) 1117–1122. https://doi.org/10.1073/pnas.1612920114.

[71] L.G. Howes, Selective COX-2 inhibitors, NSAIDs and cardiovascular events – is celecoxib the safest choice?, Ther Clin Risk Manag. 3 (2007) 831–845.

[72] N.K. Altorki, R.S. Keresztes, J.L. Port, D.M. Libby, R.J. Korst, D.B. Flieder, C.A. Ferrara, D.F. Yankelevitz, K. Subbaramaiah, M.W. Pasmantier, A.J. Dannenberg, Celecoxib, a selective cyclo-oxygenase-2 inhibitor, enhances the response to preoperative paclitaxel and carboplatin in early-stage non-small-cell lung cancer, J Clin Oncol. 21 (2003) 2645–2650. https://doi.org/10.1200/JCO.2003.07.127.

[73] M. Gulyas, J.S.M. Mattsson, A. Lindgren, L. Ek, K. Lamberg Lundström, A. Behndig, E. Holmberg, P. Micke, B. Bergman, S.L.C.S. Group, COX-2 expression and effects of celecoxib in addition to standard chemotherapy in advanced non-small cell lung cancer, Acta Oncologica. 57 (2018) 244–250.

[74] J. Li, F. Cao, H. Yin, Z. Huang, Z. Lin, N. Mao, B. Sun, G. Wang, Ferroptosis: past, present and future, Cell Death & Disease. 11 (2020) 1–13. https://doi.org/10.1038/s41419-020-2298-2.

[75] J.-Y. Lee, M. Nam, H.Y. Son, K. Hyun, S.Y. Jang, J.W. Kim, M.W. Kim, Y. Jung, E. Jang, S.-J. Yoon, J. Kim, J. Kim, J. Seo, J.-K. Min, K.-J. Oh, B.-S. Han, W.K. Kim, K.-H. Bae, J. Song, J. Kim, Y.-M. Huh, G.-S. Hwang, E.-W. Lee, S.C. Lee, Polyunsaturated fatty acid biosynthesis pathway determines ferroptosis sensitivity in gastric cancer, PNAS. 117 (2020) 32433–32442. https://doi.org/10.1073/pnas.2006828117.

[76] Y. Xiao, Y. Gu, P. Purwaha, K. Ni, B. Law, S. Mallik, S.Y. Qian, Characterization of free radicals formed from COX-catalyzed DGLA peroxidation, Free Radic Biol Med. 50 (2011) 1163–1170. https://doi.org/10.1016/j.freeradbiomed.2011.02.001.

[77] Y. Gu, Y. Xu, B. Law, S.Y. Qian, The First Characterization of Free Radicals Formed From Cellular COX-Catalyzed Peroxidation, Free Radic Biol Med. 57 (2013) 49–60.

[78] L. Pang, H. Shah, H. Wang, D. Shu, S.Y. Qian, V. Sathish, EpCAM-Targeted 3WJ RNA Nanoparticle Harboring Delta-5-Desaturase siRNA Inhibited Lung Tumor Formation via DGLA Peroxidation, Molecular Therapy - Nucleic Acids. 22 (2020) 222–235.

[79] H. Shah, L. Pang, H. Wang, D. Shu, S.Y. Qian, V. Sathish, Growth inhibitory and anti-metastatic activity of epithelial cell adhesion molecule targeted three-way junctional delta-5-desaturase siRNA nanoparticle for breast cancer therapy, Nanomedicine: Nanotechnology, Biology and Medicine. 30 (2020) 102298.

[80] Y. Xu, X. Yang, P. Zhao, Z. Yang, C. Yan, B. Guo, S.Y. Qian, Knockdown of delta-5-desaturase promotes the anti-cancer activity of dihomo-γ-linolenic acid and enhances the efficacy of chemotherapy in colon cancer cells expressing COX-2, Free Radic. Biol. Med. 96 (2016) 67–77. https://doi.org/10.1016/j.freeradbiomed.2016.04.016.

[81] X. Yang, Y. Xu, A. Brooks, B. Guo, K.W. Miskimins, S.Y. Qian, Knockdown delta-5-desaturase promotes the formation of a novel free radical byproduct from COX-catalyzed ω-6 peroxidation to induce apoptosis and sensitize pancreatic cancer cells to chemotherapy drugs, Free Radical Biology and Medicine. 97 (2016) 342–350.

[82] S. Shimizu, K. Akimoto, Y. Shinmen, H. Kawashima, M. Sugano, H. Yamada, Sesamin is a potent and specific inhibitor of delta 5 desaturase in polyunsaturated fatty acid biosynthesis, Lipids. 26 (1991) 512–516. https://doi.org/10.1007/BF02536595.

[83] S. Shimizu, S. Jareonkitmongkol, H. Kawashima, K. Akimoto, H. Yamada, Inhibitory effect of curcumin on fatty acid desaturation in Mortierella alpina 1S-4 and rat liver microsomes, Lipids. 27 (1992) 509–512. https://doi.org/10.1007/BF02536132.

[84] M.G. Obukowicz, A. Raz, P.D. Pyla, J.G. Rico, J.M. Wendling, P. Needleman, Identification and characterization of a novel delta6/delta5 fatty acid desaturase inhibitor as a potential anti-inflammatory agent, Biochem Pharmacol. 55 (1998) 1045–1058.

[85] H. Yashiro, S. Takagahara, Y.O. Tamura, I. Miyahisa, J. Matsui, H. Suzuki, S. Ikeda, M. Watanabe, A Novel Selective Inhibitor of Delta-5 Desaturase Lowers Insulin Resistance and Reduces Body Weight in Diet-Induced Obese C57BL/6J Mice, PLoS One. 11 (2016). https://doi.org/10.1371/journal.pone.0166198.

[86] H. Nagase, S. Takagahara, Y. Satomi, A. Ando, K. Kubo, S. Ikeda, Effects of compound-326, a selective delta-5 desaturase inhibitor, in ApoE knockout mice with two different protocols for atherosclerosis development, J Pharm Pharm Sci. 24 (2021) 71–83.

[87] J. Fujimoto, R. Okamoto, N. Noguchi, R. Hara, S. Masada, T. Kawamoto, H. Nagase, Y.O. Tamura, M. Imanishi, S. Takagahara, K. Kubo, K. Tohyama, K. Iida, T. Andou, I. Miyahisa, J. Matsui, R. Hayashi, T. Maekawa, N. Matsunaga, Discovery of 3,5-Diphenyl-4-methyl-1,3-oxazolidin-2-ones as Novel, Potent, and Orally Available Δ-5 Desaturase (D5D) Inhibitors, J. Med. Chem. 60 (2017) 8963–8981.

[88] I. Miyahisa, H. Suzuki, A. Mizukami, Y. Tanaka, M. Ono, M.S. Hixon, J. Matsui, T-3364366 Targets the Desaturase Domain of Delta-5 Desaturase with Nanomolar Potency and a Multihour Residence Time, ACS Med Chem Lett. 7 (2016) 868–872. https://doi.org/10.1021/acsmedchemlett.6b00241.

[89] Compound for inhibition of delta-5-desaturase (d5d) and treatment of cancer and inflammation - Patent US-2019070193-A1 - PubChem, (n.d.).

[90] M. Sadiq, L. Pang, M. Johnson, V. Sathish, Q. Zhang, D. Wang, 2D Nanomaterial, Ti3C2 MXene-Based Sensor to Guide Lung Cancer Therapy and Management, Biosensors (Basel). 11 (2021). https://doi.org/10.3390/bios11020040.

[91] Y. Xu, L. Pang, H. Wang, C. Xu, H. Shah, P. Guo, D. Shu, S.Y. Qian, Specific delivery of delta-5-desaturase siRNA via RNA nanoparticles supplemented with dihomo-γ-linolenic acid for colon cancer suppression, Redox Biol. 21 (2019) 101085.

[92] X. Yang, Y. Xu, T. Wang, D. Shu, P. Guo, K. Miskimins, S.Y. Qian, Inhibition of cancer migration and invasion by knocking down delta-5-desaturase in COX-2 overexpressed cancer cells, Redox Biol. 11 (2017) 653–662. https://doi.org/10.1016/j.redox.2017.01.016.

[93] X. Yang, Y. Xu, D. Gao, L. Yang, S.Y. Qian, Dihomo-γ-linolenic acid inhibits growth of xenograft tumors in mice bearing human pancreatic cancer cells (BxPC-3) transfected with delta-5-desaturase shRNA, Redox Biology. 20 (2019) 236–246.

[94] H. Yin, G. Xiong, S. Guo, C. Xu, R. Xu, P. Guo, D. Shu, Delivery of Anti-miRNA for Triple-Negative Breast Cancer Therapy Using RNA Nanoparticles Targeting Stem Cell Marker CD133, Mol. Ther. 27 (2019) 1252–1261.

[95] B. dos Santos Rodrigues, S. Arora, T. Kanekiyo, J. Singh, Efficient neuronal targeting and transfection using RVG and transferrin-conjugated liposomes, Brain Research. 1734 (2020) 146738. https://doi.org/10.1016/j.brainres.2020.146738.

[96] R.J. George, M.A. Sturmoski, S. Anant, C.W. Houchen, EP4 mediates PGE2 dependent cell survival through the PI3 kinase/AKT pathway, Prostaglandins & Other Lipid Mediators. 83 (2007) 112–120. https://doi.org/10.1016/j.prostaglandins.2006.10.005.

[97] A.A. Birukova, T. Zagranichnaya, P. Fu, E. Alekseeva, W. Chen, J.R. Jacobson, K.G. Birukov, Prostaglandins PGE2 and PGI2 promote endothelial barrier enhancement via

PKA- and Epac1/Rap1-dependent Rac activation, Experimental Cell Research. 313 (2007) 2504–2520. https://doi.org/10.1016/j.yexcr.2007.03.036.

[98] Involvement of COX-2/PGE2 Pathway in the Upregulation of MMP-9 Expression in Pancreatic Cancer, (n.d.). https://www.hindawi.com/journals/grp/2011/214269/ (accessed June 23, 2021).

[99] Cisplatin-Based Adjuvant Chemotherapy in Patients with Completely Resected Non–Small-Cell Lung Cancer, New England Journal of Medicine. 350 (2004) 351–360.

[100] S. Yuan, H. Chen, Mathematical rules for synergistic, additive, and antagonistic effects of multi-drug combinations and their application in research and development of combinatorial drugs and special medical food combinations, Food Science and Human Wellness. 8 (2019) 136–141. https://doi.org/10.1016/j.fshw.2019.01.003.

[101] H. Katagiri, M. Takahashi, K. Wakai, H. Sugiura, T. Kataoka, K. Nakanishi, Prognostic factors and a scoring system for patients with skeletal metastasis, The Journal of Bone and Joint Surgery. British Volume. 87-B (2005) 698–703. https://doi.org/10.1302/0301-620X.87B5.15185.

[102] J.-Y. Han, Y.-J. Chung, S.W. Park, J.S. Kim, M.-G. Rhyu, H.-K. Kim, K.S. Lee, The relationship between cisplatin-induced apoptosis and p53, bcl-2 and bax expression in human lung cancer cells, Korean J Intern Med. 14 (1999) 42–52.

[103] S. Elmore, Apoptosis: A Review of Programmed Cell Death, Toxicol Pathol. 35 (2007) 495–516. https://doi.org/10.1080/01926230701320337.

[104] J.C. Reed, Bcl-2 family proteins: regulators of apoptosis and chemoresistance in hematologic malignancies, Semin Hematol. 34 (1997) 9–19.

[105] J. Laudanski, W. Niklinska, T. Burzykowski, L. Chyczewski, J. Niklinski, Prognostic significance of p53 and bcl-2 abnormalities in operable nonsmall cell lung cancer, The European Respiratory Journal. 17 (2001) 660–666.

[106] H. Han, B. Yang, H.J. Nakaoka, J. Yang, Y. Zhao, K. Le Nguyen, A.T. Bishara, T.K. Mandalia, W. Wang, Hippo signaling dysfunction induces cancer cell addiction to YAP, Oncogene. 37 (2018) 6414–6424. https://doi.org/10.1038/s41388-018-0419-5.

[107] S.W. Plouffe, A.W. Hong, K.-L. Guan, Disease implications of the Hippo/YAP pathway, Trends in Molecular Medicine. 21 (2015) 212–222.

[108] M.F. Linton, S. Fazio, Cyclooxygenase products and atherosclerosis, Drug Discovery Today: Therapeutic Strategies. 5 (2008) 25–36. https://doi.org/10.1016/j.ddstr.2008.05.006.

[109] C.A. Rouzer, L.J. Marnett, Cyclooxygenases: structural and functional insights, Journal of Lipid Research. 50 (2009) S29–S34. https://doi.org/10.1194/jlr.R800042-JLR200.

[110] X. Sun, Q. Li, Prostaglandin EP2 receptor: Novel therapeutic target for human cancers (Review), International Journal of Molecular Medicine. 42 (2018) 1203–1214.

[111] K. Tsuge, T. Inazumi, A. Shimamoto, Y. Sugimoto, Molecular mechanisms underlying prostaglandin E2-exacerbated inflammation and immune diseases, International Immunology. 31 (2019) 597–606. https://doi.org/10.1093/intimm/dxz021.

[112] G.Y. Di Veroli, C. Fornari, D. Wang, S. Mollard, J.L. Bramhall, F.M. Richards, D.I. Jodrell, Combenefit: an interactive platform for the analysis and visualization of drug combinations, Bioinformatics. 32 (2016) 2866–2868.

[113] M. Matsumoto, W. Nakajima, M. Seike, A. Gemma, N. Tanaka, Cisplatin-induced apoptosis in non-small-cell lung cancer cells is dependent on Bax- and Bak-induction pathway and synergistically activated by BH3-mimetic ABT-263 in p53 wild-type and

mutant cells, Biochemical and Biophysical Research Communications. 473 (2016) 490–496. https://doi.org/10.1016/j.bbrc.2016.03.053.

[114] P. Gallinari, S.D. Marco, P. Jones, M. Pallaoro, C. Steinkühler, HDACs, histone deacetylation and gene transcription: from molecular biology to cancer therapeutics, Cell Res. 17 (2007) 195–211. https://doi.org/10.1038/sj.cr.7310149.

[115] M. Huang, J. Zhang, C. Yan, X. Li, J. Zhang, R. Ling, Small molecule HDAC inhibitors: Promising agents for breast cancer treatment, Bioorganic Chemistry. 91 (2019) 103184. https://doi.org/10.1016/j.bioorg.2019.103184.

[116] S. Ropero, M. Esteller, The role of histone deacetylases (HDACs) in human cancer, Molecular Oncology. 1 (2007) 19–25. https://doi.org/10.1016/j.molonc.2007.01.001.

[117] Y. Li, E. Seto, HDACs and HDAC Inhibitors in Cancer Development and Therapy, Cold Spring Harb Perspect Med. 6 (2016) a026831. https://doi.org/10.1101/cshperspect.a026831.

[118] D. Plesca, S. Mazumder, A. Almasan, Chapter 6 DNA Damage Response and Apoptosis, in: Methods in Enzymology, Academic Press, 2008: pp. 107–122.

[119] Y.E. Kim, J. Chen, R. Langen, J.R. Chan, Monitoring apoptosis and neuronal degeneration by real-time detection of phosphatidylserine externalization using a polarity-sensitive indicator of viability and apoptosis, Nat Protoc. 5 (2010) 1396–1405.

[120] Y.E. Kim, J. Chen, J.R. Chan, R. Langen, Engineering a polarity-sensitive biosensor for time-lapse imaging of apoptotic processes and degeneration, Nat Methods. 7 (2010) 67–73. https://doi.org/10.1038/nmeth.1405.

[121] S.-H. Chen, G. Zhaori, Potential clinical applications of siRNA technique: benefits and limitations, Eur. J. Clin. Invest. 41 (2011) 221–232. https://doi.org/10.1111/j.1365-2362.2010.02400.x.

[122] A. Wittrup, J. Lieberman, Knocking down disease: a progress report on siRNA therapeutics, Nat Rev Genet. 16 (2015) 543–552. https://doi.org/10.1038/nrg3978.

[123] B. Hu, L. Zhong, Y. Weng, L. Peng, Y. Huang, Y. Zhao, X.-J. Liang, Therapeutic siRNA: state of the art, Sig Transduct Target Ther. 5 (2020) 1–25.

[124] H. Dana, G.M. Chalbatani, H. Mahmoodzadeh, R. Karimloo, O. Rezaiean, A. Moradzadeh, N. Mehmandoost, F. Moazzen, A. Mazraeh, V. Marmari, M. Ebrahimi, M.M. Rashno, S.J. Abadi, E. Gharagouzlo, Molecular Mechanisms and Biological Functions of siRNA, Int J Biomed Sci. 13 (2017) 48–57.

[125] L. Aagaard, J.J. Rossi, RNAi therapeutics: principles, prospects and challenges, Advanced Drug Delivery Reviews. 59 (2007) 75–86.

[126] S.M. Elbashir, J. Harborth, W. Lendeckel, A. Yalcin, K. Weber, T. Tuschl, Duplexes of 21-nucleotide RNAs mediate RNA interference in cultured mammalian cells, Nature. 411 (2001) 494–498. https://doi.org/10.1038/35078107.

[127] D.W. Bartlett, M.E. Davis, Insights into the kinetics of siRNA-mediated gene silencing from live-cell and live-animal bioluminescent imaging, Nucleic Acids Res. 34 (2006) 322–333. https://doi.org/10.1093/nar/gkj439.

[128] Y. Huang, S.N. Vasilatos, L. Boric, P.G. Shaw, N.E. Davidson, Inhibitors of histone demethylation and histone deacetylation cooperate in regulating gene expression and inhibiting growth in human breast cancer cells, Breast Cancer Res Treat. 131 (2012) 777–789. https://doi.org/10.1007/s10549-011-1480-8.

[129] Y. Weng, H. Xiao, J. Zhang, X.-J. Liang, Y. Huang, RNAi therapeutic and its innovative biotechnological evolution, Biotechnol Adv. 37 (2019) 801–825.

[130] Phase 1 Trial of an RNA Interference Therapy for Acute Intermittent Porphyria | NEJM, (n.d.). https://www.nejm.org/doi/full/10.1056/NEJMoa1807838 (accessed June 28, 2021).

[131] S. Agarwal, A.R. Simon, V. Goel, B.A. Habtemariam, V.A. Clausen, J.B. Kim, G.J. Robbie, Pharmacokinetics and Pharmacodynamics of the Small Interfering Ribonucleic Acid, Givosiran, in Patients With Acute Hepatic Porphyria, Clinical Pharmacology & Therapeutics. 108 (2020) 63–72. https://doi.org/10.1002/cpt.1802.

[132] A.L. Jackson, S.R. Bartz, J. Schelter, S.V. Kobayashi, J. Burchard, M. Mao, B. Li, G. Cavet, P.S. Linsley, Expression profiling reveals off-target gene regulation by RNAi, Nat Biotechnol. 21 (2003) 635–637. https://doi.org/10.1038/nbt831.

[133] M.E. Kleinman, K. Yamada, A. Takeda, V. Chandrasekaran, M. Nozaki, J.Z. Baffi, R.J.C. Albuquerque, S. Yamasaki, M. Itaya, Y. Pan, B. Appukuttan, D. Gibbs, Z. Yang, K. Karikó, B.K. Ambati, T.A. Wilgus, L.A. DiPietro, E. Sakurai, K. Zhang, J.R. Smith, E.W. Taylor, J. Ambati, Sequence- and target-independent angiogenesis suppression by siRNA via TLR3, Nature. 452 (2008) 591–597. https://doi.org/10.1038/nature06765.

[134] A.D. Judge, M. Robbins, I. Tavakoli, J. Levi, L. Hu, A. Fronda, E. Ambegia, K. McClintock, I. MacLachlan, Confirming the RNAi-mediated mechanism of action of siRNA-based cancer therapeutics in mice, J Clin Invest. 119 (2009) 661–673.

[135] A.D. Judge, G. Bola, A.C.H. Lee, I. MacLachlan, Design of noninflammatory synthetic siRNA mediating potent gene silencing in vivo, Mol Ther. 13 (2006) 494–505.

[136] R. Kanasty, J.R. Dorkin, A. Vegas, D. Anderson, Delivery materials for siRNA therapeutics, Nat Mater. 12 (2013) 967–977. https://doi.org/10.1038/nmat3765.

[137] Y. Fedorov, E.M. Anderson, A. Birmingham, A. Reynolds, J. Karpilow, K. Robinson, D. Leake, W.S. Marshall, A. Khvorova, Off-target effects by siRNA can induce toxic phenotype, RNA. 12 (2006) 1188–1196. https://doi.org/10.1261/rna.28106.

[138] P. Guo, RNA nanotechnology: engineering, assembly and applications in detection, gene delivery and therapy, J Nanosci Nanotechnol. 5 (2005) 1964–1982.

[139] P. Guo, The emerging field of RNA nanotechnology, Nature Nanotechnology. 5 (2010) 833–842. https://doi.org/10.1038/nnano.2010.231.

[140] P. Guo, Structure and function of φ29 hexameric RNA that drives the viral DNA packaging motor: Review, in: Progress in Nucleic Acid Research and Molecular Biology, Academic Press, 2002: pp. 415–472. https://doi.org/10.1016/S0079-6603(02)72076-X.

[141] S. Guo, X. Piao, H. Li, P. Guo, Methods for construction and characterization of simple or special multifunctional RNA nanoparticles based on the 3WJ of phi29 DNA packaging motor, Methods. 143 (2018) 121–133. https://doi.org/10.1016/j.ymeth.2018.02.025.

[142] H. Li, P.G. Rychahou, Z. Cui, F. Pi, B.M. Evers, D. Shu, P. Guo, W. Luo, RNA Nanoparticles Derived from Three-Way Junction of Phi29 Motor pRNA Are Resistant to I-125 and Cs-131 Radiation, Nucleic Acid Ther. 25 (2015) 188–197.

[143] P. Tarapore, Y. Shu, P. Guo, S.-M. Ho, Application of phi29 motor pRNA for targeted therapeutic delivery of siRNA silencing metallothionein-IIA and survivin in ovarian cancers, Mol. Ther. 19 (2011) 386–394. https://doi.org/10.1038/mt.2010.243.

[144] X. Piao, H. Wang, D.W. Binzel, P. Guo, Assessment and comparison of thermal stability of phosphorothioate-DNA, DNA, RNA, 2'-F RNA, and LNA in the context of Phi29 pRNA 3WJ, RNA. 24 (2018) 67–76. https://doi.org/10.1261/rna.063057.117.

[145] D. Shu, Y. Shu, F. Haque, S. Abdelmawla, P. Guo, Thermodynamically stable RNA three-way junction for constructing multifunctional nanoparticles for delivery of therapeutics, Nature Nanotechnology. 6 (2011) 658–667.

[146] Y. Shu, F. Pi, A. Sharma, M. Rajabi, F. Haque, D. Shu, M. Leggas, B.M. Evers, P. Guo, Stable RNA nanoparticles as potential new generation drugs for cancer therapy, Advanced Drug Delivery Reviews. 66 (2014) 74–89. https://doi.org/10.1016/j.addr.2013.11.006.

[147] D. Cui, C. Zhang, B. Liu, Y. Shu, T. Du, D. Shu, K. Wang, F. Dai, Y. Liu, C. Li, F. Pan, Y. Yang, J. Ni, H. Li, B. Brand-Saberi, P. Guo, Regression of Gastric Cancer by Systemic Injection of RNA Nanoparticles Carrying both Ligand and siRNA, Sci Rep. 5 (2015) 10726. https://doi.org/10.1038/srep10726.

[148] S. Guo, C. Xu, H. Yin, J. Hill, F. Pi, P. Guo, Tuning the size, shape and structure of RNA nanoparticles for favorable cancer targeting and immunostimulation, Wiley Interdiscip Rev Nanomed Nanobiotechnol. 12 (2020) e1582. https://doi.org/10.1002/wnan.1582.

[149] S. Guo, N. Tschammer, S. Mohammed, P. Guo, Specific delivery of therapeutic RNAs to cancer cells via the dimerization mechanism of phi29 motor pRNA, Hum. Gene Ther. 16 (2005) 1097–1109. https://doi.org/10.1089/hum.2005.16.1097.

[150] F. Haque, D. Shu, Y. Shu, L.S. Shlyakhtenko, P.G. Rychahou, B.M. Evers, P. Guo, Ultrastable synergistic tetravalent RNA nanoparticles for targeting to cancers, Nano Today. 7 (2012) 245–257. https://doi.org/10.1016/j.nantod.2012.06.010.

[151] P. Rychahou, Y. Shu, F. Haque, J. Hu, P. Guo, B.M. Evers, Methods and assays for specific targeting and delivery of RNA nanoparticles to cancer metastases, Methods Mol. Biol. 1297 (2015) 121–135. https://doi.org/10.1007/978-1-4939-2562-9_9.

[152] Z. Li, L. Yang, H. Wang, D.W. Binzel, T.M. Williams, P. Guo, Non-Small-Cell Lung Cancer Regression by siRNA Delivered Through Exosomes That Display EGFR RNA Aptamer, Nucleic Acid Ther. (2021). https://doi.org/10.1089/nat.2021.0002.

[153] H. Liu, S. Guo, R. Roll, J. Li, Z. Diao, N. Shao, M.R. Riley, A.M. Cole, J.P. Robinson, N.M. Snead, G. Shen, P. Guo, Phi29 pRNA vector for efficient escort of hammerhead ribozyme targeting survivin in multiple cancer cells, Cancer Biol. Ther. 6 (2007) 697–704. https://doi.org/10.4161/cbt.6.5.3962.

[154] G. Spizzo, D. Fong, M. Wurm, C. Ensinger, P. Obrist, C. Hofer, G. Mazzoleni, G. Gastl, P. Went, EpCAM expression in primary tumour tissues and metastases: an immunohistochemical analysis, J. Clin. Pathol. 64 (2011) 415–420.

[155] M.A. Mohtar, S.E. Syafruddin, S.N. Nasir, L.T. Yew, Revisiting the Roles of Pro-Metastatic EpCAM in Cancer, Biomolecules. 10 (2020).

[156] N.-B. Liabakk, I. Talbot, R.A. Smith, K. Wilkinson, F. Balkwill, Matrix metalloprotease 2 (MMP-2) and matrix metalloprotease 9 (MMP-9) type IV collagenases in colorectal cancer, Cancer Research. 56 (1996) 190–196.

[157] V. Ellenrieder, B. Alber, U. Lacher, S.F. Hendler, A. Menke, W. Boeck, M. Wagner, M. Wilda, H. Friess, M. Büchler, Role of MT-MMPs and MMP-2 in pancreatic cancer progression, International Journal of Cancer. 85 (2000) 14–20.

[158] G. Moreno-Bueno, E. Cubillo, D. Sarrió, H. Peinado, S.M. Rodríguez-Pinilla, S. Villa, V. Bolós, M. Jordá, A. Fabra, F. Portillo, Genetic profiling of epithelial cells expressing E-cadherin repressors reveals a distinct role for Snail, Slug, and E47 factors in epithelial-mesenchymal transition, Cancer Research. 66 (2006) 9543–9556.

[159] G. Zheng, J.G. Lyons, T.K. Tan, Y. Wang, T.-T. Hsu, D. Min, L. Succar, G.K. Rangan, M. Hu, B.R. Henderson, Disruption of E-cadherin by matrix metalloproteinase directly mediates epithelial-mesenchymal transition downstream of transforming growth factor-β1 in renal tubular epithelial cells, The American Journal of Pathology. 175 (2009) 580–591.

[160] S. Gao, F. Dagnaes-Hansen, E.J.B. Nielsen, J. Wengel, F. Besenbacher, K.A. Howard, J. Kjems, The Effect of Chemical Modification and Nanoparticle Formulation on Stability and Biodistribution of siRNA in Mice, Mol Ther. 17 (2009) 1225–1233.

[161] S. Huerta-Yépez, A.B. Tirado-Rodriguez, O. Hankinson, Role of diets rich in omega-3 and omega-6 in the development of cancer, Boletín Médico Del Hospital Infantil de México. 73 (2016) 446–456. https://doi.org/10.1016/j.bmhimx.2016.11.001.

[162] R. Pai, B. Soreghan, I.L. Szabo, M. Pavelka, D. Baatar, A.S. Tarnawski, Prostaglandin E2 transactivates EGF receptor: a novel mechanism for promoting colon cancer growth and gastrointestinal hypertrophy, Nat. Med. 8 (2002) 289–293. https://doi.org/10.1038/nm0302-289.

[163] J.K. Brunelle, A. Letai, Control of mitochondrial apoptosis by the Bcl-2 family, J Cell Sci. 122 (2009) 437–441. https://doi.org/10.1242/jcs.031682.

[164] P.C. Calses, J.J. Crawford, J.R. Lill, A. Dey, Hippo Pathway in Cancer: Aberrant Regulation and Therapeutic Opportunities, Trends in Cancer. 5 (2019) 297–307.

[165] F.-X. Yu, B. Zhao, K.-L. Guan, Hippo Pathway in Organ Size Control, Tissue Homeostasis, and Cancer, Cell. 163 (2015) 811–828.

[166] B. Zhao, Q.-Y. Lei, K.-L. Guan, The Hippo–YAP pathway: new connections between regulation of organ size and cancer, Current Opinion in Cell Biology. 20 (2008) 638–646. https://doi.org/10.1016/j.ceb.2008.10.001.

[167] S. Piccolo, S. Dupont, M. Cordenonsi, The biology of YAP/TAZ: hippo signaling and beyond, Physiol Rev. 94 (2014) 1287–1312. https://doi.org/10.1152/physrev.00005.2014.

[168] H. Achiwa, Y. Yatabe, T. Hida, T. Kuroishi, K. Kozaki, S. Nakamura, M. Ogawa, T. Sugiura, T. Mitsudomi, T. Takahashir, Prognostic significance of elevated cyclooxygenase 2 expression in primary, resected lung adenocarcinomas, Clinical Cancer Research. 5 (1999) 1001–1005.

[169] L. Pang, H. Shah, S. Qian, V. Sathish, Iminodibenzyl redirected cyclooxygenase-2 catalyzed dihomo-γ-linolenic acid peroxidation pattern in lung cancer, Free Radical Biology and Medicine. (2021). https://doi.org/10.1016/j.freeradbiomed.2021.06.004.

[170] H.-Y. Jung, T.H. Kim, J.-E. Lee, H.K. Kim, J.H. Cho, Y.S. Choi, S. Shin, S.-H. Lee, H. Rhee, H.K. Lee, H.J. Choi, H.Y. Jang, S. Lee, J.H. Kang, Y.A. Choi, S. Lee, J. Lee, Y.L. Choi, J. Kim, PDX models of human lung squamous cell carcinoma: consideration of factors in preclinical and co-clinical applications, Journal of Translational Medicine. 18 (2020) 307. https://doi.org/10.1186/s12967-020-02473-y.

[171] Y. Jiang, J. Zhao, Y. Zhang, K. Li, T. Li, X. Chen, S. Zhao, S. Zhao, K. Liu, Z. Dong, Establishment of lung cancer patient-derived xenograft models and primary cell lines for lung cancer study, J Transl Med. 16 (2018) 138. https://doi.org/10.1186/s12967-018-1516-5.

[172] A. Kellar, C. Egan, D. Morris, Preclinical Murine Models for Lung Cancer: Clinical Trial Applications, BioMed Research International. 2015 (2015) e621324.

[173] L. Parlea, A. Puri, W. Kasprzak, E. Bindewald, P. Zakrevsky, E. Satterwhite, K. Joseph, K.A. Afonin, B.A. Shapiro, Cellular Delivery of RNA Nanoparticles, ACS Comb Sci. 18 (2016) 527–547. https://doi.org/10.1021/acscombsci.6b00073.

[174] M. Maugeri-Saccà, R. De Maria, The Hippo pathway in normal development and cancer, Pharmacology & Therapeutics. 186 (2018) 60–72.